AD-A160 137 METALLIC INDUCTION REACTION ENGINE(U) ELECTROMAGNETIC LAUNCH RESEARCH INC CAMBRIDGE MA P P MONGEAU ET AL. 28 DEC 84 EML-85-AF001 AFOSR-TR-85-0773 1/2

UNCLASSIFIED F49620-83-C-0126 F/G 21/3 NL

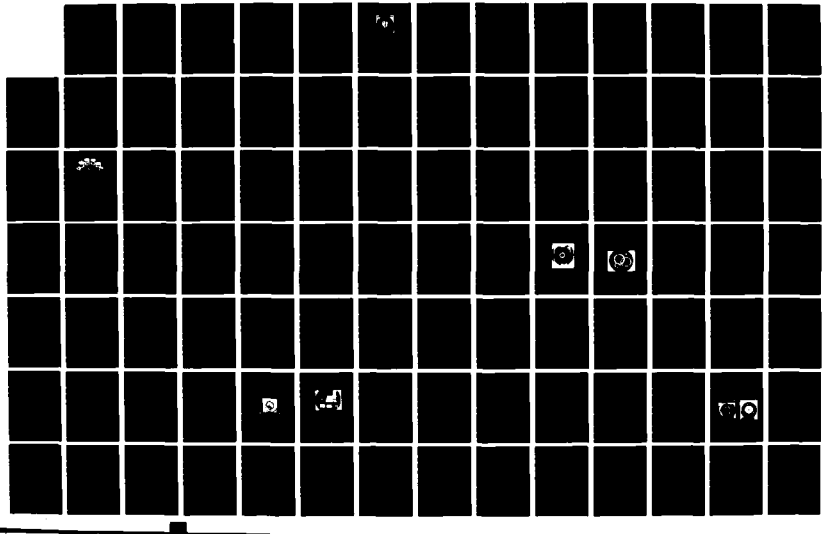

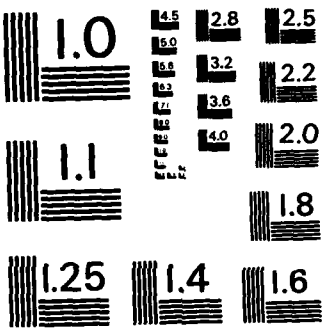

MICROCOPY RESOLUTION TEST CHART
NATIONAL BUREAU OF STANDARDS-1963-A

AFOSR-TR-

METALLIC INDUCTION REACTION ENGINE

F49620-83-C-0126
Final Report

UNCLASSIFIED

SECURITY CLASSIFICATION OF THIS PAGE

REPORT DOCUMENTATION PAGE

AD-A160 137

1a. REPORT SECURITY CLASSIFICATION UNCLASSIFIED	1b. RESTRICTIVE MARKINGS
2a. SECURITY CLASSIFICATION AUTHORITY	3. DISTRIBUTION/AVAILABILITY OF REPORT Approved for public release; Distribution is unlimited.
2b. DECLASSIFICATION/DOWNGRADING SCHEDULE	
4. PERFORMING ORGANIZATION REPORT NUMBER(S) EML-85-AF001	5. MONITORING ORGANIZATION REPORT NUMBER(S) AFOSR-TR- 85-0213
6a. NAME OF PERFORMING ORGANIZATION Electromagnetic Launch Research, Inc.	6b. OFFICE SYMBOL (If applicable)
7a. NAME OF MONITORING ORGANIZATION Air Force Office of Scientific Research	
6c. ADDRESS (City, State and ZIP Code) 625 Putnam Avenue Cambridge, Massachusetts 02139	7b. ADDRESS (City, State and ZIP Code) Bolling AFB DC 20332-6448
8a. NAME OF FUNDING/SPONSORING ORGANIZATION AIR FORCE OFFICE OF SCIENTIFIC RESEARCH	8b. OFFICE SYMBOL (If applicable) NA
9. PROCUREMENT INSTRUMENT IDENTIFICATION NUMBER F49620-83-C-0126	
8c. ADDRESS (City, State and ZIP Code) BOLLING AFB DC 20332-6448	10. SOURCE OF FUNDING NOS

PROGRAM ELEMENT NO.	PROJECT NO.	TASK NO.	WORK UNIT NO.
61102F	2308	A1	

11. TITLE (Include Security Classification)
Metallic Induction Reaction Engine

12. PERSONAL AUTHOR(S)
Mongeau, Peter Parr, and Hart, Douglas Payton

13a. TYPE OF REPORT	13b. TIME COVERED	14. DATE OF REPORT (Yr., Mo., Day)	15. PAGE COUNT
Final	33 JUL 01 to 84 JUN 30	84 DEC 28	140

16. SUPPLEMENTARY NOTATION

17. COSATI CODES		
FIELD	GROUP	SUB. GR.
21	03	

18. SUBJECT TERMS (Continue on reverse if necessary and identify by block number)
Electric Propulsion, Pulse Coil, Pulsed Power, Accelerator

DTIC ELECTE JAN 15 1985 A

19. ABSTRACT (Continue on reverse if necessary and identify by block number)

Advances in electrical propulsion technology have inspired a variety of approaches for orbit raising propulsion. One such technique, the metallic induction reaction engine, uses a solid metallic reaction mass rather than a gas or plasma to achieve high thrust density and efficiency. The reaction mass is inductively accelerated by a magnetic pulse coil, thereby eliminating the problems of erosion and wear.

The basic mechanisms and limits of the conversion of electrical energy into kinetic energy by the metallic induction reaction engine are analyzed. To facilitate this, a single shot experimental engine was constructed and operated over one hundred times, including several tests with conversion efficiencies greater than 50%. Further analyses were performed by developing a numerical model. The velocity and current predicted by this model agree to within 15% of the experimental data over the entire range of operation. Extrapolation to higher performance operation has revealed that there are adverse coupling effects and circuit impedance effects which can limit the ultimate performance of the metallic induction reaction engine. Both the experimental tests and the numerical model indicate that the specific impulse of the engine is more dependent on the density of the reaction mass and the strength of the accelerating magnetic field than it is on material conductivity.

20. DISTRIBUTION/AVAILABILITY OF ABSTRACT	21. ABSTRACT SECURITY CLASSIFICATION
UNCLASSIFIED/UNLIMITED ☒ SAME AS RPT. ☐ DTIC USERS ☐	UNCLASSIFIED

22a. NAME OF RESPONSIBLE INDIVIDUAL	22b. TELEPHONE NUMBER (Include Area Code)	22c. OFFICE SYMBOL
LEONARD F. CAVENY	(202) 767-4937	AFOSR/NA

DD FORM 1473, 83 APR EDITION OF 1 JAN 73 IS OBSOLETE. UNCLASSIFIED

SECURITY CLASSIFICATION OF THIS PAGE

EXECUTIVE SUMMARY

Advances in electric propulsion technology have inspired a variety of orbit raising thrusters. One such thruster, the metallic induction reaction engine, uses magnetic induction to efficiently convert electrical energy into kinetic energy. Conceptually this thruster is very similar to an inductive argon thruster except a highly conductive metal is used as a reaction mass rather than an ionized gas [Daily 81]. Like the argon thruster, a ring is formed from the reaction mass and placed in close proximity to a magnetic pulse coil. Stored electrical energy is then discharged into the pulse coil. Current flowing in the coil magnetically induces an opposing current in the reaction mass ring. The magnetic fields generated by these two currents interact to produce a force which accelerates the reaction mass ring away from the pulse coil thereby producing thrust.

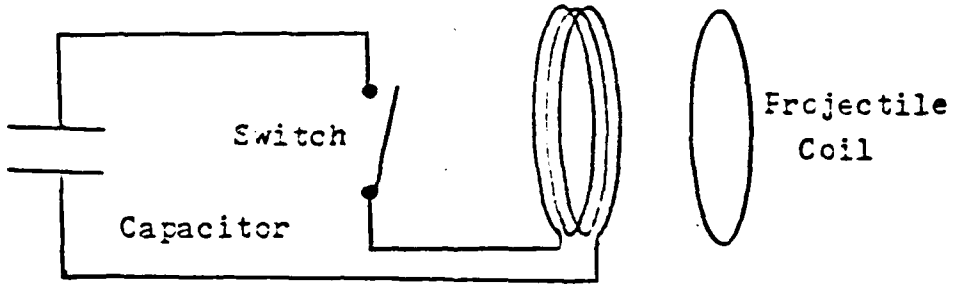

Figure 1: Reaction Engine Schematic

Although the fundamental operating principles of the metallic induction reaction engine have been previously established, little was known about the basic operating mechanisms and limitations of this device [Mongeau 81]. During the past two years, Electromagnetic Launch Research, Inc. has been investigating the pulsed induction acceleration process. It is the goal of this research to establish the basic energy transfer machanisms and the performance limitations of this

device.

The first step in accomplishing these goals was to construct an experimental test apparatus in which the pulsed inductive acceleration process could be easily observed. This apparatus consists of an 18 inch diameter glass vacuum chamber mounted on a movable steel channel frame. At one end of the chamber is an access port which allows various pulse coil designs to be quickly bolted into place for testing and at the other end of the chamber is a lexan viewing port for photographic observations of the reaction mass acceleration. Electrical energy is stored in a 90 microfarad, 20 kilovolt capacitor bank and discharged into the pulse coils through a mechanical dielectric switch. Instrumentation includes measurements of voltage and current of the pulse coil circuit and velocity of the reaction mass rings. Over one hundered tests using aluminum and copper reaction mass materials have been performed with this apparatus including several tests with conversion efficiencies greater than 50 percent and velocities in excess of 700 meters per second.

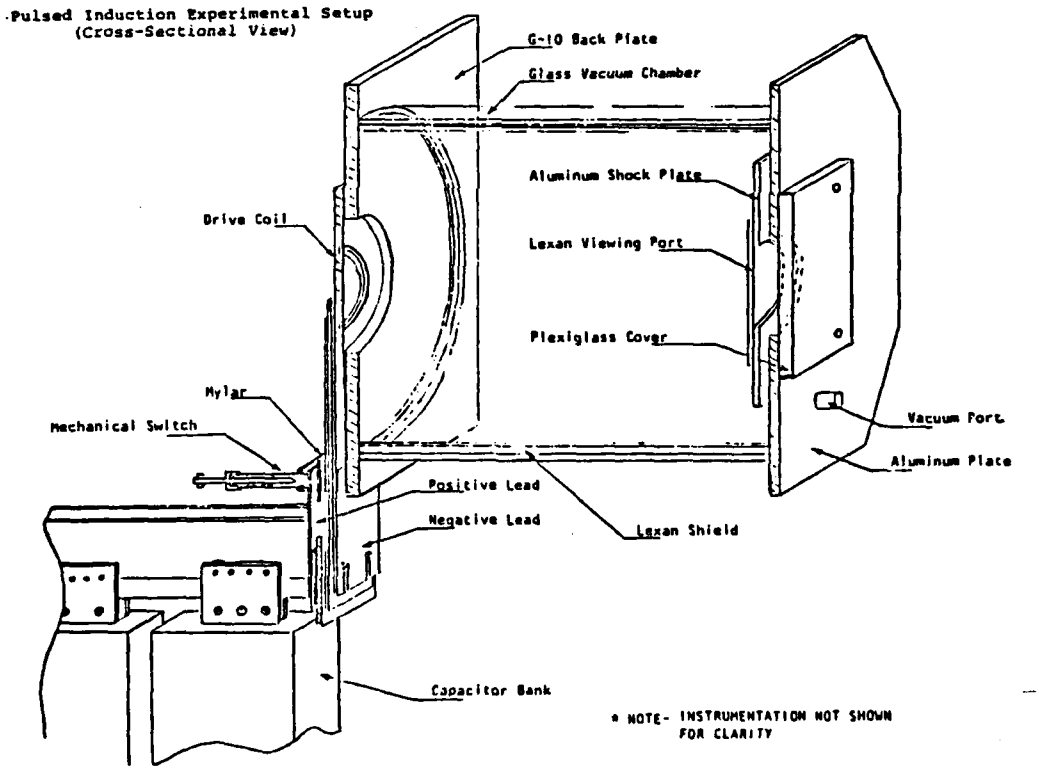

Figure 2: Experimental Setup

A-1

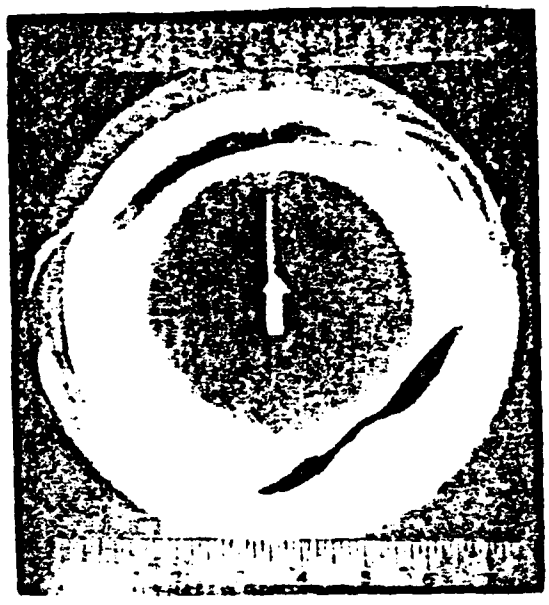

Figure 3: Aluminum Reaction Mass Ring in Flight (750 m/s)

Although the experimental apparatus proved to be a useful tool in analysing the pulsed inductive acceleration process, it provided only a limited amount of information. Information such as reaction mass temperature, current, inductive and resistive voltage drops, etc. could not be obtained by direct measurement. Because of this, a detailed numerical model was developed. This model combines material properties with magnetic coupling parameters to simulate a metallic induction reaction engine system. The numerically obtained values of current, voltage, and reaction mass velocity from this model proved to be accurate to within 15 percent of the experimentally obtained values over the entire range of operation.

Table 1: Experimental and Numerical Performance Comparison

Pulse Coil #1 (3 Turns, 2.85 uH, 1.1 mΩ)

Aluminum Reaction Mass (8.68 grams, 0.33 uH)

Initial Cap. Voltage	Reaction Ring Velocity (Calc.)	Reaction Ring Velocity (Meas.)	System Efficiency
9 kV	495 m/s	498 m/s	29.5 %
10	565	532	27.3
11	635	617	30.3
13	776	725	30.0
14	847	754	28.0

Pulse Coil #2 (2 turns, 1.4 uH, 0.1 mΩ)

Aluminum Reaction Mass (12.6 grams, 0.28 uH)

10 kV	331 m/s	365 m/s	18.7 %
13	463	440	16.0

Pulse Coil #3 (4 turns, 2.12 uH, 0.7 mΩ)

Aluminum Reaction Mass (0.7 grams, 0.2 uH)

7 kV	451 m/s	576 m/s	3.4 %
8	493	485	1.8
9	560	640	2.5

Copper Reaction Mass (2.15 grams, 0.2 uH)

6 kV	258 m/s	207 m/s	2.8

Both the experimental and numerical simulations of the metallic induction reaction engine indicate that optimum performance is obtained with low density highly conductive reaction mass materials. Furthur analysis performed with the numerical model indicates that there exists a back EMF saturation effect which inhibits the energy discharge into the reaction mass/pulse coil system. This saturation effect can be greatly reduced by using pulse coils shaped to reduce the initial accelerating force on the reaction mass ring during the start of the acceleration process. One coil shape that is being considered for this application is known as a compound coil.

A compound coil is actually two coils, one placed inside the other. They are positioned in such a way that a reaction mass ring can be placed between them. Because the reaction mass ring rests near the center of the coil where the mutual inductance gradient between the reaction mass ring and the pulse coil is at its lowest, the force on the ring and thus the acceleration of the ring is virtually independent of the energy input into the system. A compound coil of this type was constructed. However, because of instrumentation difficulties, a detailed analysis of it's performance has not been established.

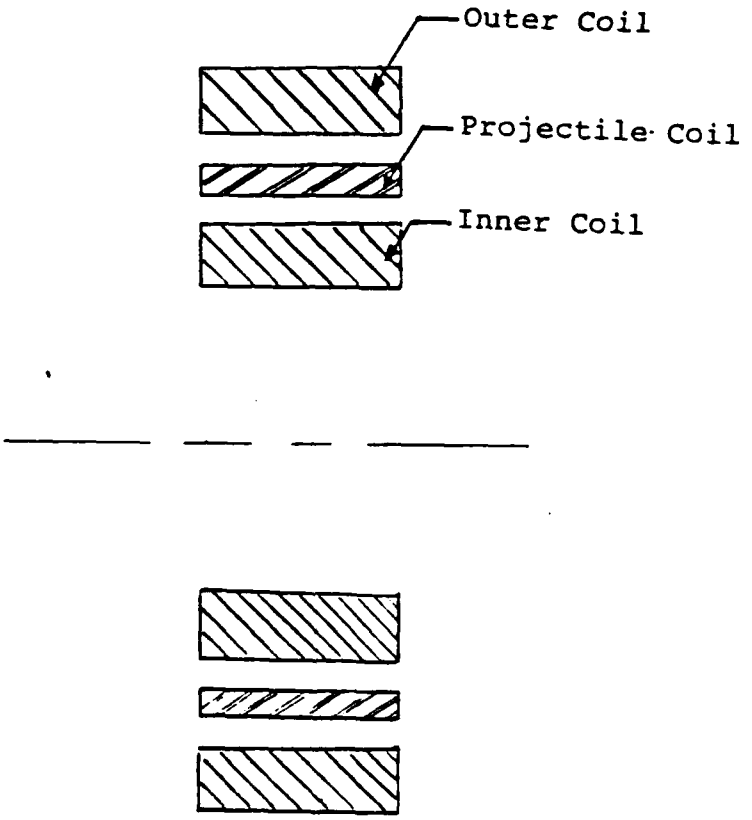

Figure 4: Compound Coil

Aside from back EMF effects, there also exist inherent material resistive properties which can limit the performance of a metallic induction reaction engine system. When the reaction mass is accelerated, its temperature increases due to ohmic heating from an induced current. The temperature of the reaction mass ring can become so great that it will vaporize. However, as

the reaction mass's temperature increases so does it's resistivity. This increase in resistivity can prevent the inductive transfer of energy from the pulse coil circuit to the reaction mass ring. However, it is assumed that if a sufficient voltage can be induced in the reaction mass ring, it will ionize and continue to conduct electricity well past its vaporization point. Presently an experimental apparatus is being constructed to demonstrate this ionization process and to observe the effect it has on the ultimate performance of a metallic induction reaction engine system. This test apparatus consists of a thin glass vacuum chamber mounted to a pulse coil. Various reaction mass materials can be placed in this chamber and inductively excited by discharging a capacitor bank through the pulse coil. Because the chamber is thin, it prevents the reaction mass ring from moving away from the pulse coil. This allows the ionization process to be observed independent of back EMF effects and changes in coupling conditions. Instrumentation of this apparatus will consist of measurements of the pulse coil current and voltage, the reaction mass ring current and photographic observations of the reaction mass ionization.

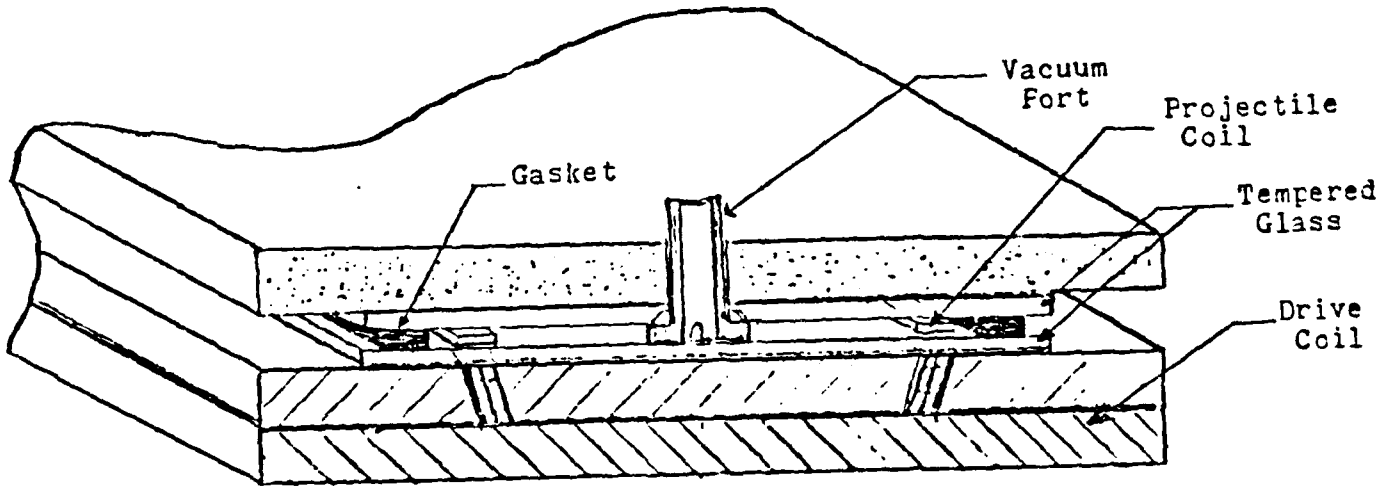

Figure 5: Ionization Apparatus

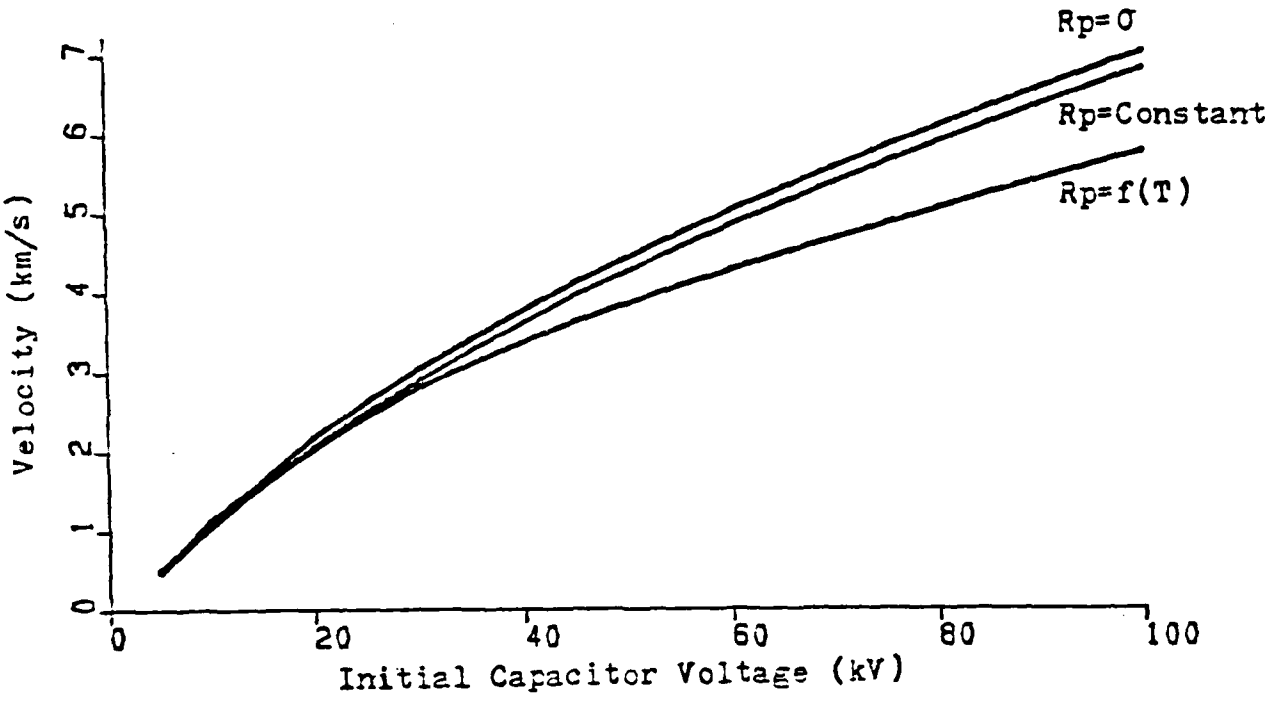

Figure 6: Resistance Effect on Aluminum Reaction Mass

One of the major difficulties encountered during experimental tests has been the failure of pulse coils. To date, the pulse coil designs used in the experimental tests have not been able to stand up to the full 20 kilovolts of the capacitor bank. Three different pulse coil designs have been tested. These designs were based on experimental and theoretical research performed for previous pulsed inductive acceleration projects [McKinney 84], [Clifton 84]. All of the coils built have used solid dielectric materials to insulate the current turns and to provide structural support. Failure of the dielectric material generally results in permanent failure of the coil and a new coil must be constructed to replace the failed one. Coil construction can be a long and tedious process that slows experimental work and adds to the overall cost of the research. In an attempt to alleviate this difficulty, a pulse coil has been designed that uses an oil dielectric rather than a solid dielectric. It is believed that the self healing properties of the oil dielectric will prevent permanent damage to the coil in the advent of an electrical break down. Should permanent damage occur, the modular construction of this coil will allow it to be quickly disassembled and the failed component replaced. Construction and testing of this coil will be completed by late February.

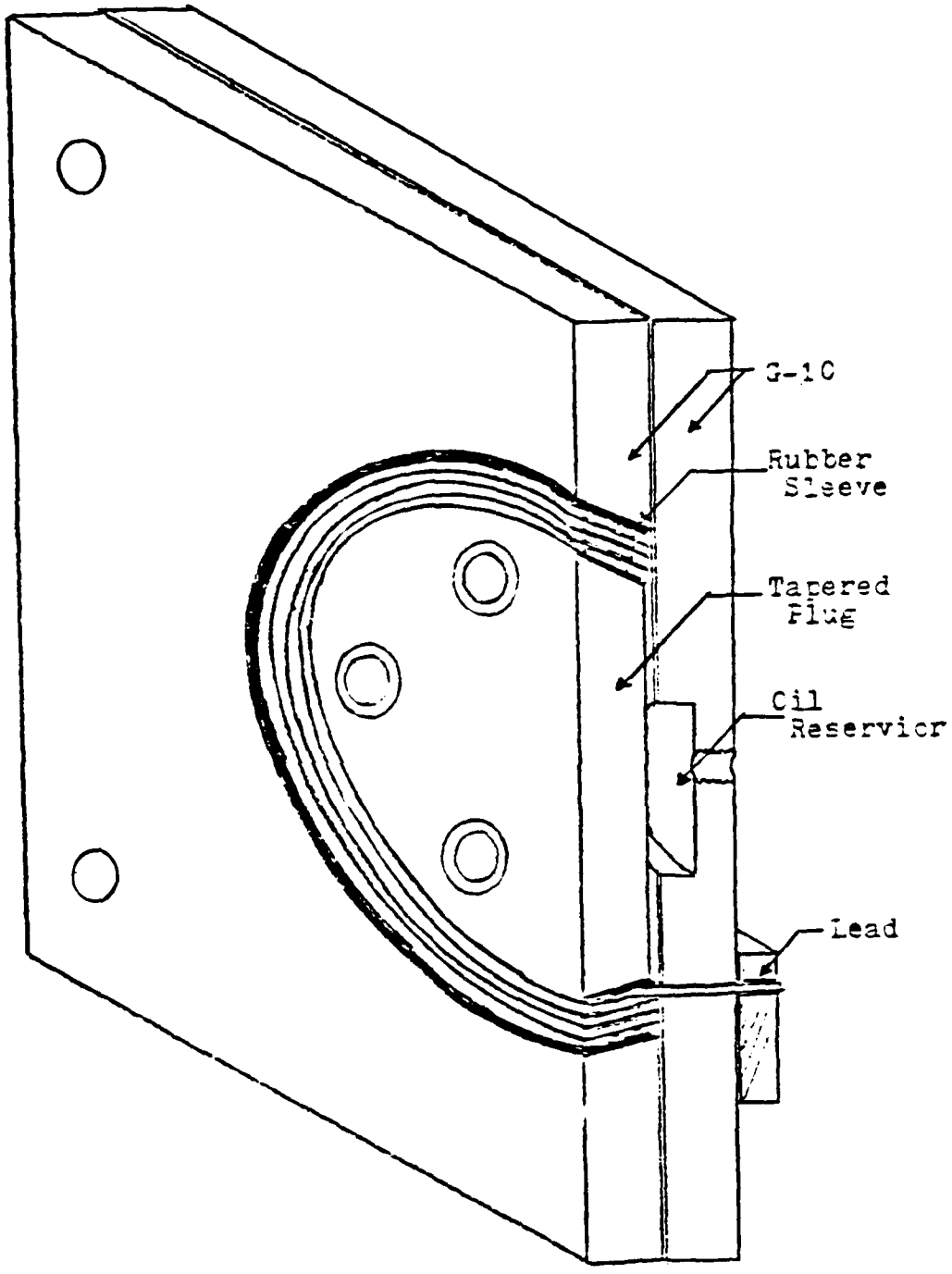

Figure 7: Rebuildable Pulse Coil

This report represents two years of an ongoing three year research program to study the basic mechanisms and limitations of the metallic induction reaction engine. The research was performed at Electromagnetic Launch Research, Inc. Cambridge Massachusetts by Peter P. Mongeau and Douglas P. Hart. It was supported by the Air Force Office of Scientific Research contract number F49620-83-C-0126. The results of this research were published in thesis form as partial fulfillment of the requirements for the degree of Masters of Science at the Massachusetts Institute of Technology (see Appendix). Summaries are being prepared for publication in the proceedings of the Electric Propulsion Conference in Alexandria, Virginia and the Pulsed Power Conference in Arlington, Virginia.

METALLIC INDUCTION REACTION ENGINE

by

Douglas Payton Hart

Bachelor of Science
University of Illinois
Aero/Astronautical Engineering
Champaign-Urbana, 1983

SUBMITTED TO THE DEPARTMENT OF MECHANICAL ENGINEERING IN PARTIAL FULFILLMENT OF THE REQUIREMENTS FOR THE DEGREE OF

MASTER OF SCIENCE

at the

MASSACHUSETTS INSTITUTE OF TECHNOLOGY

December 1984

Signature of Author .....
Department of Mechanical Engineering
December 31, 1984

Certified by .....
Dr. Peter P. Mongeau
Thesis Supervisor

Certified by .....
Dr. Ain A. Sonin
Department Reader

Accepted by .....
Dr. Ain A. Sonin, Chairman
Departmental Graduate Committee

METALLIC INDUCTION REACTION ENGINE

by

Douglas Payton Hart

Submitted to the Department of Mechanical Engineering on December 31, 1984 in partial fulfillment of the requirements for the degree of Master of Science.

ABSTRACT

Advances in electrical propulsion technology have inspired a variety of approaches for orbit raising propulsion. One such technique, the metallic induction reaction engine, uses a solid metallic reaction mass rather then a gas or plasma to achieve high thrust density and efficiency. The reaction mass is inductively accelerated by a magnetic pulse coil, thereby eliminating the problems of erosion and wear.

The basic mechanisms and limits of the conversion of electrical energy into kinetic energy by the metallic induction reaction engine are analyzed. To facilitate this, a single shot experimental engine was constructed and operated over one hundred times, including several tests with conversion efficiencies greater then 50%. Further analyses were performed by developing a numerical model. The velocity and current predicted by this model agree to within 15% of the experimental data over the entire range of operation. Extrapolation to higher performance operation has revealed that there are adverse coupling effects and circuit impedance effects which can limit the ultimate performance of the metallic induction reaction engine. Both the experimental tests and the numerical model indicate that the specific impulse of the engine is more dependent on the density of the reaction mass and the strength of the accelerating magnetic field than it is on material conductivity.

Thesis Supervisor: Dr. Peter Mongeau
Title: Research Scientist, Electromagnetic Launch Research, Inc., M.I.T.

TABLE OF CONTENTS

LIST OF FIGURES

LIST OF TABLES

ACKNOWLEDGMENTS

The work reported in this thesis was performed at M.I.T., and at Electromagnetic Launch Research, Inc. in Cambridge, Massachusetts. It was supported by the Air Force Office of Scientific Research contract number F49620-83-C-0126.

To the cast of characters at Electromagnetic Launch Research, Inc.,

Francis (Sam) Goodall,	Artist
Lisa Gredin,	Co-agonizer
Whitney Hamnett,	Philosopher
Robert (Kim) Kimberk,	Intellectual
Juliet Kolm,	Prankster
William (Bill) Snow	Workaholic
John Yadisernia,	Entrepreneur

Thank you.

Your friendship and understanding will not be forgotten.

A special word of thanks goes to Henry Kolm, and Peter Mongeau who gave me an opportunity of a lifetime and the guidance to bring it to fruition.

Anne Laughlin, fiancee and friend, if it were not for your support, I would never have come this far.

CHAPTER 1

INTRODUCTION

A metallic induction reaction engine is a type of space propulsion device which uses magnetic induction to convert electrical energy into kinetic energy. Conceptually it is a very simple device. A metal reaction mass such as aluminum or any other good metallic conductor is formed into a ring. Stored electrical energy is then discharged into a magnetic coil. Current in the coil magnetically induces an opposing current in the reaction mass ring. In this way, a magnetic force is generated between the two coils which pushes them apart. This process is repeated ten to a hundred times a second and thus, a fairly constant thrust is produced.

The metallic induction reaction engine was pioneered by Peter Mongeau in 1980 as an alternative to the high specific impulse thrusters normally associated with electrical propulsion. It's high efficiency and moderate specific impulse operation make it an ideal candidate for rapid transfer of large payloads from low earth orbit to geosynchronous orbit.

In this chapter, the major components of the metallic induction reaction engine and the method in which they operate to produce thrust are discussed. Also included is a

discussion of some of the advantages and disadvantages of this device.

1.1 Basic Configuration

The metallic induction reaction engine consists of only four major components, the drive coil, the bucket coil, the power source, and the current switch. Although there are many other parts which tie into these components, their functions are of little importance to the fundamental understanding of the engine itself. Figure 1.1 shows a basic schematic of the metallic induction reaction engine and the general layout of its major components.

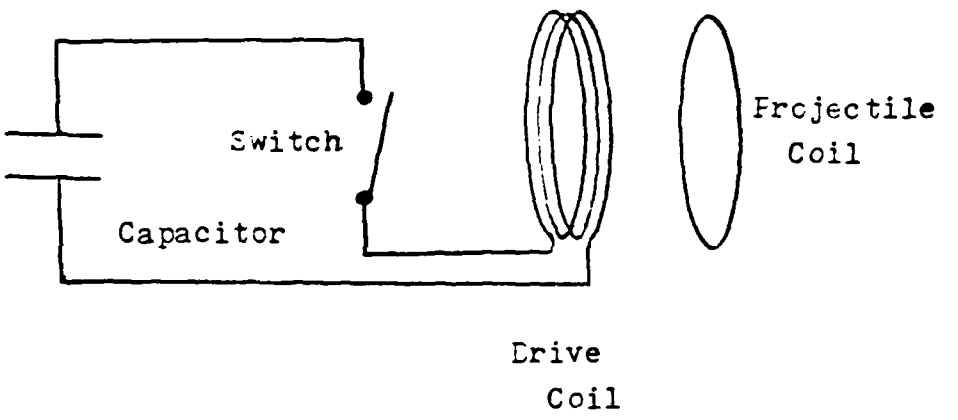

Figure 1.1: System Diagram

1.1.1 Drive Coil

The drive coil is the heart of the metallic induction reaction engine system. Its primary function is to produce a magnetic field from stored electrical energy. In order for this magnetic field to have a useful form, the drive coil must be shaped so that it forms a close magnetic coupling with the reaction mass. There are many different types of magnetic coils which can be used as drive coils. One coil that is well suited to the reaction engine system is called a face coil. A face coil is simply a magnetic coil which is wound parallel to a plane normal to the coil's axis of symmetry.

1.1.2 Projectile Coil

The projectile coil is a coil formed out of the reaction mass and placed in close proximity to the drive coil. This coil can be made out of almost any conductive substance but the best materials appear to be those that have very low densities and high conductivity such as aluminum, magnesium, and lithium. An example of a projectile coil and face coil can be seen in figure 1.2. Details on projectile coil materials and magnetic coupling will be discussed later.

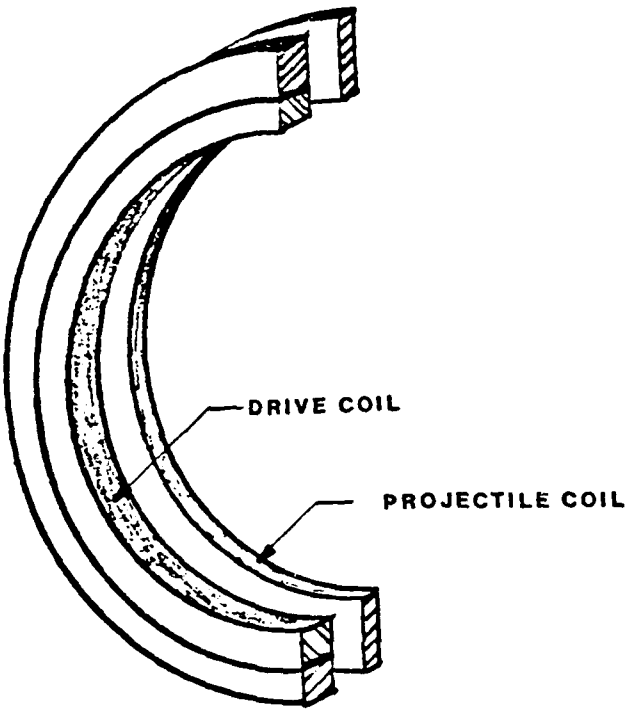

Figure 1.2: Typical Face Coil and Projectile Coil

1.1.3 Power Source

During operation, the metallic induction reaction engine requires a great deal of power; on the order of megawatts. Power supplies capable of meeting this requirment tend to be large, heavy, and costly. However, the metallic induction reaction engine operates in a pulse mode in which power is only drawn for very short periods of time, 1 to 2 milliseconds. Therefore, energy can be stored in capacitors and delivered in quick, high powered spurts during operation.

1.1.4 Current Switch

While the capacitors are being charged to their operating voltage, they are disconected from the drive coil by a switch. There are several types of commercially available switches that meet the power requirments of the metallic induction reaction engine. Included amoung these are gas gap, vacuum and ignitron switches. The gas gap and vacuum switches are relatively inexpensive and are sufficient for most applications.

Gas gap and vacuum switches operate in much the same way. A low pressure gas or a vacuum is used to hold off the voltage between two opposing electrodes. When a high voltage, 50 to 60 kilovolts, is applied to a third triggering electrode, an ionized plasma forms. This plasma causes the dielectric gap between the other two electrodes to break down and conduct electricity. Figure 1.3 shows several different types of gas gap and vacuum switches.

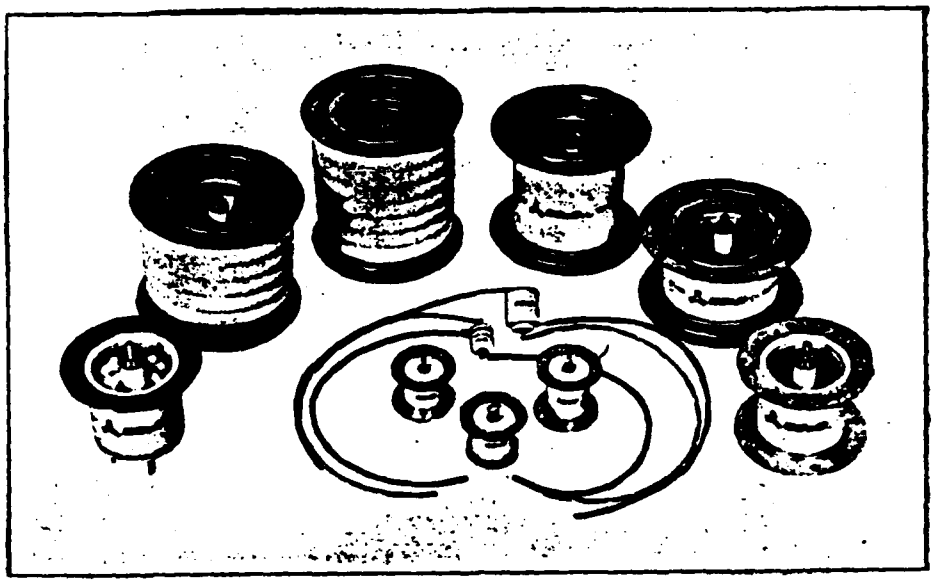

Figure 1.3: Gas Gap Switches

1.2 Operating Cycle

The metallic induction reaction engine operates in a repeating cyclic mode. This cyclic operation is composed of four basic steps. First, the capacitors are charged to the operating voltage by a DC power supply. Then, a projectile coil is formed in front of the drive coil out of the reaction mass. The current switch is closed and the capacitors discharge into the drive coil. Because the projectile coil is closely coupled with the drive coil, a current is induced in it in response to the current in the drive coil. The interaction of the magnetic fields produced by these currents causes a strong force which accelerates the two coils apart. This cycle is repeated 10 to 100 times a second thus generating a fairly

constant thrust. The following sections discuss the details of the metallic induction reaction engine's operation in more detail.

1.2.1 Charging

The capacitors of the metallic induction reaction engine are charged using a DC power supply. This power supply can be in the form of solar cells, a nuclear reactor, or any other power source which can be adapted to generate high voltage energy. The amount of energy stored in the capacitors per cycle of operation is equal to;

$$Ue \approx CV^2/2 \qquad (1.2.1)$$

where Ue is the amount of energy stored , C is the capacitance, and V is the voltage the capacitors are charged to.

1.2.2 Ring Formation

The projectile rings which couple to the drive coil are formed out of the reaction mass. These rings can be formed by spraying, extruding, or stamping the rings from any conductive material. The details of this are beyond the scope of this thesis and are not presented here. However, projectile ring formation is not forseen as a major design constraint.

1.2.3 Discharge

After the capacitors are charged and the projectile coil is in place, the switch is closed and current is allowed to flow through the drive coil. This discharge of energy follows an RCL type discharge due to the inductance of the drive coil, the projectile coil, and the leads. The total energy delivered to the drive circuit is simply;

$$Ue = \int_0^{\tau_o} VI \, dt \qquad (1.2.2)$$

where I is the drive coil current and V is the capacitor voltage.

1.2.4 Induced Current

Because the drive coil and the projectile coil are magnetically coupled, they behave in much the same way a transformer does. That is, as current flows through the drive coil, a magnetic field forms. At the same time, a current is induced in the projectile coil causing an opposing magnetic field. This phenomenon arises from the conservation of magnetic flux.

1.2.5 Acceleration

The magnetic field formed by the drive coil and projectile coil interact to produce a force that pushes them apart. This

force can be large enough to accelerate the projectile coil to tens of kilometers per second within a few centimeters.

1.3 Advantages

There are several distinct advantages to the metallic induction reaction engine in comparison to other forms of electrical propulsion. These advantages include simplicity, reliability, readily available reaction mass, moderate specific impulse, and high efficiency. Because of these advantages the metallic induction reaction engine is a viable option to conventional forms of propulsion.

1.3.1 Simplicity

The metallic induction reaction engine is a fairly simple device. There are no moving parts which can wear against each other and there is only one power source required for operation.

1.3.2 Minimal Surface Contact

Many electrical propulsion devices rely on the reaction material coming in contact with some form of electrode. Because of this, they often have trouble with electrode erosion and deterioration. The metallic induction reaction engine, however, induces a current in the reaction mass by

magnetically coupling to it rather than making direct mechanical contacts. This lack of physical contact greatly increases the reliability of the device.

1.3.3 Readily Available Reaction Mass

Because the metallic induction reaction engine uses conductive reaction materials such as aluminum and magnesium, its reaction mass can be obtained from a wide variety of sources. This means that the payload being delivered to orbit may not have to carry its reaction mass along as dead weight. For instance, the outer fuel tank of the space shuttle could be cut up and fed into the engine. Another advantage to using a metallic reaction mass such as aluminum or magnesium is that they are nontoxic and easy to store in condensed form.

1.3.4 Moderate Specific Impulse

Electrical propulsion systems traditionally have very high specific impulses. Although this is generally considered an advantage over conventional chemical propulsion, this is not always the case. Daily and Loveberg showed that because of the high cost of putting an object into space, there is an optimum finite specific impulse at which an orbital thruster should operate. This optimum specific impulse is dependent on the market economy and how long investors are willing to have

their investments tied up. In general, this optimum specific impulse is in the range in which the metallic induction reaction engine efficiently operates, fifteen hundered to two thousand seconds. A graph of specific impulse versus time to orbit can be seen in figure 1.4.

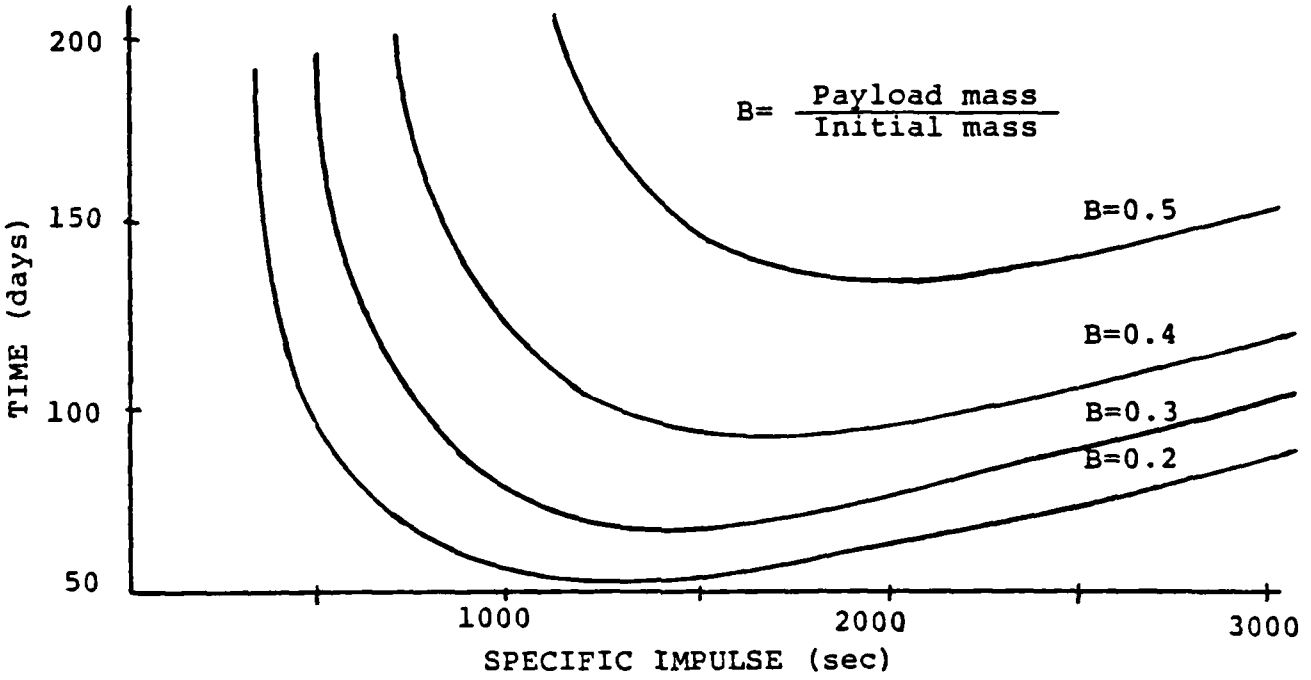

Figure 1.4: Time to Orbit vs. Specific Impulse

1.4 Disadvantages

Although the metallic induction reaction engine has many advantages, it is not without its problems. Most of the

disadvantages associated with this engine are also disadvantages faced by many other electrical thrusters. These disadvantages include high power, high voltage, and rapid switching requirments.

1.4.1 High Power

Many electric propulsion systems such as MPDs and arc jets draw a great deal of power during operation. The metallic induction reaction engine also falls in this category. In order to obtain this power it is necessary to use an energy storage device such as a capacitor. Capacitors are in general very large and heavy for the amount of energy they are capable of storing. Fortunately, like the MPD thrusters, the metallic induction reaction engine only has to store enough energy at one time for a single pulse. However, these capacitors still represent a major part of the overall weight and size of the engine.

Another problem with the use of capacitors is that they have a limited cyclic lifetime of charging and discharging. Typical capacitor lifetimes fall short of the requirments for many space missions. It is obvious that a better source of power is needed but until one is discovered or capacitors are improved upon, the metallic induction reaction engine, like many other electrical propulsion systems, is at the mercy of present technology.

1.4.2 High Voltage

Operation of the metallic induction reaction engine depends upon the magnetic coupling of the projectile coil to the drive coil. This magnetic coupling only occurs within a short distance from the coil. Because of this, high voltages must be used to transfer energy to the drive coil and projectile coil before they can move an appreciable distance from each other.

1.4.3 Rapid Switching

During operation, the metallic induction reaction engine accelerates 10 to 100 projectile coils a second. Each one of these coils reaches their final exit velocity within about one millisecond from the time energy first begins to discharge into the drive circuit. Unless a switch is used which can commutate within this time, any energy left in the drive circuit after the projectile coil is fully accelerated is converted into heat. At the present time, a switch does not exist that can commutate at this rate while handling high currents and voltages. However, interest in pulsed power has sparked a large development effort and, with a little luck, a switch of this type may exist in the near future.

CHAPTER 2

THEORY OF OPERATION

All devices based on the principle of electromagnetic acceleration rely on the same fundamental equations of motion. The metallic induction reaction engine is no exception. In this chapter, the equations governing pulsed induction acceleration are derived and the principles behind the conversion of electrical energy to kinetic energy are considered. Careful attention is paid to the efficiency at which this energy conversion takes place.

2.1 Derivation of Constitutive Equations

The equations governing pulsed induction acceleration are fairly easy to derive. They emerge from well understood principles of kinematics, electrodynamics and thermodynamics. Although all of the these equations are closely coupled with one another, they can be thought of as representing separate and distinct effects. This results in a set of simultaneous differential equations representing all of the major physical processes taking place in pulsed induction acceleration.

2.1.1 Kinematics

The only kinematic processes taking place in the metallic induction reaction engine are the ones ocurring at the projectile/drive coil interface. The force pushing the projectile coil away from the drive coil can be expressed as

$$F = IpId(dMpd/dz) \qquad (2.1.1)$$

where Ip is the projectile coil current, Id is the drive coil current and dM/dz is the mutual inductance gradient between the projectile coil and the drive coil. Then, from Newton's law the instantaneous acceleration of the projectile coil can be written as simply

$$dv/dt = IpId(dM/dz)/m \qquad (2.1.2)$$

where v is the velocity of the projectile coil and m is the mass of the projectile coil.

2.1.2 Electrodynamics

The equations representing the electrodynamic effects of pulsed induction acceleration are easily derived by noting the similarity between a projectile/drive coil system and a transformer. The major electrical parameters of the metallic induction reaction engine can be lumped together and analyzed as a simple electrical circuit (see figure 2.1).

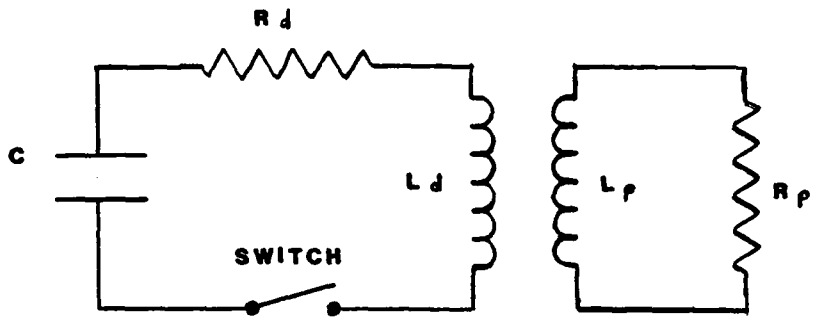

Figure 2.1: Lumped Parametric Model

By summing the voltages around the circuit loops, we obtain the equations

$$Vd = IdRd + Ld(dId/dt) + Mpd(dIp/dt) + Ip(dMpd/dz)v \quad (2.1.3)$$

and

$$0 = IpRp + Lp(dIp/dt) + Mpd(dId/dt) + Id(dMpd/dz)v \quad (2.1.4)$$

where

Vd is the voltage across the drive coil

IdRd and IpRp are the resistive voltages

Ld(dId/dt) + Mpd(dIp/dt) and
Lp(dIp/dt) + Mpd(dId/dt) are the induced voltages

and

Ip(dMpd/dz)v and Id(dMpd/dz)v are the back EMF voltages

Note that the only parameters that are not found in typical transformer circuts are the back EMF voltages. At high projectile velocities, these parameters can become the dominant terms in the two circuit equations. Details of this effect will be discussed in chapter 6.

Combining equations 2.1.3 and 2.1.4 with the constitutive relationship

$$dV/dt = Id/C \qquad (2.1.5)$$

where C is capacitance, we obtain a complete set of equations representing the discharge of electrical energy in the drive coil circuit.

2.1.3 Thermodynamics

Although the kinematic and electrodynamic equations represent the major physical processes taking place, there exsists a third set of equations that can not be neglected. These equations represent the effects of ohmic heating. Ohmic heating, the heating process associated with current flowing in a less than perfect conductor, can lead to melting and even vaporization of the projectile coil. The equation governing this process can be written as

$$mCp(dT/dt) = Ip^2 Rp \qquad (2.1.6)$$

where T is the projectile coil temperature and Cp is the specific heat of the projectile material. The projectile coil resistance, Rp, can be expressed as

$$Rp = \rho\pi(ro+ri)/(ro-ri)w \qquad (2.1.7)$$

where

ro is the outside radius of the projectile coil

ri is the inside radius of the projectile coil

w is the width of the projectile coil

and

ρ is the resistivity of the projectile coil

It should be noted that the resistivity, ρ , and the specific heat, Cp, are functions of temperature. Their exact relationship with temperature depends on the material being used.

Ohmic heating is not a process limited to projectile coils alone. It also affects drive coils and leads. However, projectile coils tend to be very thin, on the order of half a millimeter, and therefore exhibit this effect to a much greater extent. When analysing a single cycle of a typical metallic induction reaction engine, ohmic heating ocurring in the drive coil and leads can generally be neglected.

2.2 System Model

One of the most important parameters of any propulsion system

is the efficiency parameter. In pulsed induction acceleration systems, this parameter can be a bit confusing. There are actually two efficiency parameters to contend with, the transfer efficiency and the system efficiency.

2.2.1 Transfer Efficiency

The transfer efficiency is the ratio of the kinetic energy output to the total energy not recovered during a discharge cycle. This relationship can be expressed as

$$\eta_{con} = 1/2\ mv^2 / (1/2\ mv^2 + (mCp_{\Delta}T)p + (mCd_{\Delta}T)d) \qquad (2.2.1)$$

where

$(mCp_{\Delta}T)p$ is the change in thermal energy of the projectile coil

and

$(mCd_{\Delta}T)d$ is the change in thermal energy of the drive coil

The transfer efficiency represents the best performance that can be obtained by a realistic system. That is, it is the efficiency that can be obtained if the unused magnetic energy in the drive coil circuit is recovered for the next cycle.

2.2.2 System Efficiency

The system efficiency is the ratio of the kinetic energy output to the total energy stored during a single cycle of operation. It can be expressed as

$$\eta sys = 1/2\ mv^2/1/2\ CV^2 \qquad (2.2.2)$$

The system efficiency represents the amount of energy that must be stored for a given kinetic output. Notice that this efficiency is equal to the transfer efficiency if the unused discharge energy in the drive circuit is not recovered.

2.3 Ideal Energy Conversion

In an attempt to separate the theoretical limits of pulsed induction acceleration performance from hardware constraints, an ideal model of inductive energy transfer was developed. This model neglects the material resistivity and drive circuit limitations. Thus, it represents the maximum performance that can be obtained by a pulsed inductive acceleration system.

Consider a projectile/drive coil system where electrical energy is forced into the system before the projectile coil has time to move away from the drive coil (see figure 2.2).

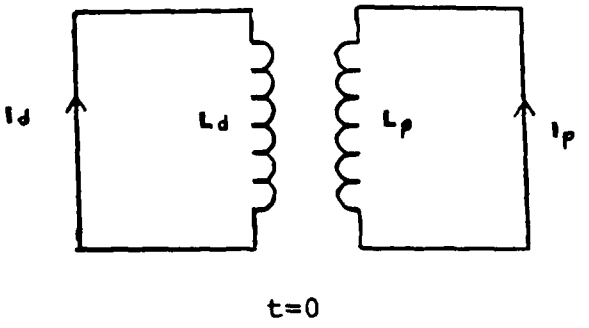

Figure 2.2: Ideal System Model

The total energy initially stored in this system is

$$Ui = 1/2\ LpIp^{i2} + MpdIp^{i}Id^{i} + 1/2\ LdId^{i2} \qquad (2.3.1)$$

By energy conservation, the final kinetic energy of the projectile coil is simply

$$Uke = Uf - Ui \qquad (2.3.2)$$

where Uf is given by the expression

$$Uf = 1/2\ LpIp^{f} + MpdIp^{f}Id^{f} + 1/2\ LdId^{f} \qquad (2.3.3)$$

The final currents, denoted by the superscript f, can be related to the initial currents through flux conservation

$$Id^{f} = LdId^{i}(1-(Mpd^{2}/LdLp)) \qquad (2.3.2)$$

$$Ip^{f} = -MpdId^{i}/Lp \qquad (2.3.3)$$

and

$$Ip^{f} = 0 \qquad (2.3.4)$$

By substituting these equations into the ratio of the kinetic energy output to the electrical energy input, an expression for the ideal efficiency of an inductive acceleration system is obtained

$$\eta_{ideal} = Mpd^{2}/LpLd \qquad (2.2.7)$$

Similarly, the specific impulse of this ideal system can be derived as

$$Isp = v/g = \sqrt{2UiMpd^{2}/mg^{2}LpLd} \qquad (2.2.8)$$

where m_c is the mass of the projectile coil and g is the gravitational constant.

This process of energy conversion is commonly known as magnetic adiabatic expansion. It is a useful model because it allows the fundamental performance limitations of the metallic induction reaction engine to be compared with other propulsion systems without having to resort to a point for point design comparison.

CHAPTER 3

EXPERIMENT

It is often difficult, if not impossible, to account for every physical phenomenon when theoretically analysing a system. Because of this, an experimental apparatus was constructed to assess the accuracy of our theory and to observe phenomena which our theoretical model did not include.

This chapter discusses the experimental prototype metallic induction reaction engine and the problems as well as the solutions encountered during its development.

3.1 Setup

The experimental device used was designed so that it could be easily operated and yet remain flexible for changes in instrumentation and coil design as new areas of interest became apparent. The experimental setup had to be low cost, simulate a space type of enviroment, and above all it had to be safe to operate at very high voltages and currents. A schematic of the experimental apparatus showing the major components can be seen in figure 3.1.

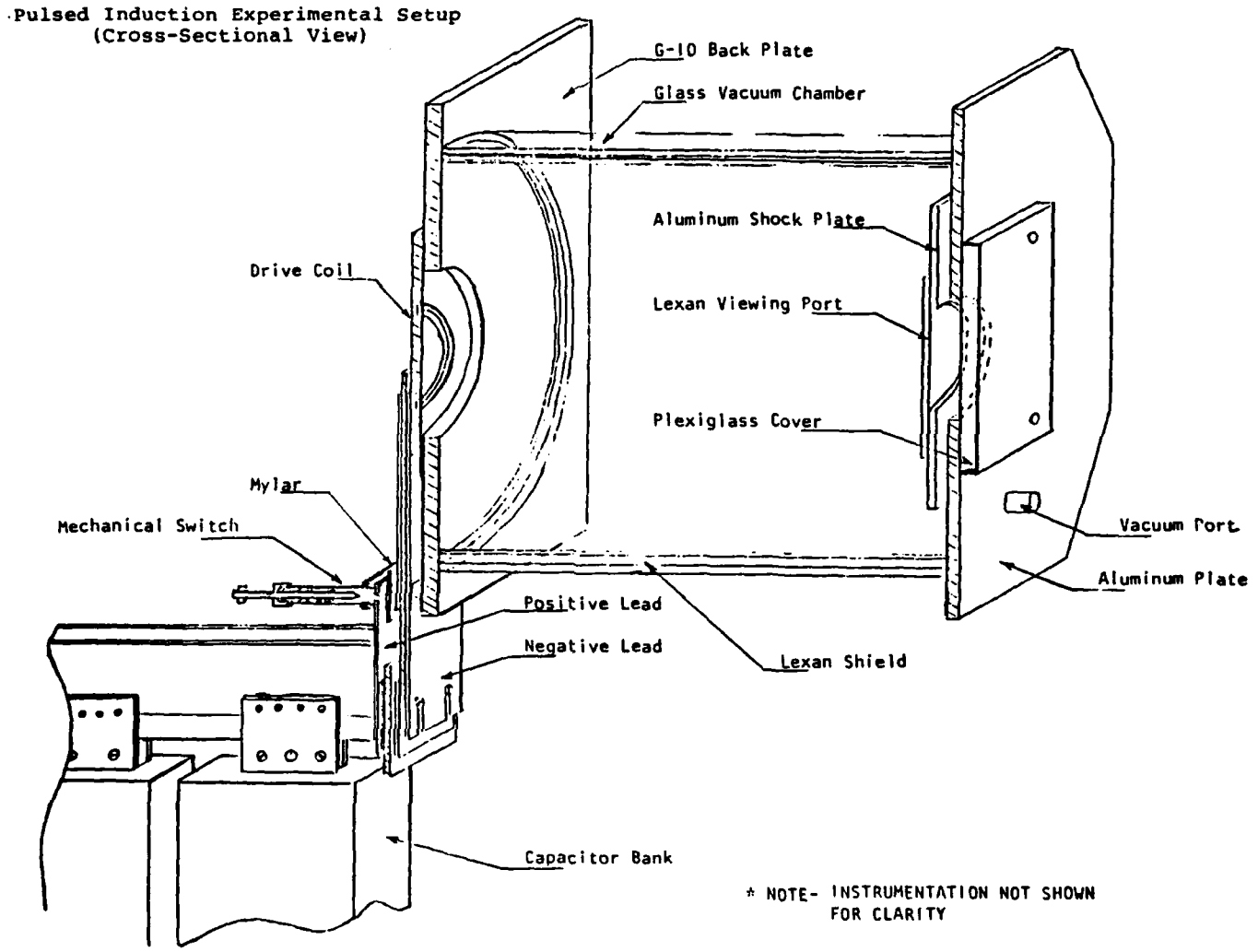

Figure 3.1: Experimental Setup

3.1.1 Drive Coil

Several different drive coils were built and tested in the metallic induction reaction engine prototype. All of the drive coils built were face coils but the scale size, number of turns, and design of each coil was changed so that the effect of various coil parameters could be observed.

The first coil designed and tested, shown in figure 3.2, was a three turn wire wrap coil. A circular groove was cut in a plate of G-10. Then, rectangular fiber glass insulated wire was wound into this grove with a thin strip of G-10 separating each turn of the coil. The coil was then potted in epoxy and placed in a vacuum chamber to remove trapped air. Finally, the surface of the coil was milled flat and a sheet of mylar glued down. The mylar acted as a smooth dielectric surface which the projectile coil could be placed on. This coil survived over fifty pulses but it was unable to stand up to high voltages and currents. It failed at sixteen thousand volts and one hundred thousand amperes when two turns of the coil near the leads shorted.

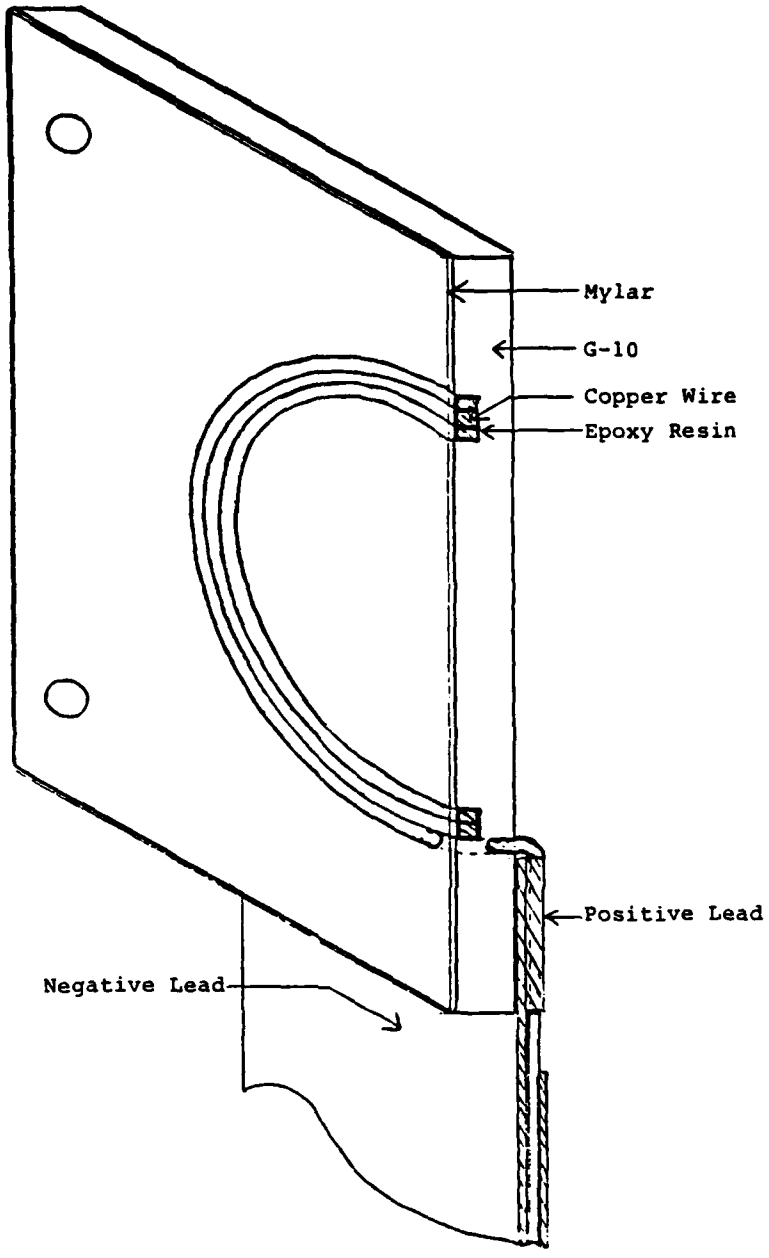

Figure 3.2: Three Turn Wire Wrapped Coil

The second coil built, shown in figure 3.3, was a two turn coil cut from a half inch sheet of copper. The turns of this coil were insulated from each other by wrapping the coil in

fiberglass and potting it in epoxy in much the same way the first coil was potted. Unfortunately during potting, dry spots formed on the surface of the coil. These dry spots eventually led to the coil's failure at twelve thousand volts and seventy five thousand amperes. An arc formed along the surface of the coil shorting it out and burning the insulation.

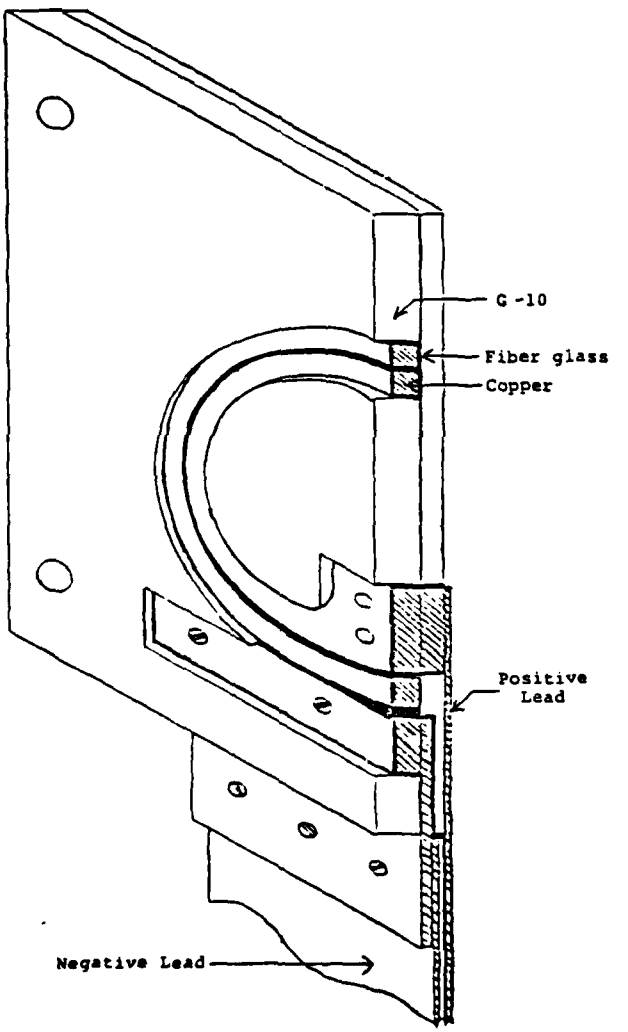

Figure 3.3: 1/2 inch Plate Copper Coil

The third coil was a four turn coil constructed in the same way as the first coil but instead of mylar insulating the surface, a layer of 0.1 millimeter G-10 was glued to the surface. This coil has been tested to nine thousand volts and twenty five thousand ampers without failure (see figure 3.4).

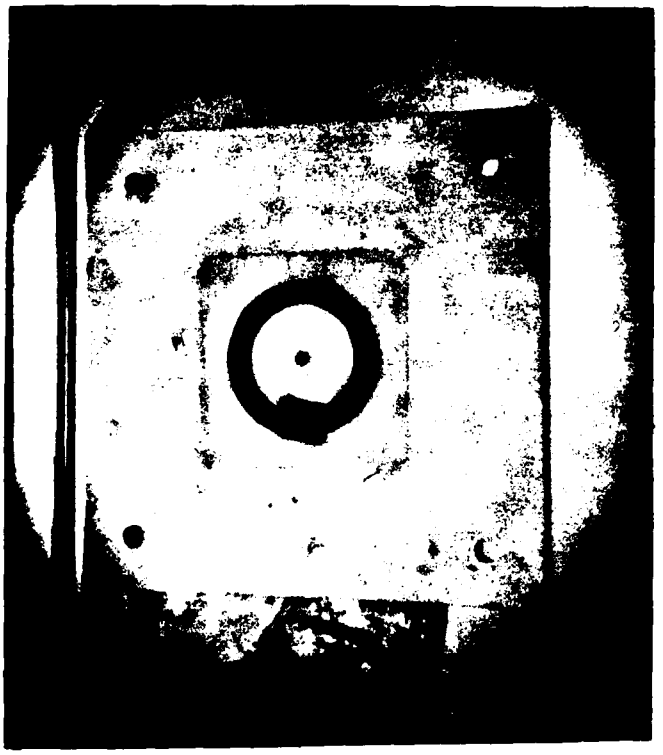

Figure 3.4: Four Turn Wire Wrapped Coil

3.1.2 Projectile Coil

The projectile coils were cut from 0.5 millimeter aluminum sheet, 0.02 millimeter aluminum foil, and several sizes of high grade aluminum and copper shim stock ranging from 0.02 millimeters to 0.25 micrometers (see figure 3.5). The

projectile coils were then adhered to the surface of the drive coil using vacuum grease or spray contact cement. The holding power of both the vacuum grease and the contact cement was minute compared to the forces accelerating the projectile coil. The vacuum grease, however, added an appreciable amount of weight to the projectile coil and coated the inside of the vacuum chamber during operation. For this reason, contact cement was used almost exclusively.

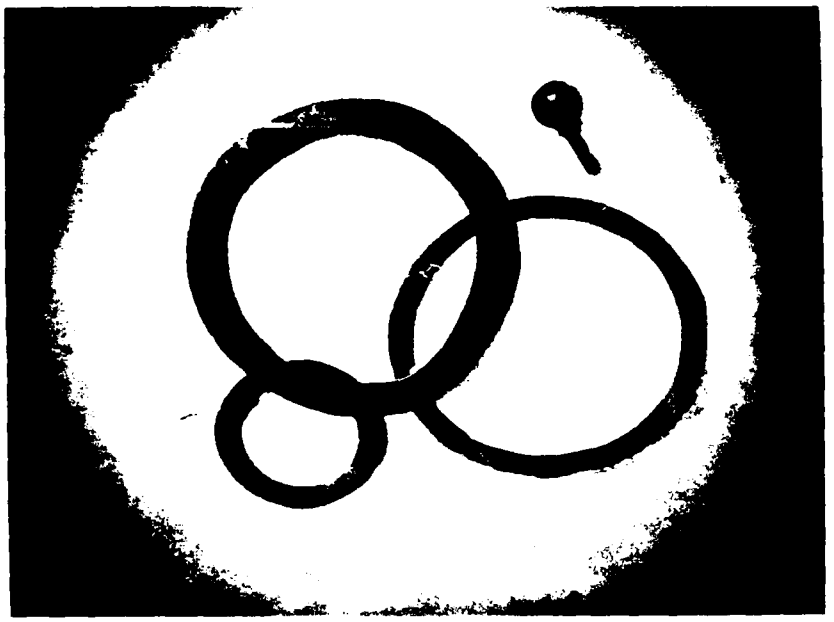

Figure 3.5: Typical Projectile Coils

3.1.3 Capacitor Bank

The capacitors used to drive the pulse coils were supplied by Tobe Duechman and rated at 20 kilovolts and 15

microfarads. Six of these capacitors were hooked in parellel to form a power supply capable of storing a total of 27 kilojoules and, unlike electrolytic capacitors, capable of delivering that energy in a few microseconds. The Tobe Duechman capacitors, although rather large and costly, proved to be a reliable source of energy.

3.1.4 Leads

The leads from the capacitors to the drive coil were one of the most critical and challenging parts of the experimental apparatus to design. They had to be capable of standing off the full 20 kilovolts of the capacitor bank and yet have very low inductance. In order to accomplish this the leads were kept as short as possible by designing the test apparatus so that the drive coil was located close to the capacitors.

3.1.5 Switch

The high current and voltage at which the test apparatus operated presented a problem in choosing a switch. The switch needed to be easy to operate, low cost, have relatively low inductance, and operate over a wide range of voltages. Two different switches were tried. The first was a gas gap switch manufactured by EG&G. Although this switch never failed in the sense that it was no longer usable, it did

present problems. It had a fairly narrow voltage range at which it would operate and would often fail to trigger at one or two kilovolts on either side of its designed operating voltage. Also, the dc to dc converter used to generate the high trigger voltages often malfunctioned or was hooked up incorrectly. After several of these fairly costly switches exploded on other experiments due to high currents caused by dielectric failure, a simpler mechanical type of switch was designed and tested [Reithel 59]. Two flat plates were added to one of the leads going from the drive coil to the capacitor bank. Between these two plates a mylar sheet was placed to keep the current from arcing. A sharp steel pin was then positioned in such a way that it could pierce the mylar and thus make contact between the plates. As soon as contact was made, an arc would form that melted the mylar and enlarged the contact area. Removable brass plates were placed around the contact area in order to reduce the effect of pitting caused by arcing, and the steel pins were designed to be easily removed and sharpened as they ablated. This switch was very inexpensive and performed well at all voltages and currents (see figure 3.6).

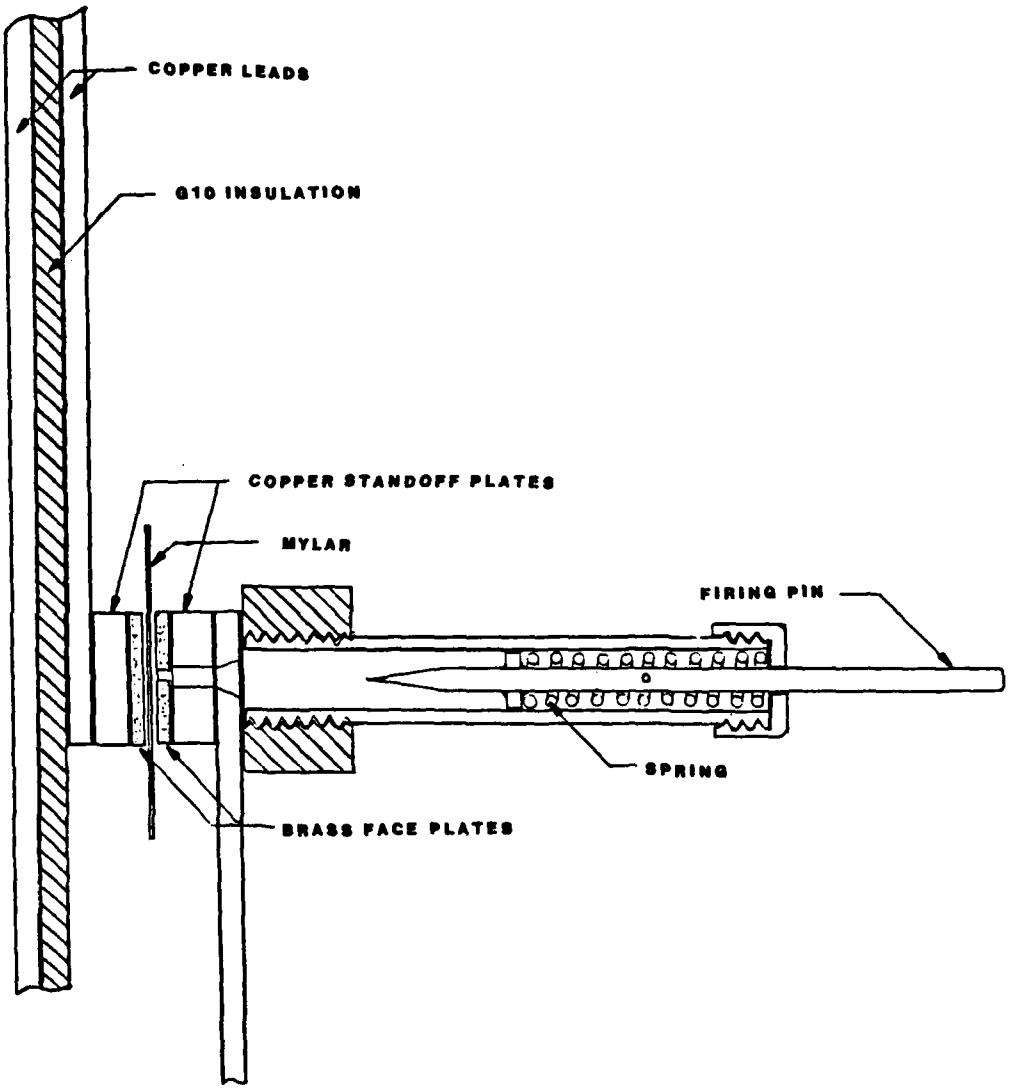

Figure 3.6: Mechanical Dielectric Switch

3.1.6 Decelerator

The decelerator was a device used to stop the projectile coils after the test apparatus was fired. It consisted of an

aluminum plate mounted on springs at the rear of the test chamber. A lexan viewing port was placed in the center of the decelerator to allow photographs to be taken of the projectile as it left the drive coil. The only problem encountered with this device was that the lexan shields had to be replaced every now and then as they became damaged by the projectile coils (see figure 3.7).

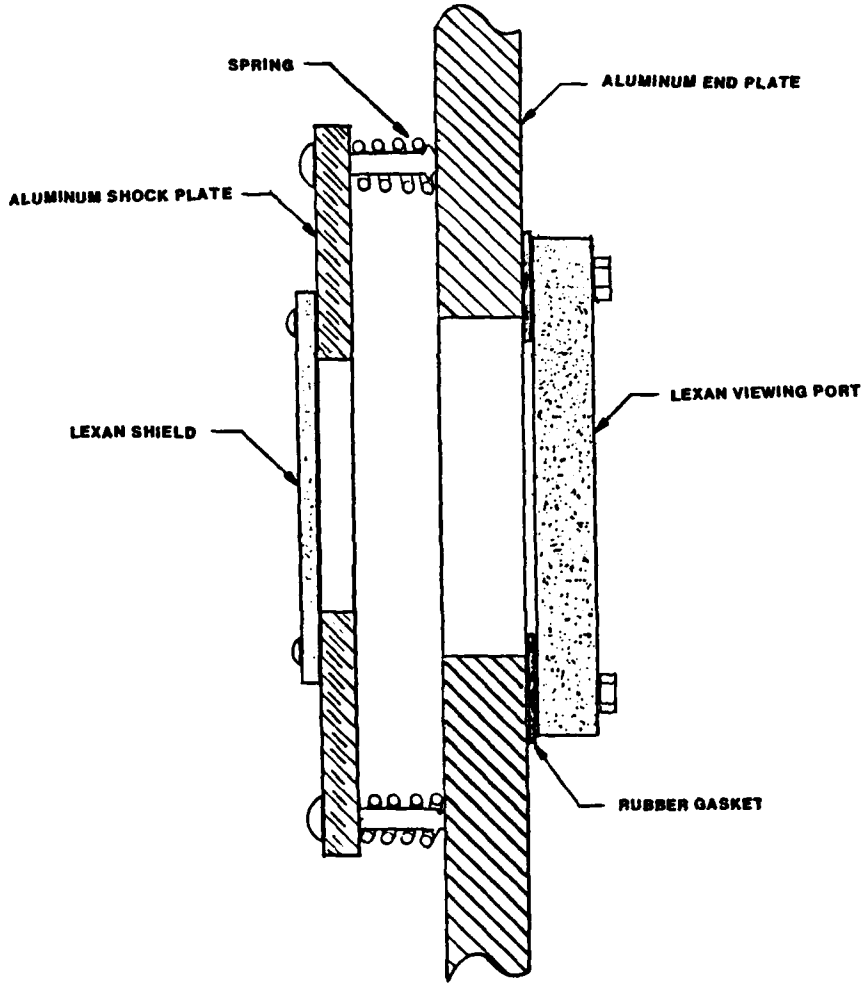

Figure 3.7: Decelerator

3.1.7 Vacuum Chamber

The vacuum chamber associated with the test apparatus consisted of an 18 inch glass cylinder mounted on a steel channel frame. This glass vacuum chamber was used to reduce the air drag of the projectile coil. A vacuum pump was connected to this cylinder by 2 inch diameter vacuum tubing. Plastic gaskets coated with silicon vacuum grease sealed the ends of the cylinder up against aluminum and G-10 end plates. A lexan shield was used to protect the cylinder from any damage that might have ocurred when a drive coil failed or a large projectile misfired.

3.2 Instrumentation

A typical operating cycle of the experimental apparatus, from the time the switch was closed to the time the projectile coil came to rest, took on the order of one to two milliseconds. This short time frame made instrumentation a challenge. Three measurements, current and voltage of the drive coil circuit, and velocity of the projectile coil, were taken during each test. Additional information on the acceleration process could be obtained from a camera and strobe setup.

3.2.1 Voltage

Voltage was measured using a Textronics P1600 high voltage

probe connected to an oscilloscope. Its accuracy was such that the nonlinearities of the magnetic coupling between the projectile coil and the drive coil could be easily seen on the oscilloscope.

3.2.2 Current

Current was measured using a Rogowski coil. Because of the wide, low inductance leads used on the test apparatus, a special Rogowski coil had to be designed that would fit around these leads. This was accomplished by winding copper wire around a flexible nylon threaded rod and insulating it with Tygon tubing. In this manner, a flexible Rogowski coil was constructed that could easily fit around either of the drive coil leads.

3.2.3 Pressure

The pressure in the test chamber was measured with a thermocouple hooked into the vacuum line between the test chamber and the vacuum pump. All tests were performed at a pressure of 60 to 100 millitorr. At this pressure, effects of aerodynamic drag were negligible.

3.2.4 Velocity

Velocity turned out to be the most difficult measurement to

obtain. A device was needed that could accurately measure the velocity of the projectile coil from a few hundred meters per second to velocities on the order of a thousand meters per second. Several different devices were designed and tested. Each of these devices performed reasonably well at low velocities. However, at high velocities electrical noise became a problem.

3.2.1.1 Time of Flight

The simplest of all the velocity sensors designed was the time of flight indicator. Because the projectile coil only accelerates for a very short period of time, it reaches its maximum velocity just a few centimeters from the drive coil. In a vacuum, there is very little resistance to the forward motion of the projectile coil thus, it maintains essentially a constant velocity from the time it leaves the drive coil to the time it hits the decelerating plate. One way to measure this velocity is to simply measure the time it takes the projectile coil to travel a given distance from the drive coil. This was acomplished by replacing the decelerator at the end of the vacuum chamber with a combination decelerator and contact switch. Details of this switch can be seen in figure 3.8. An oscilloscope was set up to trigger off of the Rogowski coil. When current began to flow through the drive coil, the

oscilloscope triggered and began to trace across the screen. Contact of the projectile coil with the switch closed the switch and caused a voltage spike to appear on the oscilloscope. Thus, the time of flight could be directly read from the oscilloscope.

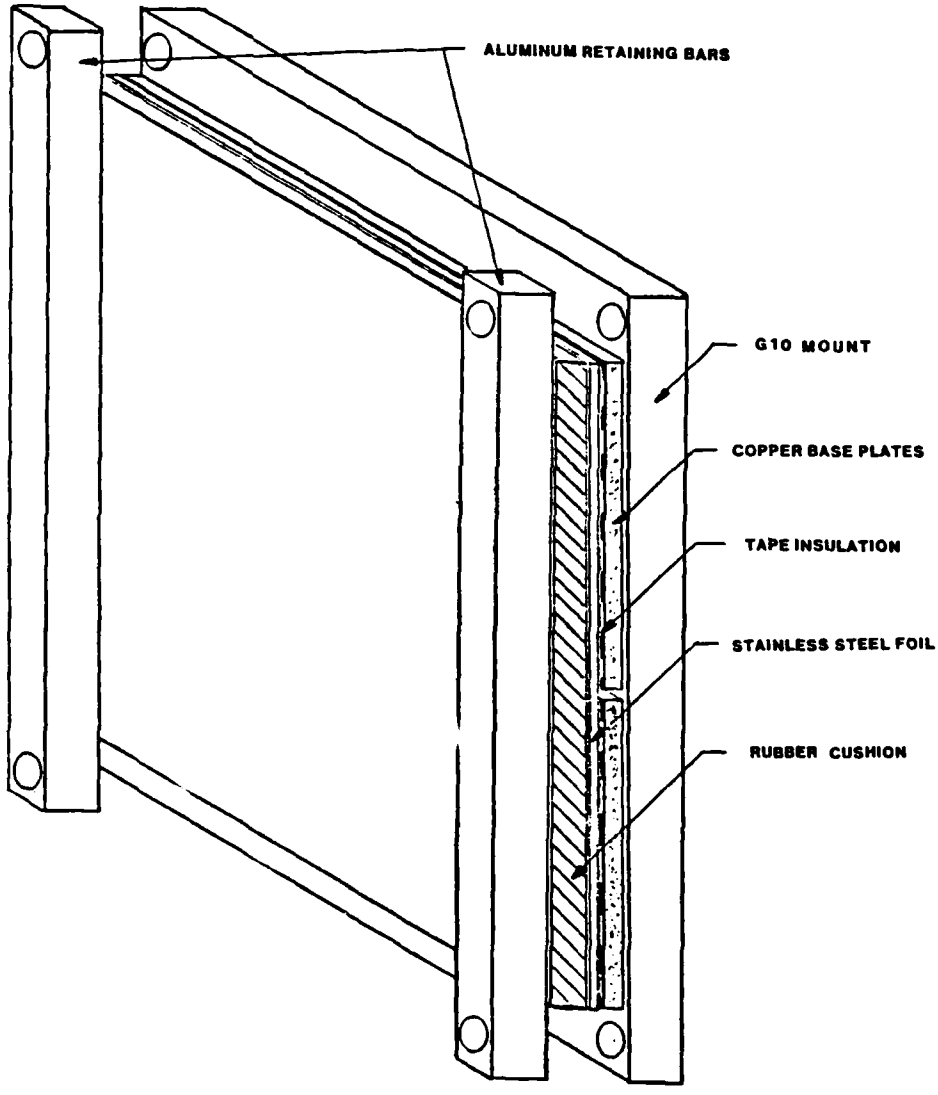

Figure 3.8: Time-of-Flight Sensor

The contact switch performed well at velocities less then five hundred meters per second. Above that, the projectile coil would destroy the contact switch by fusing the stainless steel contact sheet to the copper contact plate. Also, the electrical noise picked up from the projectile coil's magnetic field as it approached the contact plate, often made it difficult to pinpoint exactly when the projectile coil hit.

3.2.1.2 Wire Break

In an attempt to find a velocity sensor that did not have to be completely rebuilt after every test shot, a second velocity sensor was developed. This velocity sensor relied on a voltage ladder formed from thin lengths of nichrome wire connected to resistors. When one of the nichrome wires broke, the circuit voltage read on an oscilloscope would drop. Therefore the velocity of the projectile coil could be determined by placing the nichrome wires in the path of the projectile coil at known distances from the drive coil. The time at which the projectile coil broke each of the nichrome wires was read from the voltage drops indicated on the oscilloscope and the velocity was then calculated by knowing the distance of each wire from the drive coil. The schematic for the wire break circuit used can be seen in figure 3.9.

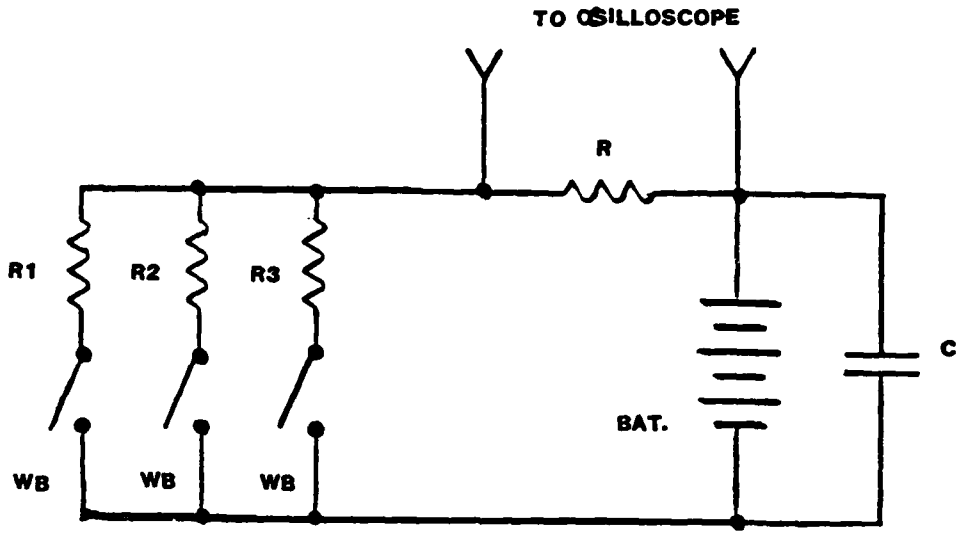

Figure 3.9: Wire Break Schematic

This method of velocity sensing worked out fairly well except that the nichrome wire acted as an antenna and the electrical noise picked up made it impossible to read velocities when operating at high voltages. This problem was solved to some extent by using twisted insulated wire. However, because the wire was doubled back on itself making it almost twice as strong, the projectile coil often failed to break it. Also, several electrical connections to the twisted wire had to be made within the vacuum chamber. This was a tedious process that slowed the experiment considerably.

3.2.1.3 Laser

An optical sensing system using lasers turned out to be the best method of measuring velocity. This method of measurement is essentially the same as the wire break except that the wires are replaced with lasers and phototransistors. The lasers were necessary to obtain enough light to activate the phototransistors from a distance of ten or more centimeters. Lasers with an output intensity of 0.5 milliwatts were used. This was more than enough power to build a reliable sensor. One difficulty in using lasers was that they must be aligned very carfully. The farther the lasers are from the phototransistor pickups, the more sensitive their alignment becomes. In order to avoid this problem, an optical diffuser made from lexan was constructed for each phototransistor pickup (see figure 3.10). The diffusers distributed the light over a larger area thus making alignment less critical. These diffusers were nothing more than small pieces of lexan that had been scratched on the surface with fine emery paper and placed in front of the fiber optic pickups. The lasers were mounted on a pedestal next to the vacuum chamber and the fiber optic pickups were mounted to an aluminum plate on the other side of the vacuum chamber.

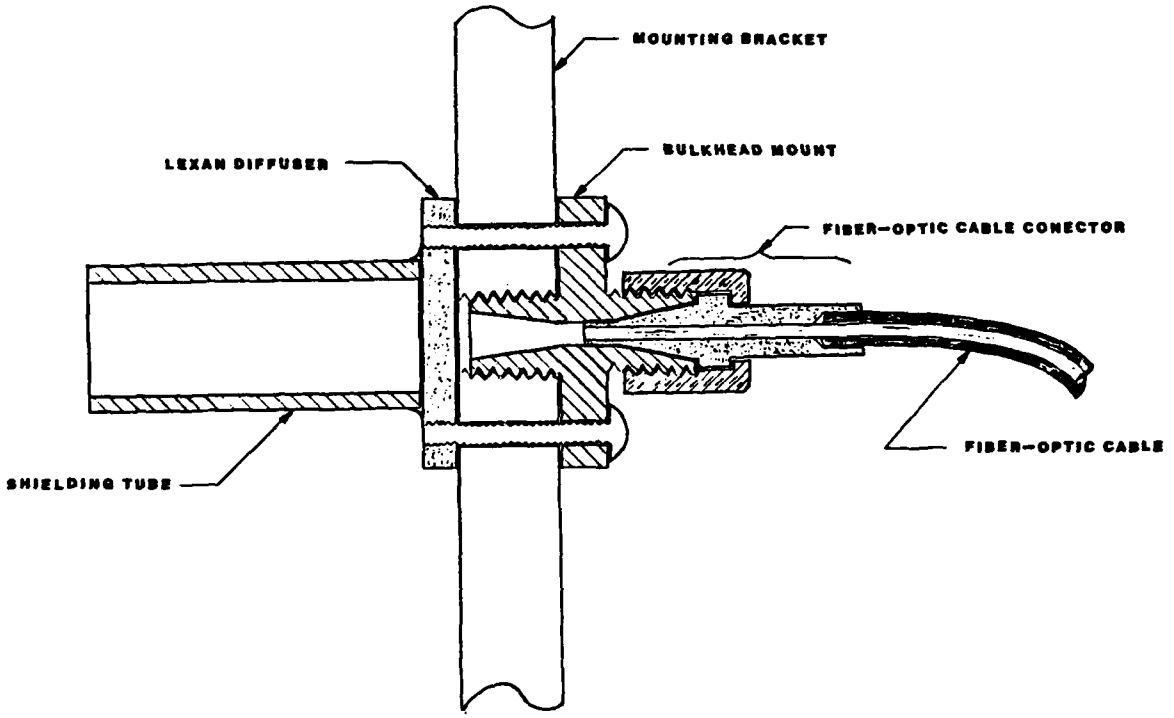

Figure 3.10: Optical Diffuser

The fiber optic cables ran from the diffusers down to an aluminum box containing the phototransistors and the signal generating circuitry. By using fiber optic cables in this manner, all the electronic circuitry could be kept well away from the drive coil and current switch thus reducing the problem of electrical noise pickup. A schematic of the signal generating circuit can be seen in figure 3.11.

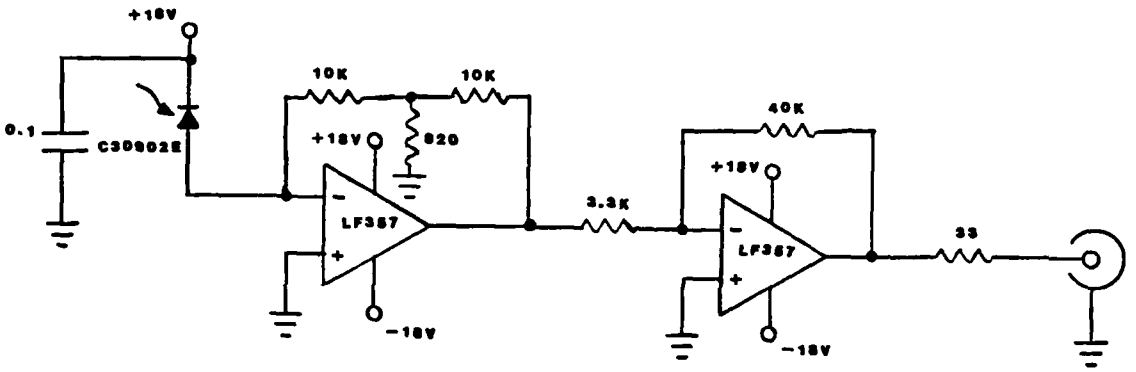

Figure 3.11: Optical Sensor

3.2.5 Inductance and Resistance

To obtain accurate data from the test apparatus, precise values of the lead inductance, the drive coil inductance, and the resistance of the system must be known. These values were measured using a digital LCR meter. By connecting the LCR meter to the drive coil leads and using insulators of various known

thicknesses to hold the projectile coil away from the drive coil, the mutual inductance between the two coils could be measured. This process helped in assessing the accuracy of the numerical model discussed in chapter five.

3.2.6 Photographic Observation

The measurements of voltage current and velocity describe a great deal of the mechanics of the pulsed inductive system. However, these measurements provide very limited knowledge of what is physically taking place during the acceleration process. In an attempt to obtain this information, a camera was set up in such a way that it could view the projectile through the plexiglass port and lexan shield at the end of the test chamber. Several battery powered flash units were used to strobe the projectile during its flight. These battery powered flash units provided high speed flashs of about 6 microseconds in length that captured the projectile on film as it moved at speeds as fast as 700 meters per second. The flash units were synchronized using an electronic timing circuit that triggered off of the Rogowski coil. A schematic of this timing circuit can be seen in figure 3.12.

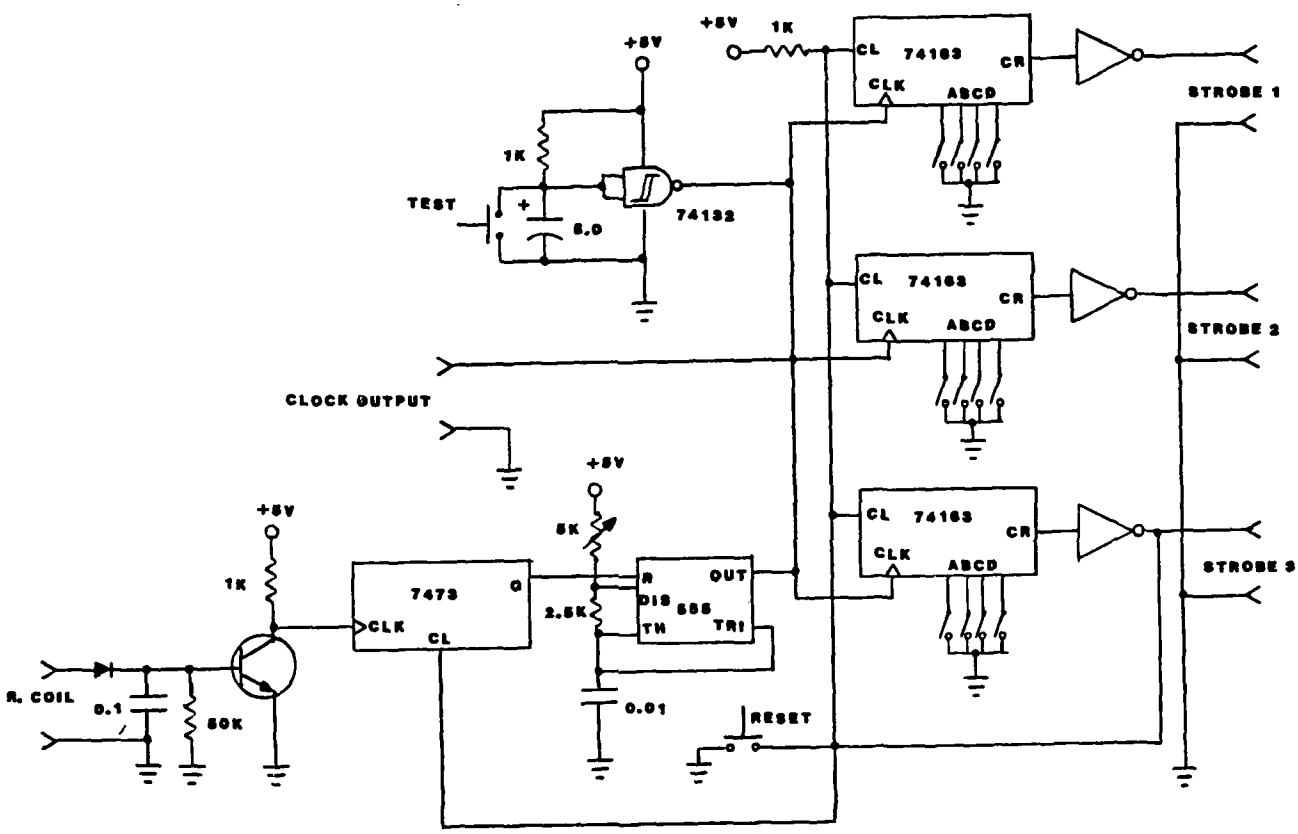

Figure 3.12: Strobe Timing Circuit

3.3 Operation

Operation of the experimental apparatus was a fairly simple but time consuming procedure. First the oscilloscopes were turned on and allowed to warm-up. A projectile coil was adhered to the face of the drive coil and the velocity sensor was connected, adjusted and tested to make sure it was functional. Then, the drive coil was bolted to the G-10 end plate on the vacuum chamber. A mylar sheet was placed between the contact plates of the mechanical switch and the switch was then tightened and adjusted. The vacuum pump was started and the bolts holding the drive coil to the vacuum chamber were tightened as the pressure in the chamber dropped. This helped prevent leaks from ocurring around the drive coil gasket. A thermocouple pressure gauge was turned on and the vacuum chamber was allowed to pump down to around 60 millitorr. While the pressure dropped, a camera was setup and the strobes and timing circuits were turned on. The mechanical switch was then armed and the voltage sensor connected to the capacitor bank. Then, a grounding strap on the capacitor bank was removed and final adjustments were made to the oscilloscopes. Ear protectors were put on, the capacitors charged, and the trigger pin was pulled from the mechanical switch. Finally, data was read from the oscilloscopes, the grounding strap was connected, and the experimental apparatus was inspected for damage. This entire procedure typically took one

to two hours to perform. If all went well, several tests could be run in a day. However, as with almost any experimental apparatus, unexpected problems often developed and had to be corrected before further tests could be made. Some of these problems and the way in which they were corrected are discussed in chapter four.

CHAPTER 4

EXPERIMENTAL RESULTS

The experimental simulation of the metallic induction reaction engine provided invaluable information on the physical workings of this device. Photographic observations and measurements of velocity, current and voltage were made. These measurements were accurate enough to indicate when the projectile coil changed from a solid to a liquid. They also showed the highly nonlinear discharge effects that result from the close magnetic coupling of the drive coil with the projectile coil.

In this chapter, some of the difficulties encountered during the operation of the experimental apparatus are discussed. Typical data traces and photographs are shown and the accuracy of the instrumentation used to obtain the data traces is analyzed. Also included in this chapter are the tabulated results of all the experimental tests performed.

4.1 Operating Difficulties

Several difficulties arose during the operation of the experimental apparatus. None of these difficulties proved to be insurmountable. However, they slowed the experiments considerably and added to the overall cost of the apparatus.

4.1.1 Electrical Noise

Of all the difficulties encountered, the effects of RFI transmision from the drive coil circuit proved to be the most troublesome. This induced electrical noise made velocity measurements extremely difficult when operating at high voltages. It caused the oscilloscopes to mistrigger, the electrical timing circuit controlling the strobes to misfire, and it introduced such a scatter of stray voltages that the measurements taken could not be distinguished from false signals. An example of this electrical noise problem can be seen in the oscilloscope trace, figure 4.1, of a three wire break velocity sensor taken during a 15 kilovolt test.

Several precautions were taken to avoid electrical noise problems. All conections between the oscilloscopes and the instruments were made with coaxial cables. Electrical circuits were shielded in aluminum boxes and, whenever possible, powered by batteries rather than external power supplies. Finally, the wire break velocity sensor was redesigned so that the wires doubled back on themselves and were twisted (see figure 4.2). Although twisting the wires of the velocity sensor helped, it was still not adequate. Eventually, a laser sensor was developed which used fiber optic cables to isolate the electrical circuitry from high voltage discharges. None of the precautions taken

completely solved the problem of electrical noise but they made it tolerable.

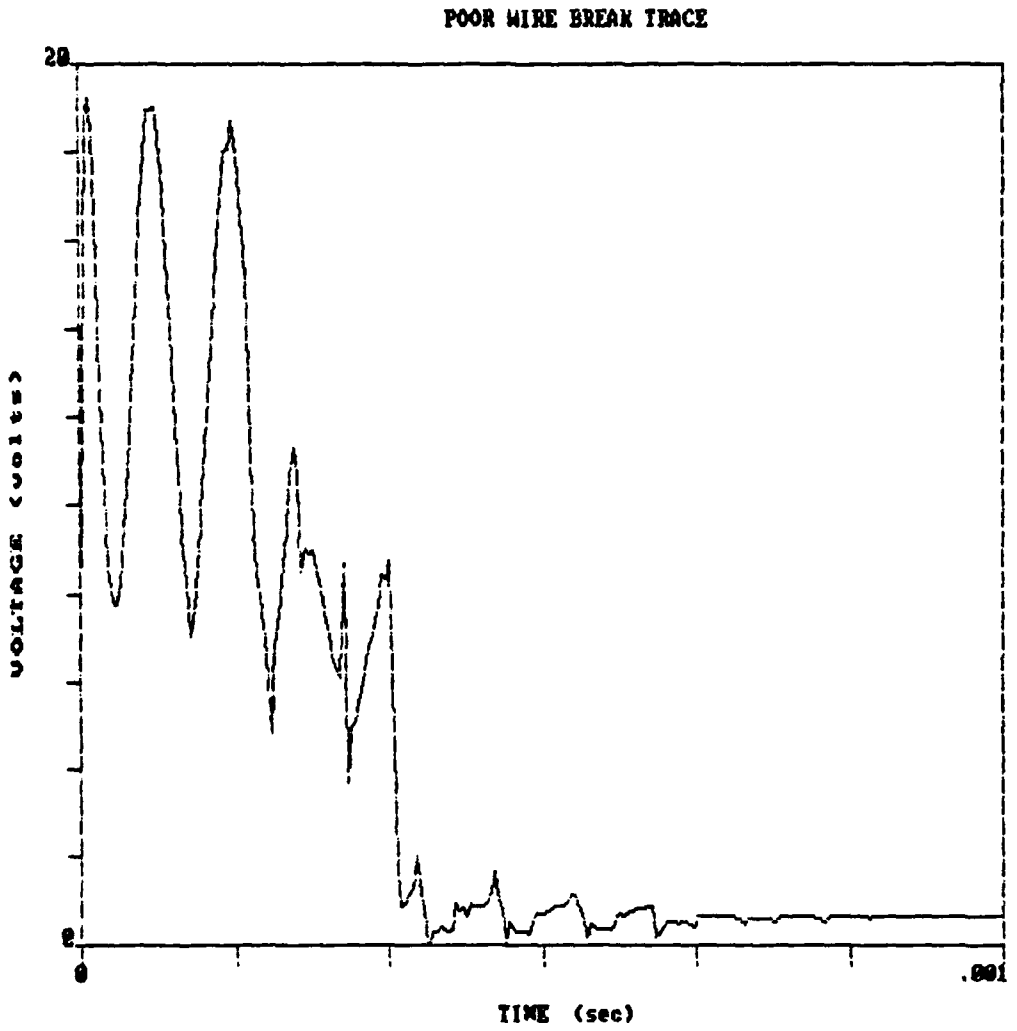

Figure 4.1: Electrical Noise Problem

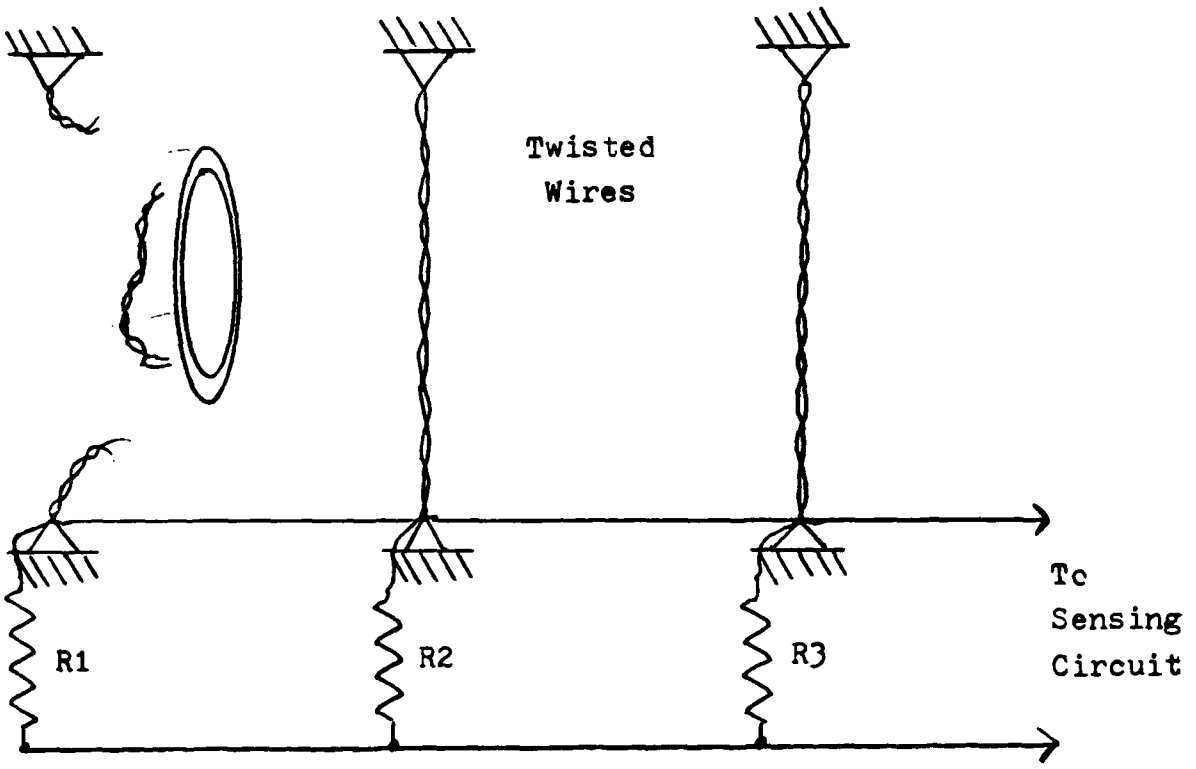

Figure 4.2: Twisted Wire Break Sensor

4.1.2 Coil Failure

The maximum performance that could be obtained by the experimental appartus was limited by the structural integrity of the drive coils used. None of the coils built could stand up to

the full 18,000 joule limit of the capacitor bank. Unfortunately, in order to observe effects such as the phase change of the projectile material, it was necessary to operate near this limit. Because of this, several coils failed during the course of the experiments. The exact mechanism of these failures has not yet been determined. However, it appears to be due to cracking in the dielectric insulator between coil turns followed by an electrical arc breakdown. (see figures 4.3).

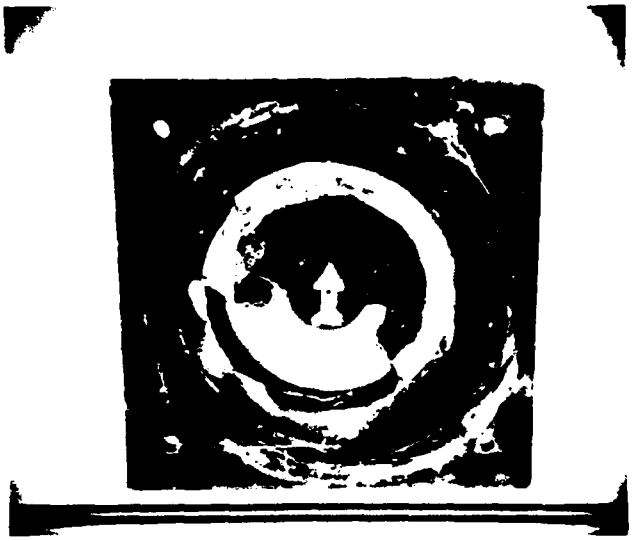

Figure 4.3: Drive Coil Failure

4.1.3 Switch Ablation

The mechanical switch used on the experimental apparatus provided a reliable means of closing the drive coil circuit. Unfortunately, the mechanism that made this switch work also led to its destruction. When the switch was triggered, a stainless steel pin would pierce a sheet of mylar used to hold off the

capacitor voltage between two brass plates. A hot conductive plasma would form and blow the mylar away from the contact area around the pin. In practice, this plasma was so hot that it would partially melt the stainless steel pin and brass plates (see figure 4.4).

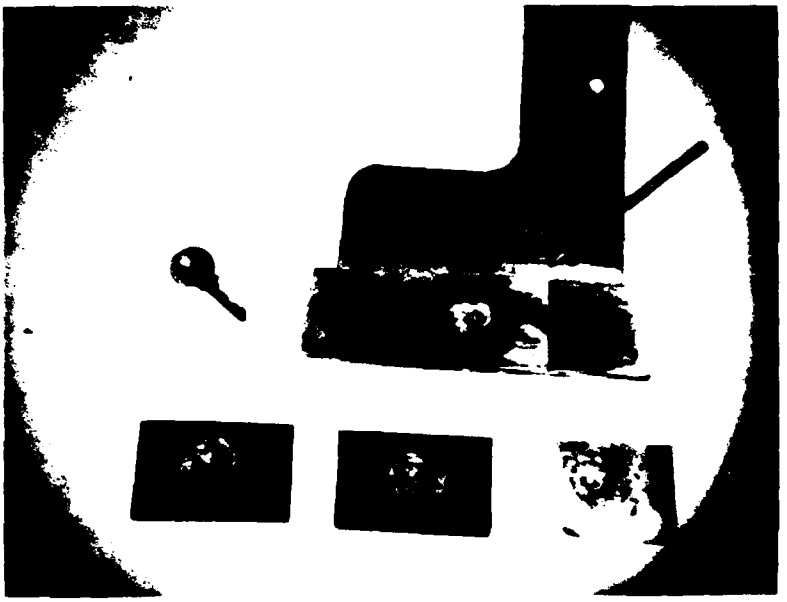

Figure 4.4: Switch Ablation

Several different materials such as tungstan carbide and high carbon steel were tried in place of the stainless steel and brass. Although almost any material with a higher melting point worked better, it was believed that the cost of these materials and the difficulty in machining them made them impractical for this switch. The best solution to this problem was to make the stainless steel pin and brass plates easy to machine and quick to replace. Typically, the point on the stainless steel pin had to be reground after each test and the brass plates had to be

replaced after about fifteen tests.

4.2 Data Summary and Tabulation

Over one hundered tests were performed with the experimental apparatus. Three different drive coils and several different sizes of aluminum and copper projectile coils were tested at capacitor voltages ranging from one kilovolt to fifteen kilovolts. Measurements of voltage, current and velocity were taken during each of these tests. Unfortunately, electrical noise made interpreting some of the data traces difficult if not impossible. However, many significant tests, including several showing the projectile coil melting, were accurately recorded.

4.2.1 Typical Data Traces

Nicolet digital oscilloscopes were used to take voltage, current and velocity readings. These oscilloscopes allowed the data to be stored on floppy disks and read into a computer where they could be graphed and compared with each other. Typical traces from the oscilloscopes can be seen in figures 4.5 through 4.9.

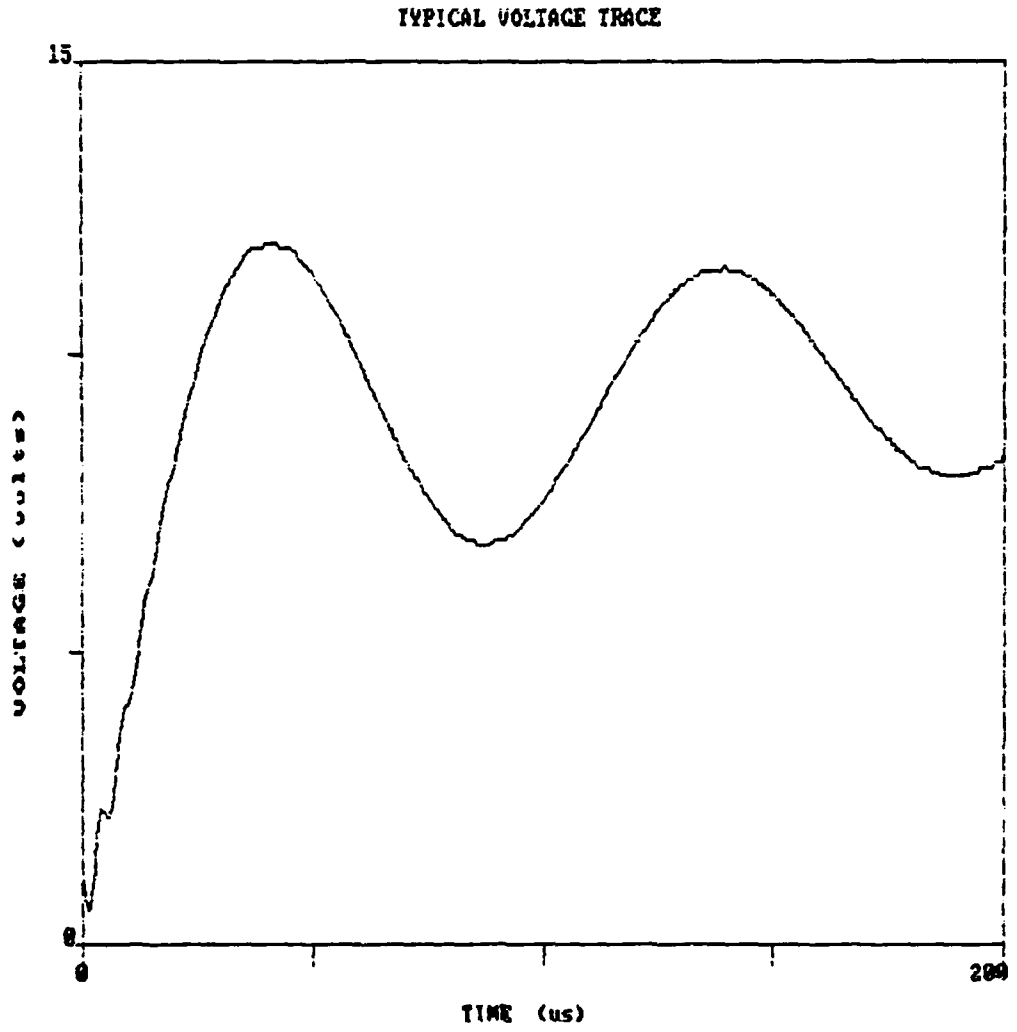

Figure 4.5: Typical Voltage Trace

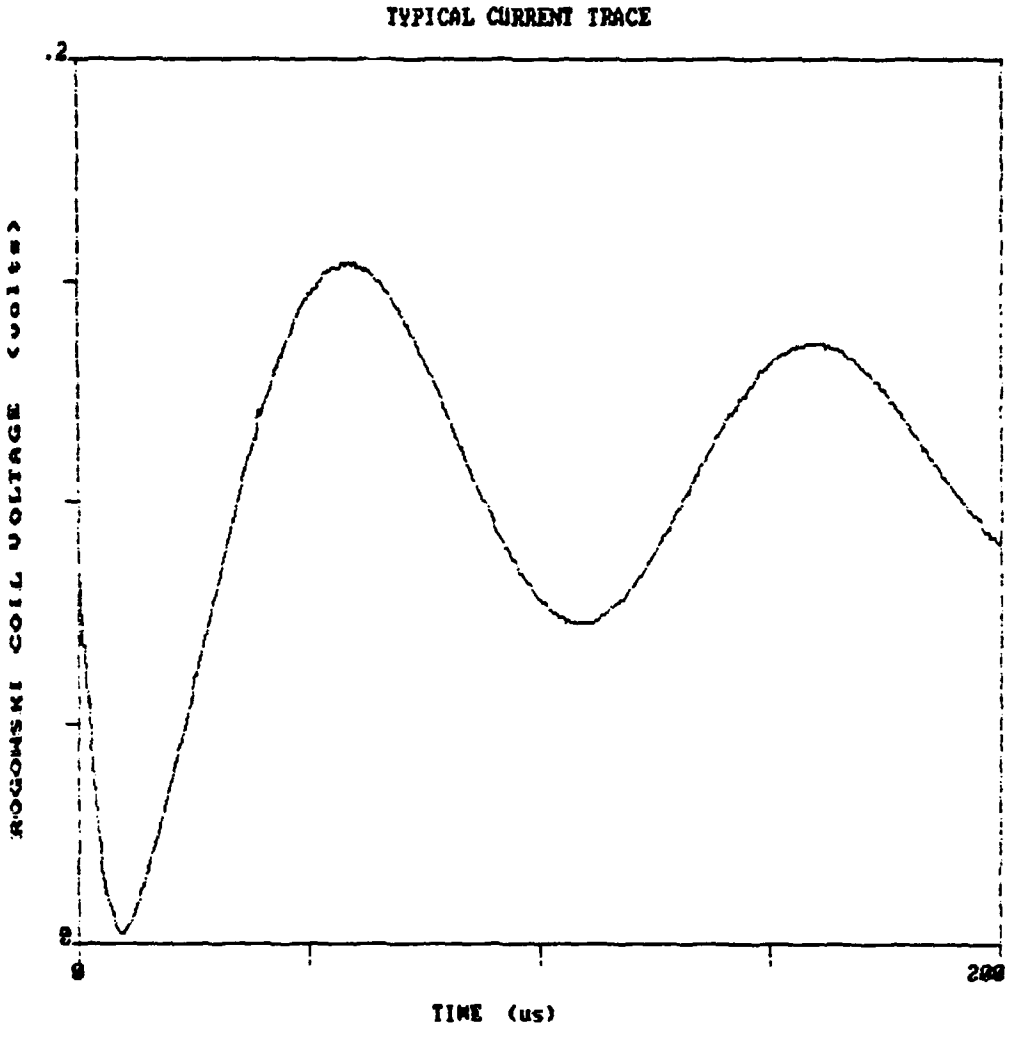

Figure 4.6: Typical Current Trace

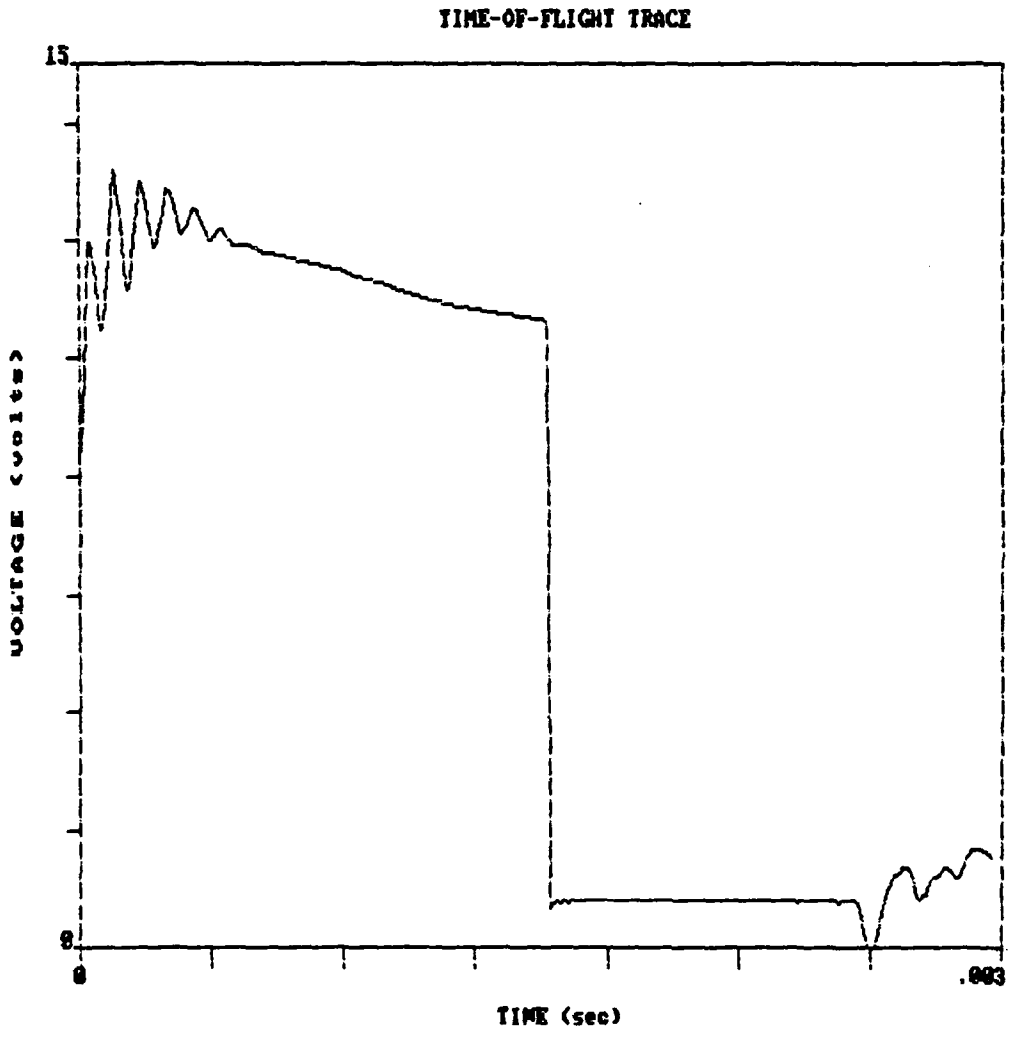

Figure 4.7: Typical Time-of-Flight Trace

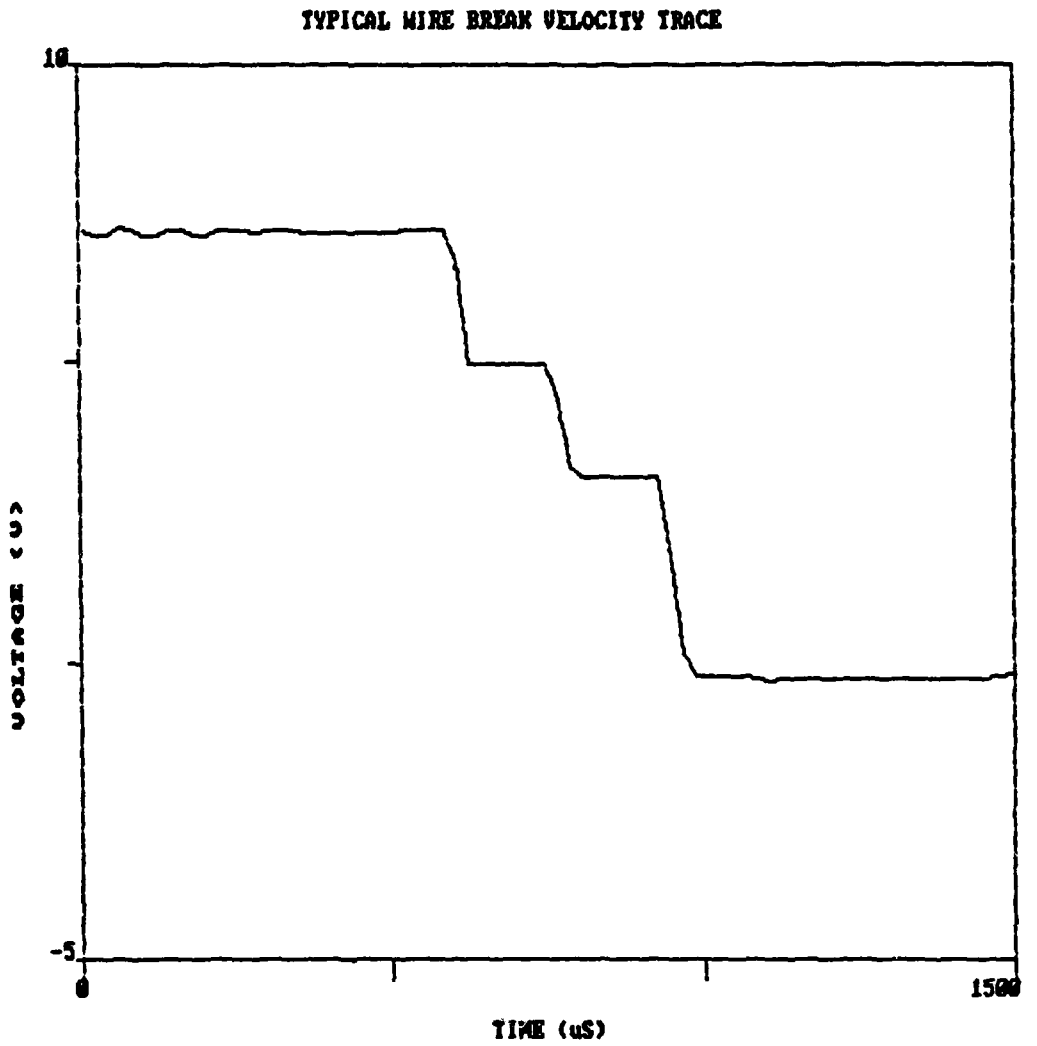

Figure 4.8: Typical Wire Break Trace

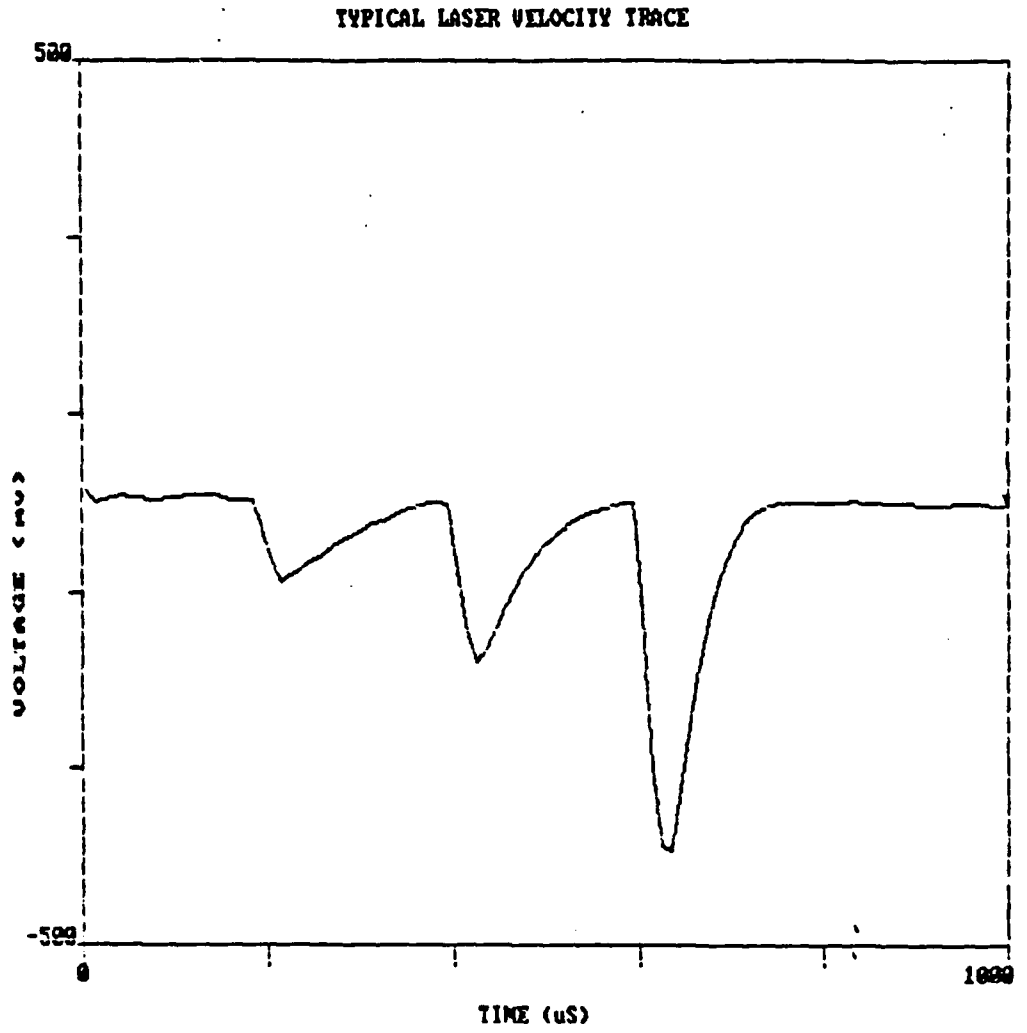

Figure 4.9: Typical Laser Velocity Trace

4.2.2 Photographic Observations

The camera proved to be a very useful experimental tool. It was the only way in which the kinematics of the projectile coil acceleration could be studied in detail. Both color and black & white photographs were taken of various projectile coils in flight. Two of these photographs can be seen in figures 4.10 (a) and (b).

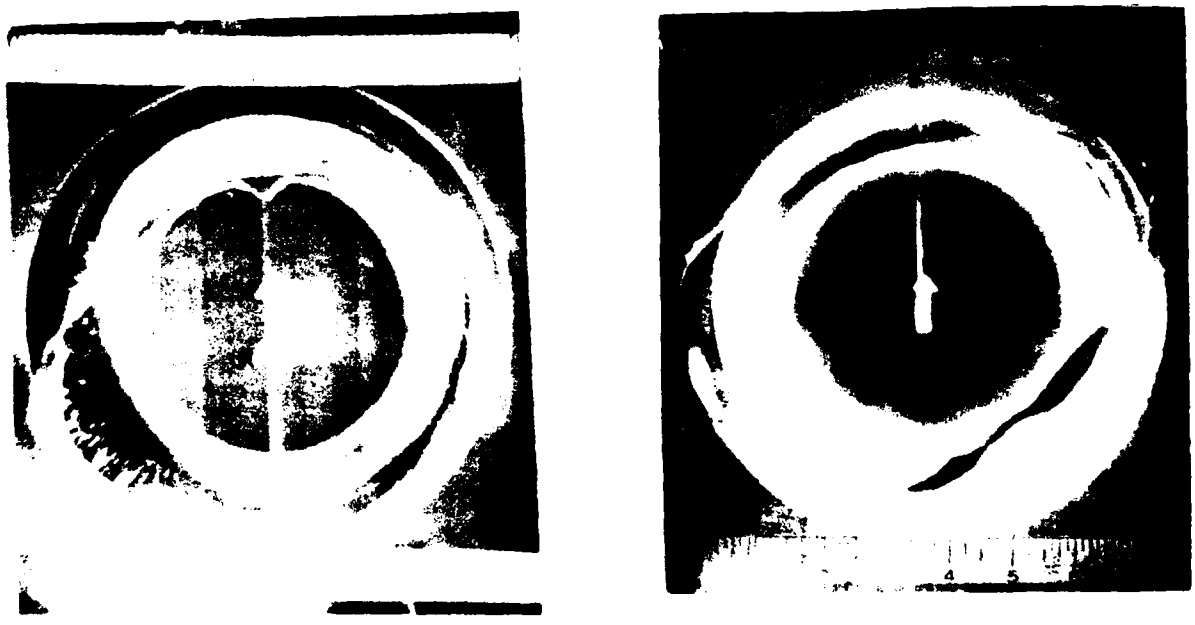

(a)
540 m/s

(b)
750 m/s

Figure 4.10: Projectile Coils in Flight

4.2.3 Tabulation of Data

Tables 4.1 through 4.3 present the performance results obtained from the experimental apparatus.

Table 4.1: Discharge Circuit Parameters

Maximum Operating Voltage	20 kV
Total Capacitance	90 uF
Switch Resistance	7.2 mΩ
Lead Inductance	0.075 uH

Table 4.2: Drive Coil Parameters

	Coil #1	Coil #2	Coil #3
Construction	Cu Wire	Cu Plate	Cu Wire
Inside Radius	7.o cm	6.3 cm	3.2 cm
Outside Radius	8.3 cm	8.4 cm	4.5 cm
Width	0.5 cm	1.3 cm	0.5 cm
# turns	3	2	4
Inductance	2.85 uH	1.4 uH	2.12 uH
Resistance	1.1 mΩ	0.1 mΩ	0.7 mΩ

Table 4.3: Experimental Data

Drive Coil #1

Aluminum Projectile Coils (8.68 grams, 0.33 uH)

Initial Cap. Voltage	Projectile Velocity	System Efficiency
9 kV	545 m/s	35.0 %
9	502	30.0
9	498	29.5
9	436	22.6
10	567	31.0
10	550	29.2
10	532	27.3
10	515	25.5
11	617	30.3
13	725	30.0
14	754	28.0

Drive Coil #2

Aluminum Projectile Coils (12.6 grams, 0.28 uH)

10 kV	365 m/s	18.7 %
13	440	16.0

Drive Coil #3

Aluminum Projectile Coils (0.7 grams, 0.2 uH)

5 kV	300 m/s	2.8 %
6	400	3.5
6	375	3.0

Aluminum Projectile Coils (0.45 grams, 0.2 uH)

7 kV	576 m/s	3.4 %
7	330	1.1
8	485	1.8
9	640	2.5

Copper Projectile Coils (2.15 grams, 0 2 uH)

6 kV	207 m/s	2.8 %

4.4 Determination of LCR Parameters

Two methods were used to obtain inductance and resistance values of the projectile coils, drive coils and leads of the experimental apparatus. One of these methods was to simply measure them directly using an LCR meter. This was done with a Wayne Kerr Automatic LCR Meter 4225. The meter was clipped to whatever was being measured and the inductance and resistance values read directly. The only problem with this method was that measurements could not be made under the same conditions that existed during a high voltage, high current discharge. To avoid this problem, the inductance and resistance values were often *calculated from* the current and voltage traces of experimental tests.

Consider the current trace, shown in figure 4.11, of a typical drive circuit discharge.

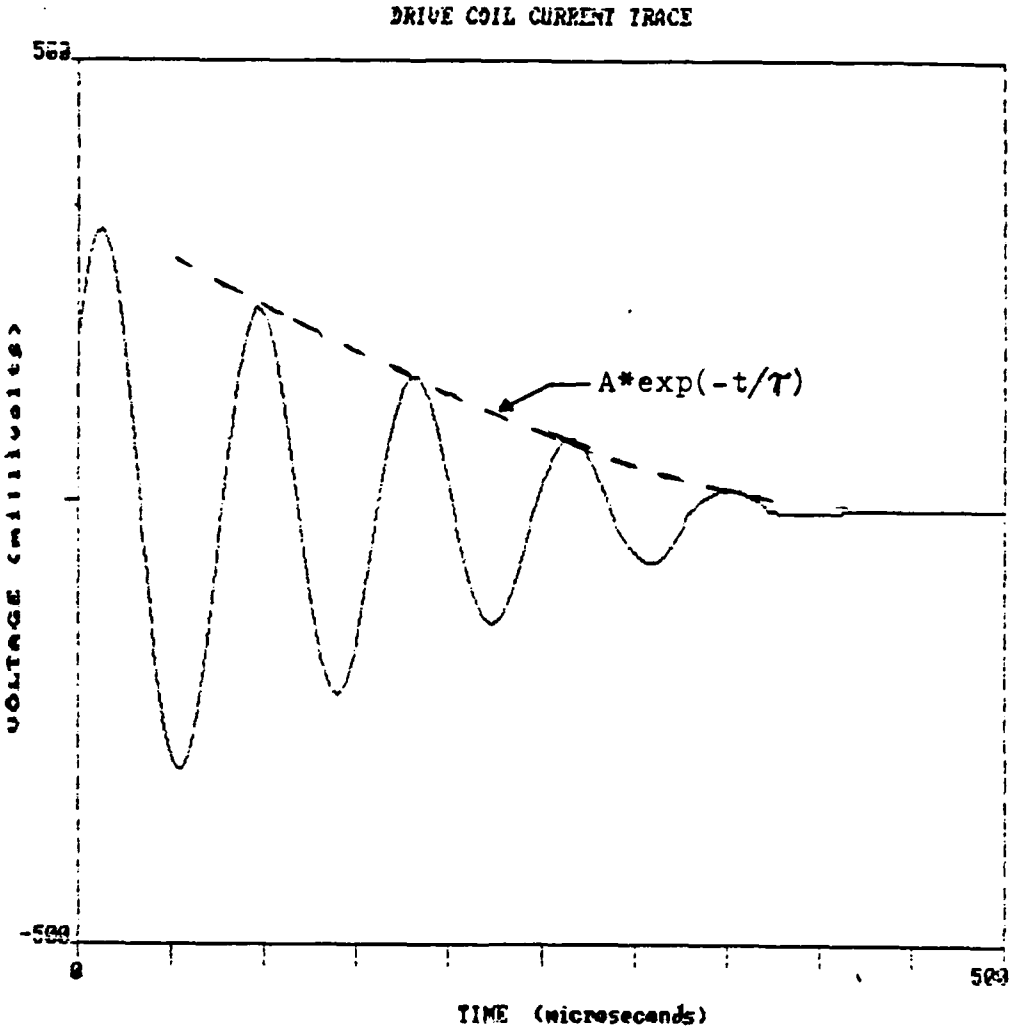

Figure 4.11: LCR Drive Circuit Trace

The peak current decays as a function of the circuit inductance and resistance,

$$I \propto \exp(-t/\tau) \qquad (4.3.1)$$

where

$$\tau = 2L/R \tag{4.3.2}$$

The period of this discharge can be written as

$$T = 2\pi\sqrt{LC} \tag{4.3.3}$$

From these relationships, the inductance and resistance of the system are simply

$$L = (\tau/2\pi)^2/C \tag{4.3.4}$$

and

$$R = 2(\tau/2\pi)^2/TC \tag{4.3.5}$$

The results of the calculations made can be seen in tables 4.1 and 4.2.

Using this same technique, values of effective inductance and resistance of the drive coil/projectile coil system can be obtained. These values represent the apparent impedances seen by the capacitor bank during discharge. They can be expressed as

$$Leff = Ld[1-(Mpd^2/LdLp)] \tag{4.3.6}$$

and

$$Reff = Rd + RpMpd^2/Lp^2 \tag{4.3.7}$$

Figure 4.12 shows the effective inductance and resistance

values for a typical drive coil/projectile coil setup. These values were obtained by holding the projectile coil at known distances from the drive coil while taking measurements with an LCR meter.

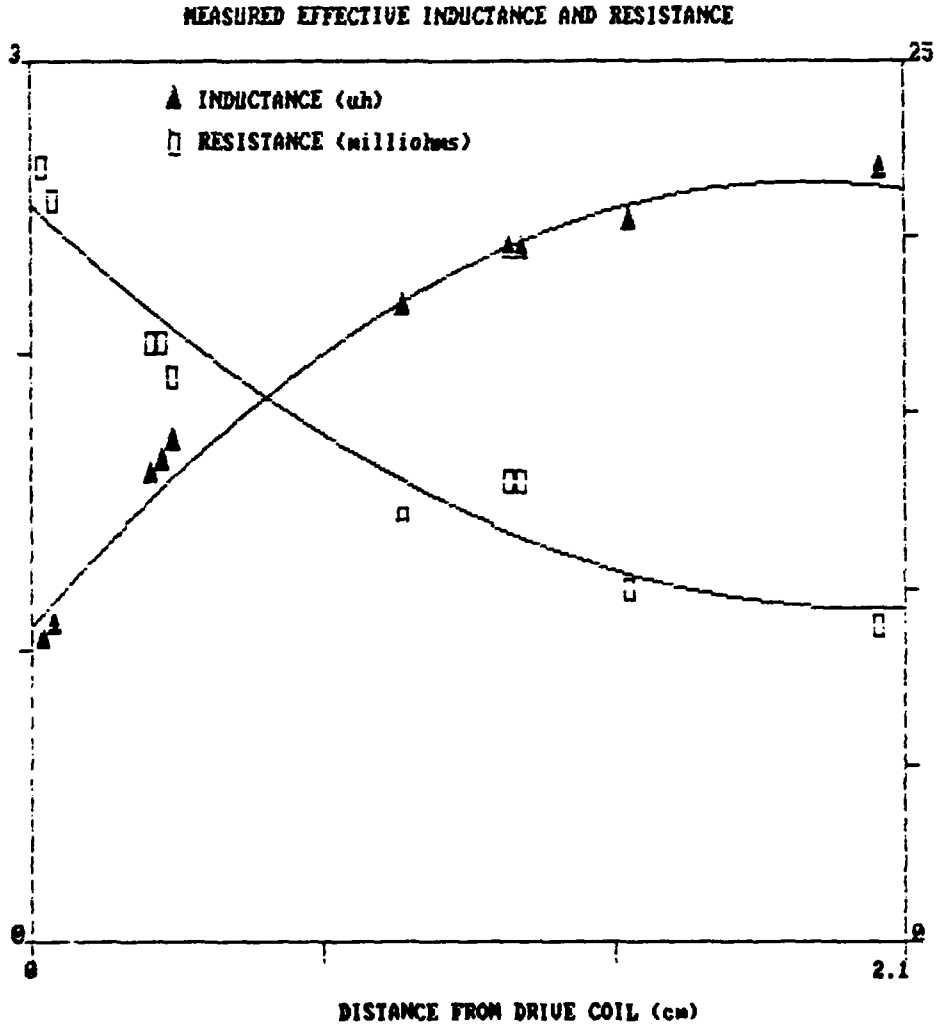

Figure 4.12: Effective Inductance and Resistance

Note that from equations 4.3.6 and 4.3.7, the mutual inductance and the mutual inductance gradient between the two

coils can be calculated. In terms of Leff,

$$Mpd = \sqrt{[1-(Leff/Ld)]LdLp} \qquad (4.3.8)$$

and

$$dMpd/dz = (Lp/2)\{[(Leff/Ld)-1]LdLp\}^{-1/2}\, dLeff/dz \qquad (4.3.9)$$

Figure 4.13 shows the results of these calculations for a typical drive coil/projectile coil setup.

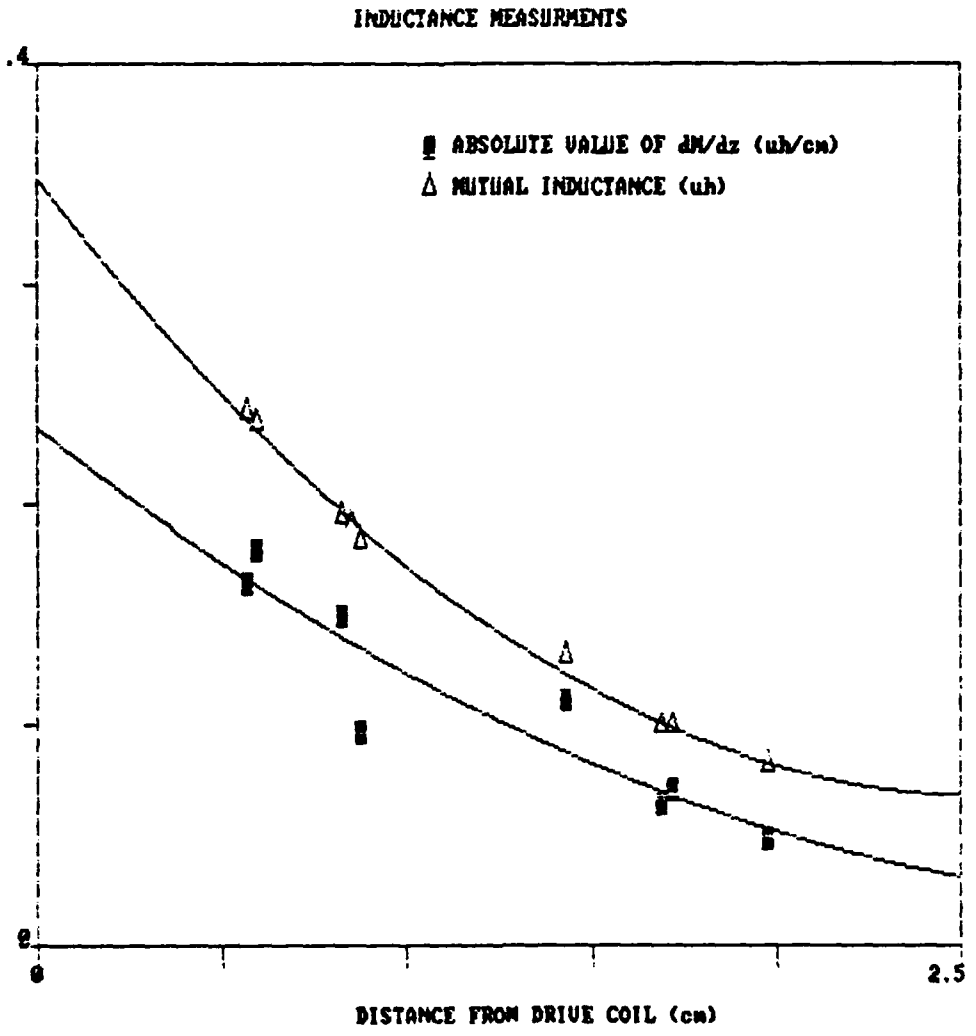

Figure 4.13: Mutual Inductance and Mutual Inductance Gradient

CHAPTER 5

NUMERICAL MODEL

Experimental tests of pulsed induction acceleration can be expensive, time consuming and, in general, provide only a limited amount of information. To obtain a complete understanding of this acceleration process, the equations governing pulsed induction acceleration must be solved. These equations are fairly easy to derive but, their solutions are not easily obtained. One way they can be solved is numerically. This chapter discusses the numerical method by which the governing differential equations of pulsed induction acceleration have been solved. Included in this numerical analysis are the temperature and phase dependent properties of the drive coil and the projectile coil as well as the magnetic and kinematic effects unique to this form of energy transfer.

5.1 Approach and Technique

The governing equations can be broken up into four main areas; electrodynamic properties such as capacitor voltage, coil currents and induced voltages, magnetic coupling parameters of the drive coil/projectile coil system, kinematics of the accelerating projectile coil, and material temperature and phase

dependent properties such as resistivity and specific heat. By splitting the equations up in this fashion, a numerical model can be formed which iteratively analyses each of these areas in turn and adjusts accordingly.

5.1.1 Simplified Equations

As shown in the previous chapter the electrodynamic equations are simply the equations derived by summing the voltages around the drive coil and projectile coil circuit loops and setting them equal to zero. That is:

$$Vd=IdRd+Ld(dId/dt)+Mpd(dIp/dt)+Ip(dMpd/dz)v \qquad (5.1.1)$$

$$Vp=IpRp+Lp(dIp/dt)+Mpd(dId/dt)+Id(dMpd/dz)v \qquad (5.1.2)$$

and from the constitutive relationships:

$$dVd/dt=Id/C \qquad (5.1.3)$$

and

$$Vp=0 \qquad (5.1.4)$$

These equations can be greatly simplified by writing them in terms of magnetic flux rather than circuit potentials. By noting that the circuit potentials are related to the change in magnetic flux through the drive coil and projectile coil

$$dYd/dt = Vd-RdId \qquad (5.1.5)$$

and

$$dYp/dt = Vp - RpIp \qquad (5.1.6)$$

equations 5.1.1 and 5.1.2 become

$$Yd = LdId + MpdIp \qquad (5.1.7)$$

and

$$Yp = LpIp + MpdId \qquad (5.1.8)$$

When these two equations are combined with the constituative equations 5.1.3 and 5.1.4 and the equation of motion

$$dv/dt = (1/m)(dMpd/dx)IpId \qquad (5.1.9)$$

a simple, explicit numerical scheme can be used to obtain time dependent solutions of coil currents, capacitor voltages, and projectile velocities. Further information such as back EMFs, resistive voltage drops, and induced voltages can be obtained by substituting the drive coil and projectile coil currents into equations 2.1.3 and 2.1.4. In the same manner by using the equation

$$mCp(dT/dt) = Ip^2 Rp \qquad (5.1.10)$$

the projectile temperature can be calculated.

5.1.2 Numerical Schemes

There are many different ways to numerically solve these sets of equations ranging from simple first order schemes such as the Euler forward and the Euler backward methods to much higher order schemes such as spectral and Rung Kutta methods. A detailed analysis of all the different methods of solution and their advantages and disadvantages is beyond the scope of this paper and will not be presented here. However, if the reader is interested in the details of other numerical schemes, there are several well written monographs listed in the reference section of this thesis.

As will be shown later, the greatest problem in trying to solve the governing differential equations is accurately deriving the magnetic coupling parameters, Mpd, dMpd/dx, Lp, and Ld. These parameters account for the the majority of calculation time and generate an appreciable amount of error. Because of this and because the governing differential equations are essentially a simplified explaination of the acceleration process, it is pointless to solve these equations with a highly accurate but complex numerical scheme. A simple explicit first order scheme can easily be implemented and is sufficiently accurate to predict the performance of a pulsed inductive system. One such scheme is the Euler forward method.

5.1.3 Euler Forward Method

The Euler forward method is a very simple and straight forward scheme to program. It is based on the assumption that the equation

$$dw/dt = R \tag{5.1.11}$$

can be written as

$$(w^n - w^{n-1})/\Delta t = R \tag{5.1.12}$$

where the superscript n+1 indicates the value of the variable at time t+^t and the superscript n indicates the value of the variable at time t.

The actual equation being solved by this scheme can be found from Taylor series expansion.

$$w^{n+1} = w^n + (\Delta t)w'^n + (\Delta t^2/2)w''^n + (\Delta t^3/3)w'^m + \ldots . O(\Delta t^4) \tag{5.1.13}$$

By substituting this expression into equation (5.1.12) we arrive at the equation

$$dw/dt + (\Delta t/2)w'' + \ldots O(\Delta t^2) = R \tag{5.1.14}$$

This scheme was one of the first numerical schemes used to solve ordinary differential equations. Although it is only a first order scheme, the time saved in programming it easily justifies its use.

5.2 Parametric Approximations

Obtaining accurate values of the magnetic coupling parameters and values of the temperature dependent resistivity properties of the coil materials are the two greatest difficulties encountered when attempting to solve the governing equations of pulsed inductive acceleration.

5.2.1 Self Inductance

Before digital computers, self inductance values of coils were found by interpolating from a series of tables and formulas. Although this method can be quite accurate, it is a laborious task that is best avoided if possible. The present availability of digital computers has made it possible to obtain self inductance values in a matter of seconds.

To understand how these values are numerically calculated, consider the coil in figure 5.1.

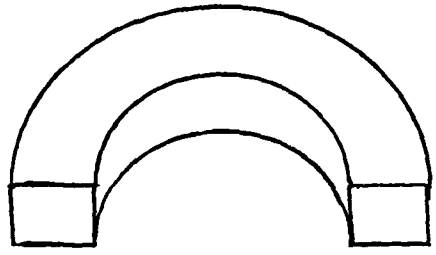

Figure 5.1: Single Turn Coil

The energy stored in this coil can be found from the equation

$$U = (1/2)LcIc^2 \qquad (5.2.1)$$

where

Lc is the coil inductance

and

Ic is the current in the coil

If the coil is broken up into a number of smaller coils such as the coil in figure 5.2, The total energy stored can be written as

$$U = \sum_{i=1}^{N}\sum_{j=1}^{N}(1/2)MijIiIj \qquad (5.2.2)$$

where N is the total number of subcoils and

$$Ii = Ij = Ic/N \qquad (5.2.3)$$

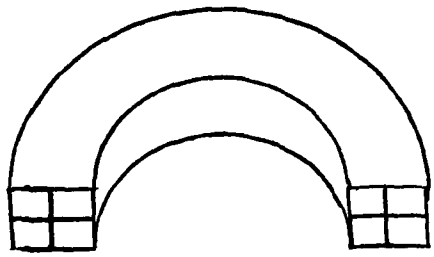

Figure 5.2: Subdivided Coil

The mutual inductance of any two subcoils is equal to the

expression

$$Mij = 2u(RiRj/m)^{1/2}[(1-m/2)K(m)-E(m)] \qquad (5.2.4)$$

where Ri and Rj are the mean radial dimensions of subcoils i and j, and

$$m = 4(RiRj)/[(Ri+Rj)^2 + Z^2] \qquad (5.2.5)$$

K(m) and E(m) are elliptical integrals of the first and second kind and can be calculated numerically using their polynomial approximations (see Appendix B).

Equation 5.2.4 only holds true if i is not equal to j. However, for small square crossectioned subcoils, Mii can be approximated as

$$Mii = Lii = 1.0E\text{-}09*G*(Ro+Ri)/2 \qquad (5.2.6)$$

where

Ro is the outer radius of the subcoil

Ri is the inner radius of the subcoil

and

$$G = 4[.5*s^2(1+(1/6)\ln(8/s^2) - 0.84834+0.2041s^2] \qquad (5.2.7)$$

$$s = (Ro-Ri)/(Ro+Ri) \qquad (5.2.8)$$

Setting equation 5.2.2 equal to equation 5.2.1 we obtain our final expression for the self inductance of a coil,

$$Lc = (1/N)^2 \sum_{i=1}^{N} \sum_{j=1}^{N} Mij \qquad (5.2.9)$$

AD-A160 137 METALLIC INDUCTION REACTION ENGINE(U) ELECTROMAGNETIC 2/2
LAUNCH RESEARCH INC CAMBRIDGE MA P P MONGEAU ET AL.
20 DEC 84 EML-85-AF001 AFOSR-TR-85-0773
UNCLASSIFIED F49620-83-C-0126 F/G 21/3 NL

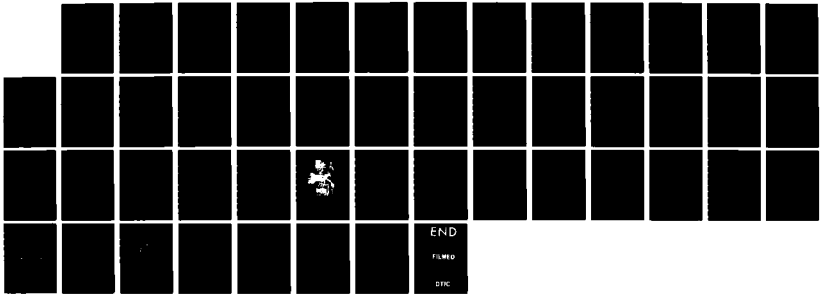

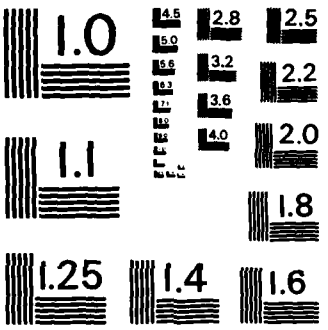

As shown by the slope of the log/log plot in figure 5.3, this method of calculation is first order accurate with respect to the number of subdivisions a coil is broken up into.

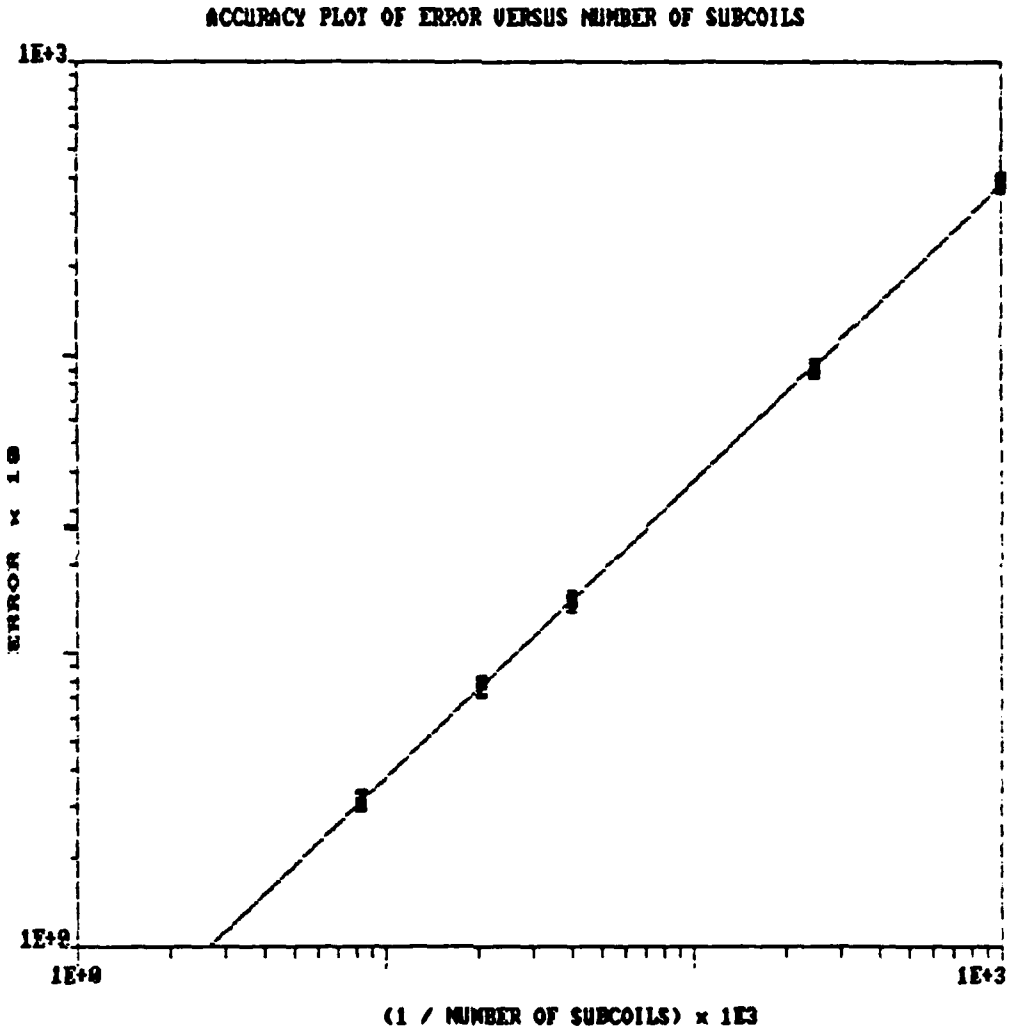

Figure 5.3: A Log/Log Accuracy Plot of Self Inducta ce

5.2.2 Mutual Inductance

The mutual inductance between two coils can be calculated using a method similar to the one used to calculate the self inductance of a single coil. Consider two coils subdivided into smaller coils totaling I and J respectively (see figure 5.4).

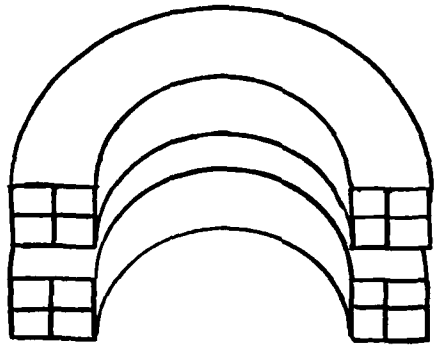

Figure 5.4: Subdivision of Two Coils

The energy stored in these two coils due to the mutual inductance between the subcoils is:

$$U = \sum_{i=1}^{I} \sum_{j=1}^{J} (1/2) M_{ij} I_i I_j \qquad (5.2.10)$$

where

I is the total number of subdivisions in coil one

and

J is the total number of subdivisions in coil two

If this equation is set equal to the macroscopic equation for the

energy stored by the mutual inductance between two coils

$$U = (1/2)M12I1I2 \qquad (5.2.11)$$

where

I1 is the current in coil one

I2 is the current in coil two

and

M12 is the mutual inductance between coil one and coil two

and by noting that Mij equals Mji our equation for the mutual inductance between two coils becomes apparent:

$$M = (1/IJ)\sum_{i=1}^{N}\sum_{j=1}^{N} Mij \qquad (5.2.12)$$

This method, like our method for calculating self inductance, is first order accurate.

5.2.3 Material Resistivity

Aside from the magnetic coupling parameters L and M, changes in material resistivity have the greatest effect on the governing equations of pulsed inductive acceleration. This nonlinear behavior of materials is a complex phenomenon to predict. Several different methods can be used to approximate this behavior as a function of temperature. However, approximations based on polynomial fitting of experimental data often have problems due to the discontinuous effects that occur

when a material undergoes a phase change. To avoid this problem, a simple "look up" table of experimental values of various material properties is often preferable to the more complex but storage efficient method of polynomial fitting.

5.2.4 Skin Depth

Related to the effect of changing material resistivity is the skin depth effect. When a conductor is placed in a rapidly changing magnetic field, the magnetic field will only penetrate the surface of the conductor to a limited extent. The depth of this penetration is known as the skin depth.

In pulsed induction acceleration, a rapidly changing magnetic field is used to induce a current in the projectile coil. Since the depth of penetration of this magnetic field is limited to the skin depth, the current induced by this field is also essentialy limited to the skin depth. This effect results in a much higher coil resistance then expected if skin depth is not considered.

Predicting this effect for numerical purposes is a complex problem. However, it has been found that for a typical system the average skin depth can be approximated by the equation

$$\delta = (2/3)[(LdC) / \sigma \pi u]^{1/2} \qquad (5.2.13)$$

where

δ is the skin depth

Ld is the drive coil inductance

and

σ is the conductivity of the drive coil material

5.3 Resolution

As with all finite difference schemes, the Euler forward method is only able to resolve waves which have periods greater then two times the smallest time step used. The reason for this can be seen in figures 5.5(a) and 5.5(b).

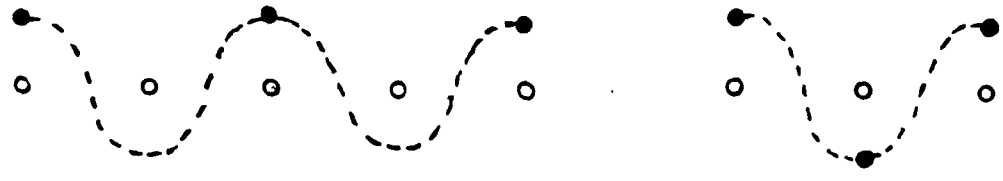

$T = 2\Delta t$ $T = \Delta t$

(a) (b)

Figure 5.5: Resolution Errors Incurred by Time Step

If a wave has a period less then or equal to two times the time step Δt, it will exhibit a dispersive type of error. That is, any change in phase in these waves will appear to happen at a different rate then it actually does. Waves with periods less

then or equal to the time step itself exibit a second type of error. These waves are either misinterpreted as having larger periods or as in figure 5(b), they are interpreted as being constant. This form of error is commonly refered to as an "aliasing error". Both aliasing errors and dispersion errors often go undetected. However, in the first order Euler forward scheme used to solve the equations of pulsed induction acceleration, these errors can cause the algorithm to become unstable and display obviously incorrect results. In general, it is best to keep the time step much smaller then the discharge period of the drive coil circuit. This insures that any small fluctuations that might exist between the drive coil circuit and the projectile coil will not go undetected.

5.4 Agreement with Experimental Results

As was shown earlier, the Euler forward method used to solve the governing equations of pulsed induction acceleration is first order accurate. That is, assuming roundoff errors are small, the difference between the exact solution of the equations and the numerical solution is directly proportional to the size of the time step used. However, until now there has been no indication that the equations derived in chapter two actually represent the physical processes taking place in a pulsed induction system. This numerical method would be useless unless there was at least some correllation between the numerically obtained results and the results observed in a typical system. As it turns out,

numerically obtained values of final velocity are, on the average, within 15% of the values observed experimentally (see Table 5.1).

Table 5.1: Comparison of Numerical Velocity with Experimental Velocity

	Initial Cap. Voltage	Measured Velocity	Calculated Velocity	Percent Error
Coil #1				
Al	9 kV	545 m/s	495 m/s	9.2 %
	9	502	495	1.4
	9	498	495	0.6
	9	436	495	13.5
	10	567	565	0.4
	10	550	565	2.7
	10	532	565	6.2
	10	515	565	9.6
	11	617	635	2.8
	13	725	776	7.0
	14	754	847	12.3
Coil #2				
Al	10 kV	365 m/s	331 m/s	9.3 %
	13	440	463	5.2
Coil #3				
Al	7 kV	576 m/s	451 m/s	21.7 %
	7	330	451	36.7
	8	485	493	1.7
	9	640	560	12.5
Cu	6	207	258	24.6

It is impossible to fully assess the accuracy of this numerical scheme over the entire range of interest. It is assumed, however, that this scheme is at least sufficiently accurate to provide a general insight into the physical processes of pulsed induction acceleration.

CHAPTER 6

SCALING AND PARAMETRIC TRADEOFFS

Experimental tests and numerical simulations indicate that the operating mechanisms of the metallic induction reaction engine are highly interdependent. Because of this, design optimization and analysis of a complete system is a very difficult task.

In this chapter, the operating mechanisms of the metallic induction reaction engine and their interdependencies are discused. A model is derived as an aide to this discusion. From this model and from the experimental and numerical studies presented in the previous chapters, general statements are made about material properties and magnetic coupling relationships.

6.1 Basic Model

Consider a simple magnetic acceleration system where a conductor is accelerated by a magnetic field with a constant density, Bo, (see figure 6.1). This is an idealized system since in practice the magnetic field density is dependent on many different parameters and is definitly not a constant. However, a system such as this provides a useful model for analysing material parameters and coupling paramters independent of their relationship with the discharge circuit.

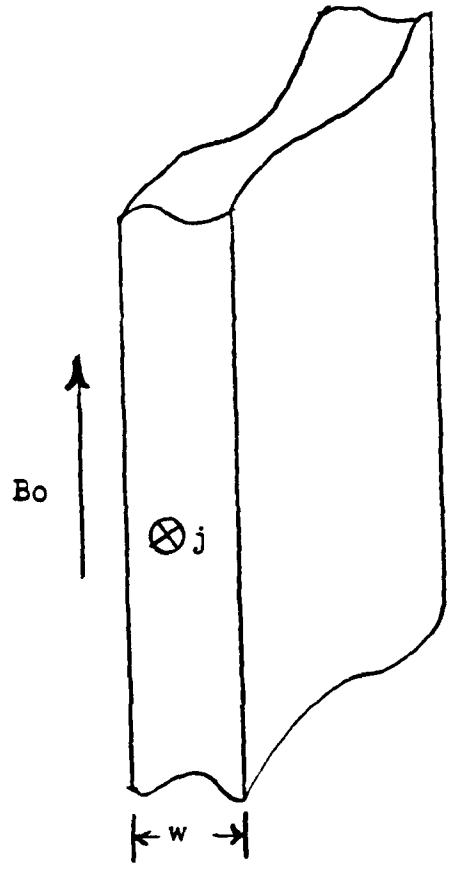

Figure 6.1: Constant Density Magnetic Field Model

Assuming that magnetic flux is conserved, the equation governing the motion of this system is

$$dp(d\,z/dt\,) = B^2/2\mu \qquad (6.1.1)$$

where $B^2/2\mu$ is the magnetic pressure exerted on the conductor.

Since the conductor is being accelerated by a constant magnetic field, this equation leads to

$$v = dz/dt = B_o^2 t/2\mu\rho w \qquad (6.1.2)$$

and

$$z = Bo^2 t^2/4\mu\rho w \qquad (6.1.3)$$

If we furthur assume that there is a finite distance, Δz, in which the conductor is magnetically coupled to the accelerating circuit, then there is a coupling time, to, equal to the equation

$$to = 2\sqrt{\mu\Delta z\rho w}/Bo \qquad (6.1.4)$$

Therefore, the maximum velocity that is attained by the conductor is simply

$$vo = Bo\sqrt{\Delta z/\mu\rho w} \qquad (6.1.5)$$

Note that because this equation is indepedent of the type of circuit used to create a magnetic field, it represents a basic scaling relationship of all magnetic accelerators.

6.1.1 Thermal Velocity

If it is assumed that the conductor is thin compared to its current skin depth, then this simple constant density magnetic field system can be analysed in terms of the conductor's thermodynamic properties.

The current density, j, of a thin conductor is relatively uniform. It can be related to the accelerating magnetic field by the expression

$$jd = i = -Bo/\mu \tag{6.1.6}$$

where i is the current per unit width of the conductor.

Substituting this into equation 6.1.1 and integrating, we obtain the maximum velocity of the conductor

$$v = \mu w J/2\rho \tag{6.1.7}$$

where J is the current integral equal to the expression

$$J = \int_0^{t_2} j^2\, dt = \int_{T_0}^{T} \sigma C\rho dT \tag{6.1.8}$$

If this velocity equation is set equal to equation 6.1.5, an expression for the conductor thickness, w, is obtained where

$$w = (4Bo^2\, \rho \Delta z/\mu^3 J^2)^{1/3} \tag{6.1.9}$$

This can be substituted back into equation 6.1.7 to yield an expression for the maximum conductor velocity in terms of the accelerating magnetic field parameters and the material properties of the conductor. The velocity written in this form is commonly known as the thermal velocity of the conductor where

$$vth = (B\sigma^2\, \Delta z\, J/2\rho^2)^{1/3} \tag{6.1.10}$$

If the conductivity of the conductor is fairly constant with

temperature, then the current integral, J, is approximately equal to the change in enthalpy of the conductor times it's conductivity

$$J = \sigma \Delta H \tag{6.1.11}$$

and equation 6.1.10 becomes

$$vth = (B\delta^2 \Delta z \sigma \Delta H / 2\rho^2)^{1/3} \tag{6.1.12}$$

6.1.2 Efficiency

The efficiency of this simple model can be derived from the equation

$$W = B\delta^2 \Delta z / 2\mu \tag{6.1.13}$$

where W is the magnetic work done to the conductor per unit area exposed to the magnetic field. Combining this with the energy lost due to ohmic heating, w^H, the efficiency equation is simply

$$\eta = W/(W+w\Delta H) \tag{6.1.14}$$

This can be written in terms of a nondimensional parameter, O, such that

$$\eta = 1/[1+(1/\theta)] \tag{6.1.15}$$

where

$$\theta = B\delta^2 \Delta z / 2\mu w \Delta H \tag{6.1.16}$$

Substituting equations 6.1.9 and 6.1.11 into 6.1.16, the expression for θ becomes

$$\theta = (Bo^{4} \Delta z^{2} \sigma / 32 \rho \Delta H)^{1/3} \qquad (6.1.17)$$

or in terms of the thermal velocity

$$\theta = v^{2} \rho / 2 \Delta H \qquad (6.1.18)$$

We now have a set of equations, 6.1.9, 6.1.12 and 6.1.18, that describe the relationships between all the parameters of this constant magnetic field model. These relationships have been plotted in terms of the specific impulse, vth/g, for several popular metals at their vaporization point (see figures 6.2 through 6.5).

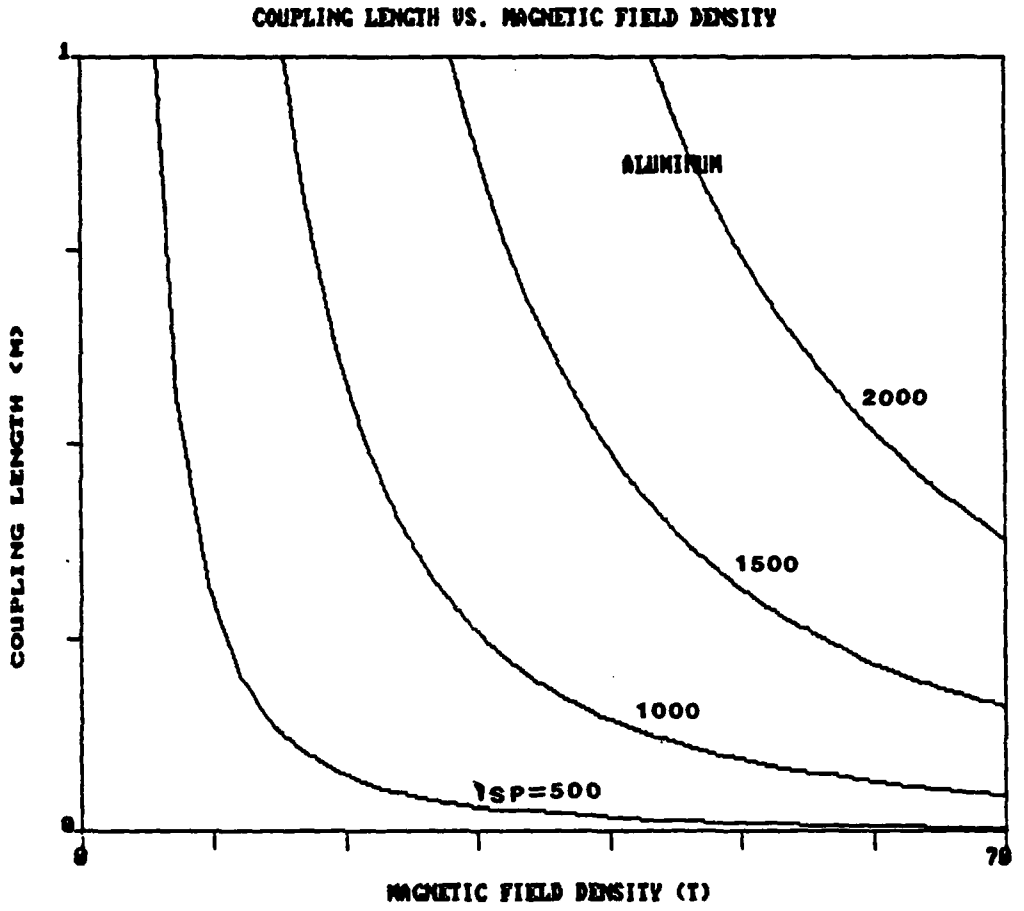

Figure 6.2: Aluminum Reaction Mass

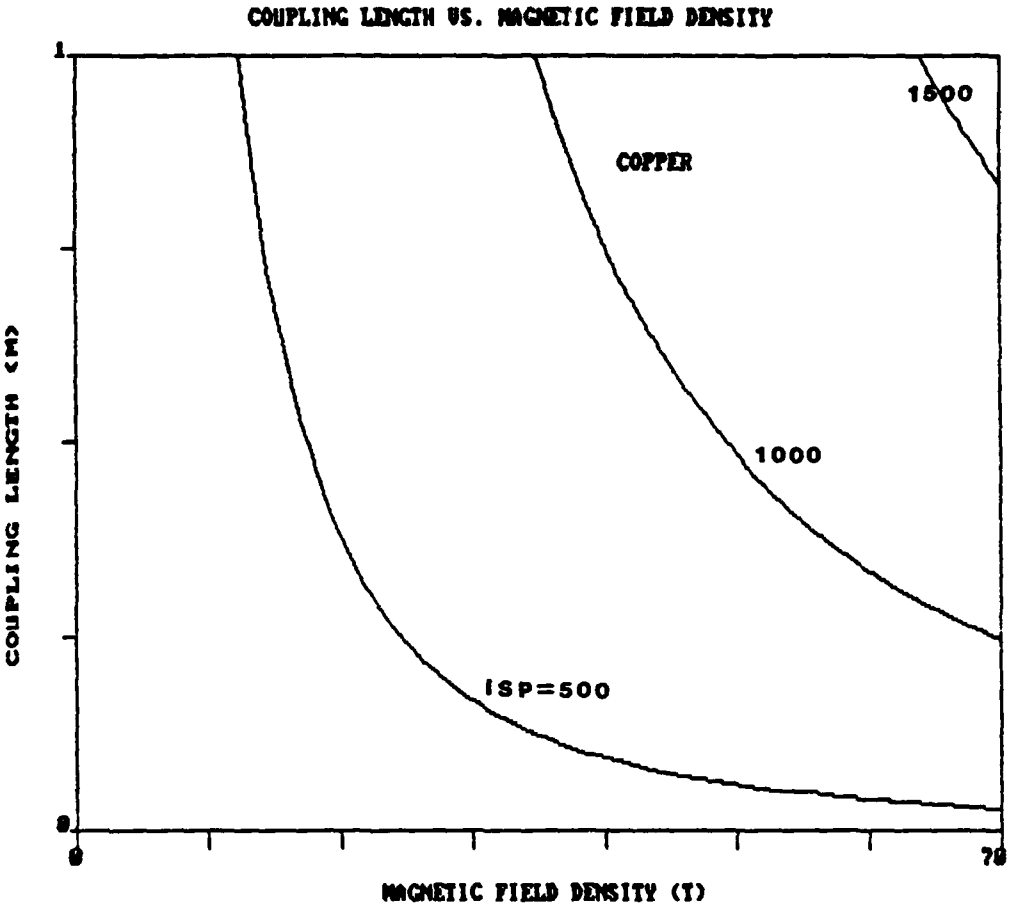

Figure 6.3: Copper Reaction Mass

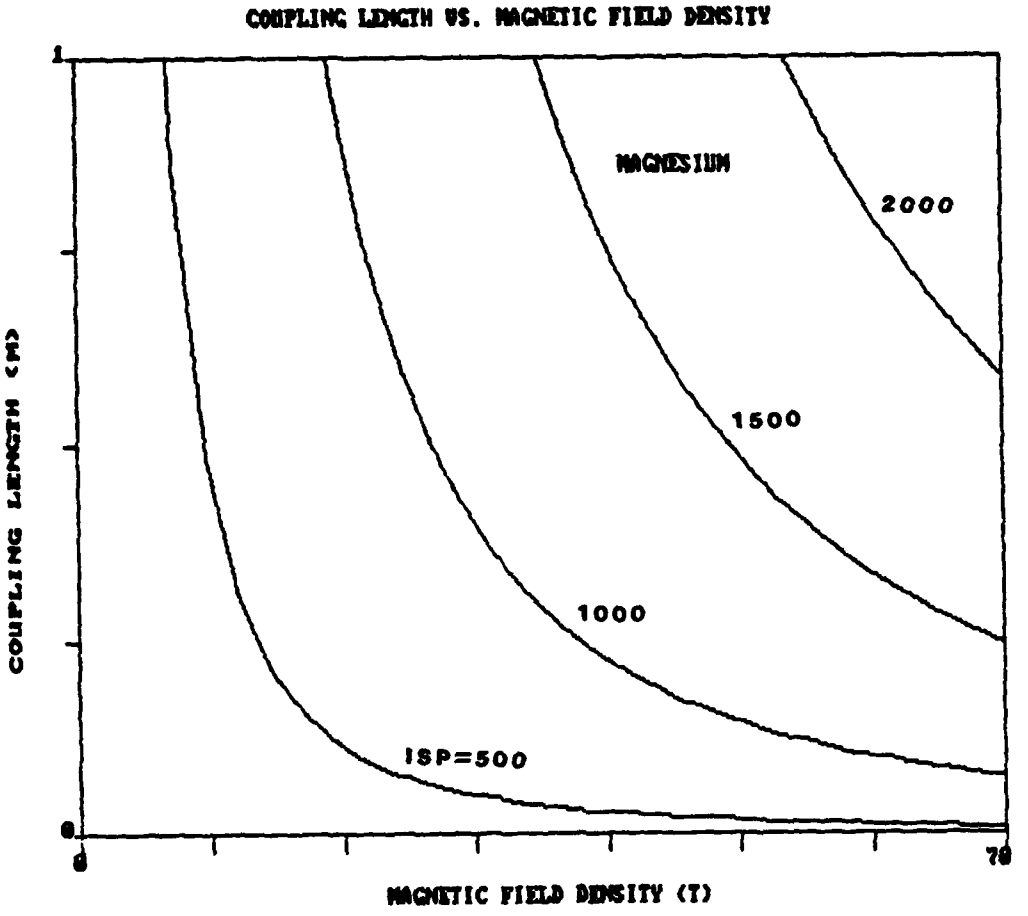

Figure 6.4: Magnesium Reaction Mass

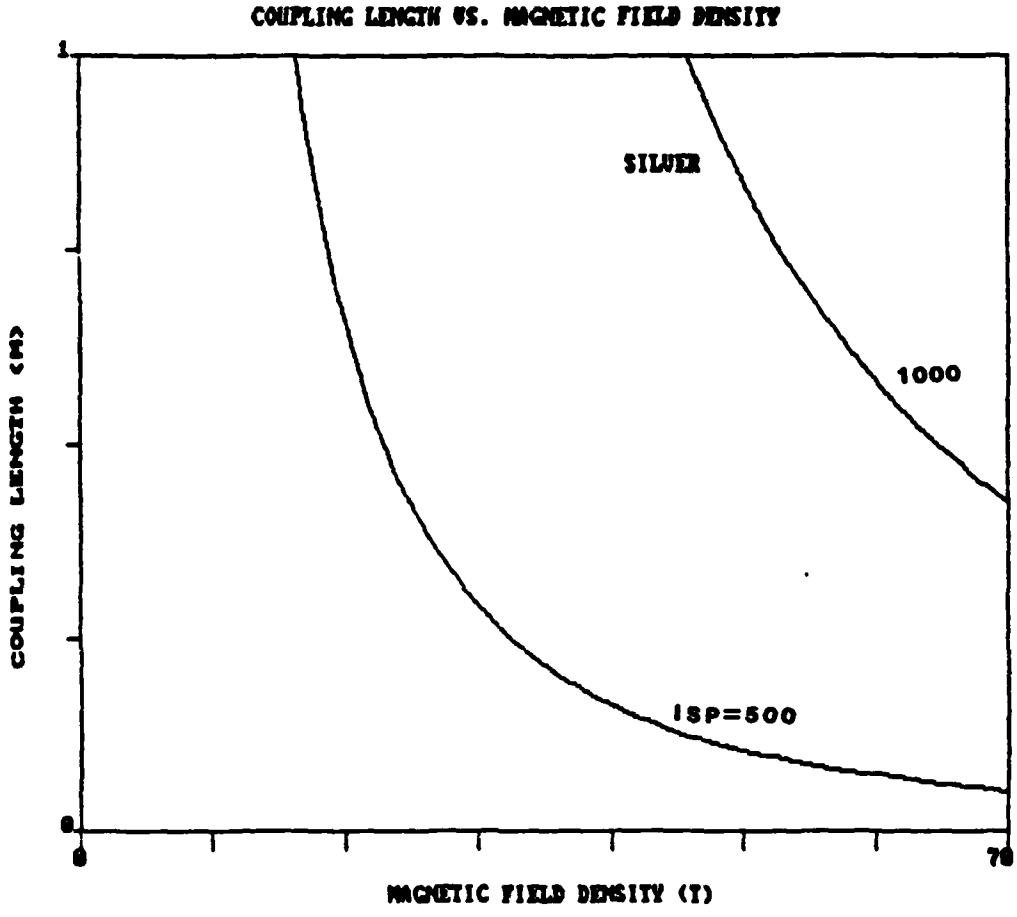

Figure 6.5: Silver Reaction Mass

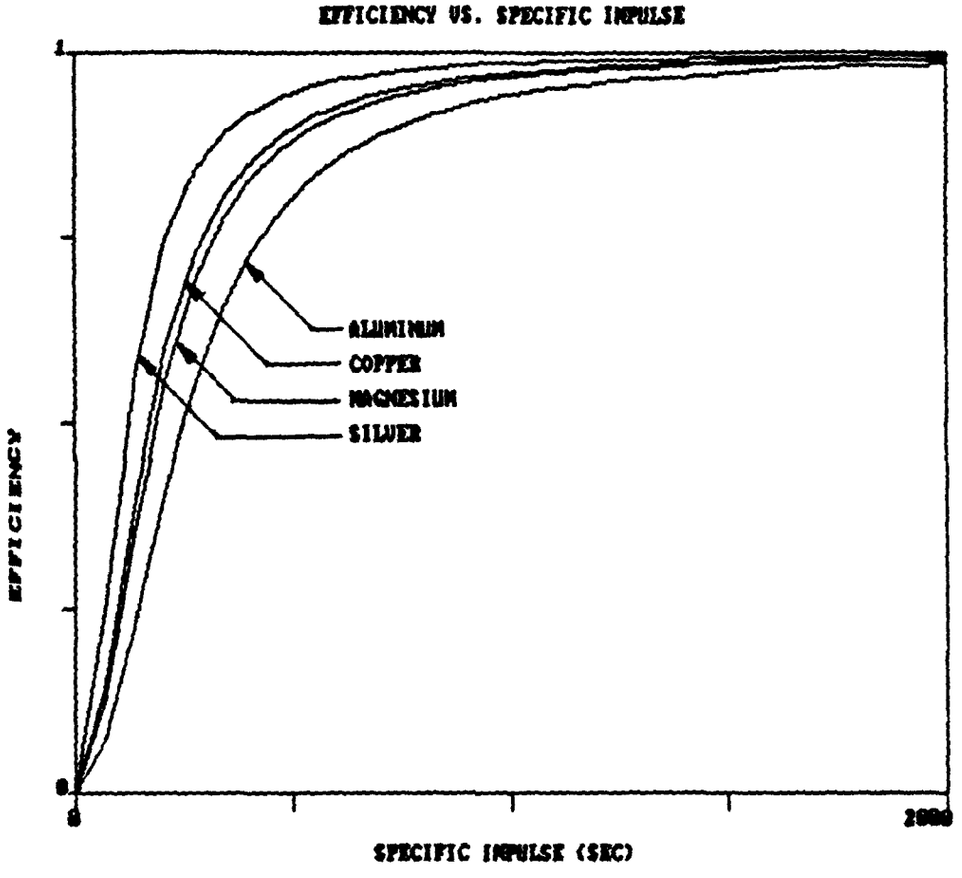

Figure 6.6: Acceleration Efficiency of Several Conductors

6.2 Inductive Model

The relationship between the parameters of the metallic

induction reaction engine are not as simple as the ones described in our basic model. The same general trends are still exhibited but nonlinear magnetic coupling characteristics and electrical discharge characteristics cannot be ignored.

6.2.1 Magnetic Coupling

In an actual projectile coil/ drive coil system, the rate of energy input is closely related to the magnetic coupling between the two coils. As shown by the effective inductance and resistance of the drive circuit, this relationship is proportional to the square of the mutual inductance

$$Leff = Ld[1-(Mpd^2/LdLp)] \tag{4.3.6}$$

and

$$Reff = Rd+RpMpd^2/Lp^2 \tag{4.3.7}$$

The kinetic energy output of the this system can also be related to the mutual inductance

$$mv^2/2 = \int_0^{\infty} Fdz = \int_{M_o}^{0} IpId\ dMpd \tag{6.2.1}$$

Note, however, that the magnetic force exerted on the projectile coil is a function of the mutual inductance gradient and not the mutual inductance

$$F = IpId\ dMpd/dz \tag{2.1.1}$$

For a particular system with a finite coupling length, this can be a problem. A large force is needed to accelerate the projectile coil to a high velocity within the coupling length. To

accomplish this, the mutual inductance gradient must also be large. This implies that the projectile coil rapidly decouples from the drive coil. Unfortuantely, the conversion of electrical energy to kinetic energy can only take place while the two coils are magneticly coupled and, therefore, the time which useful energy can be put into the system rapidly decreases as the projectile coil velocity increases (see figure 6.7).

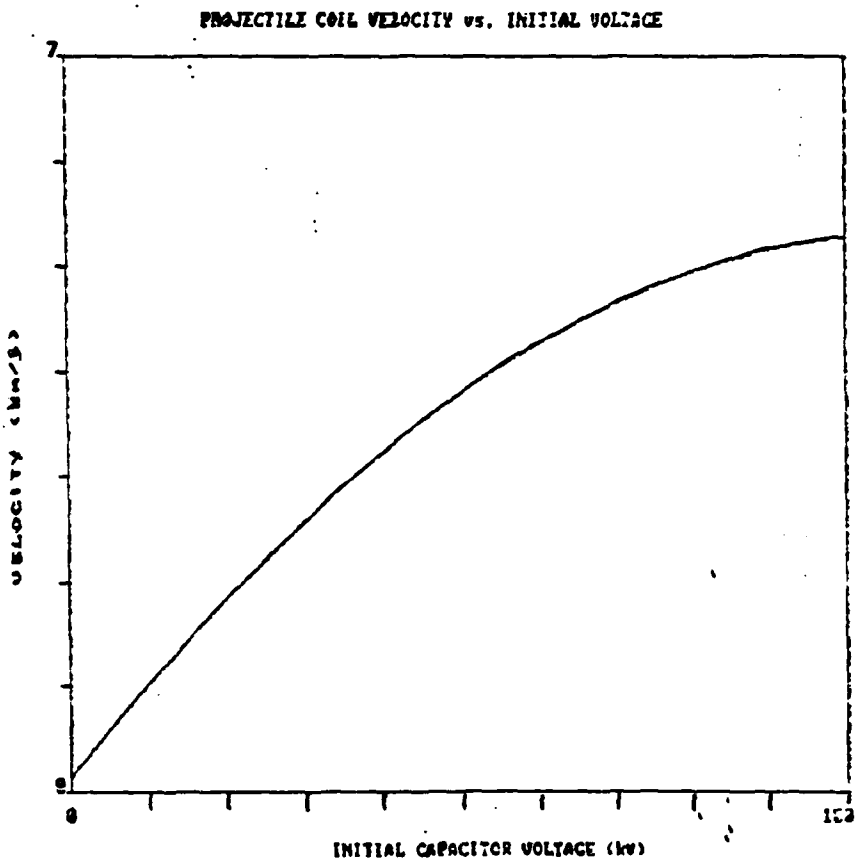

Figure 6.7: Projectile Coil Velocity Vs. Initial Capacitor Voltage

Most projectile coil/drive coil systems have a coupling length roughly equal to the mean radius of the two coils. Within

this coupling length, the mutual inductance and the mutual inductance gradient drop to a small fraction of their original values. In the constant magnetic field model, an increase in coupling length results in an increase in coupling time and projectile coil velocity. However, this relationship is more complex in an inductive system. Increasing the coupling length by expanding the mean radii of the coils, results in an increase in the impedance of the drive circuit (see figure 6.8). Therefore, although the length of time the projectile coil and drive coil remain coupled increases, the time it takes to deposit a unit amount of energy into the system also increases.

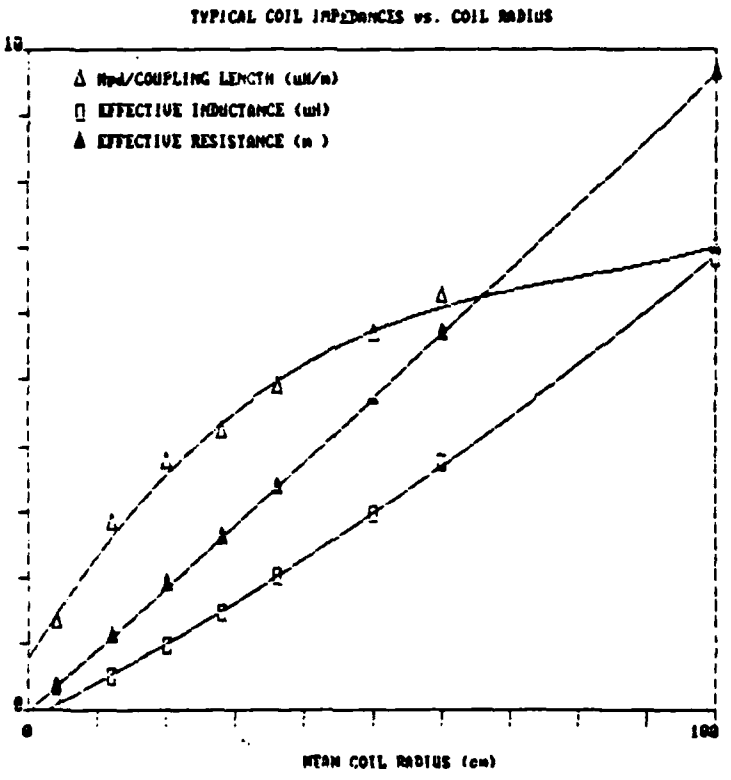

Figure 6.8: Circuit Impedance

6.2.2 Back EMF

The back EMF voltages are apparent voltages that oppose the current in the projectile coil and drive coil circuits. These voltages are the result of the projectile coil decoupling from the drive coil. In the drive coil circuit, the back Emf voltage can be expressed as

$$Vbd = Ip(dMpd/dz)v \qquad (6.2.2)$$

Similarly, in the projectile coil circuit, the back EMF voltage is

$$Vbp = Id(dMpd/dz)v \qquad (6.2.3)$$

These voltages are in effect impedance terms which limit the rate of energy flowing into the projectile coil and drive coil. Notice that they increase with the coil currents, the projectile velocity, and the mutual inductance gradient. It is not surprising that the back EMF voltages are the dominant impedance terms in a high performance system (see figure 6.9).

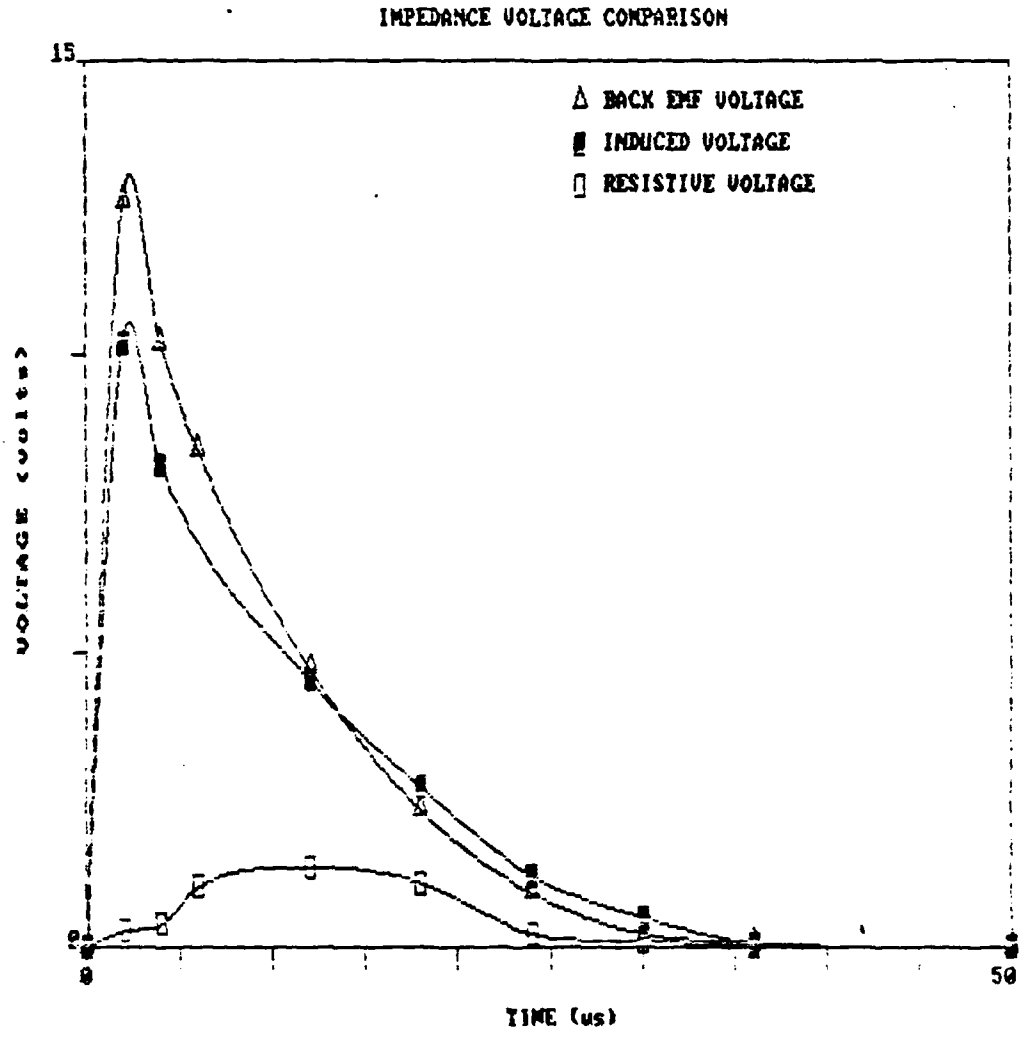

Figure 6.9: Voltage Parameter Comparison

6.2.3 Resistance

Unlike ionized gases, the resistance of metallic conductors increases with temperature. The metallic induction reaction

engine uses this property to its advantage. When the drive coil and projectile coil are closely coupled and the accelerating force is large, the resistance of the metallic projectile coil is low. Then, as the projectile coil decouples from the drive coil, ohmic heating raises it's temperature and resistance. The temperature eventually reaches the vaporization point of the material and the current in the coil rapidly decays. Because the resistance is lowest during the initial part of the acceleration process, a greater amount of energy can be deposited into the system then if the projectile coil were formed from an ionized gas. Unfortunately, the resistance of even highly conductive materials can significantly reduce the perfomance of a pulsed inductive system. The three curves ploted in figure 6.10 show the effect that resistance has on the velocity of an aluminum projectile coil. The first curve is an ideal case where the coil has no resistance. The second shows the effect of a constant resistance and the third is the case where the resistance of the projectile coil increases with temperature.

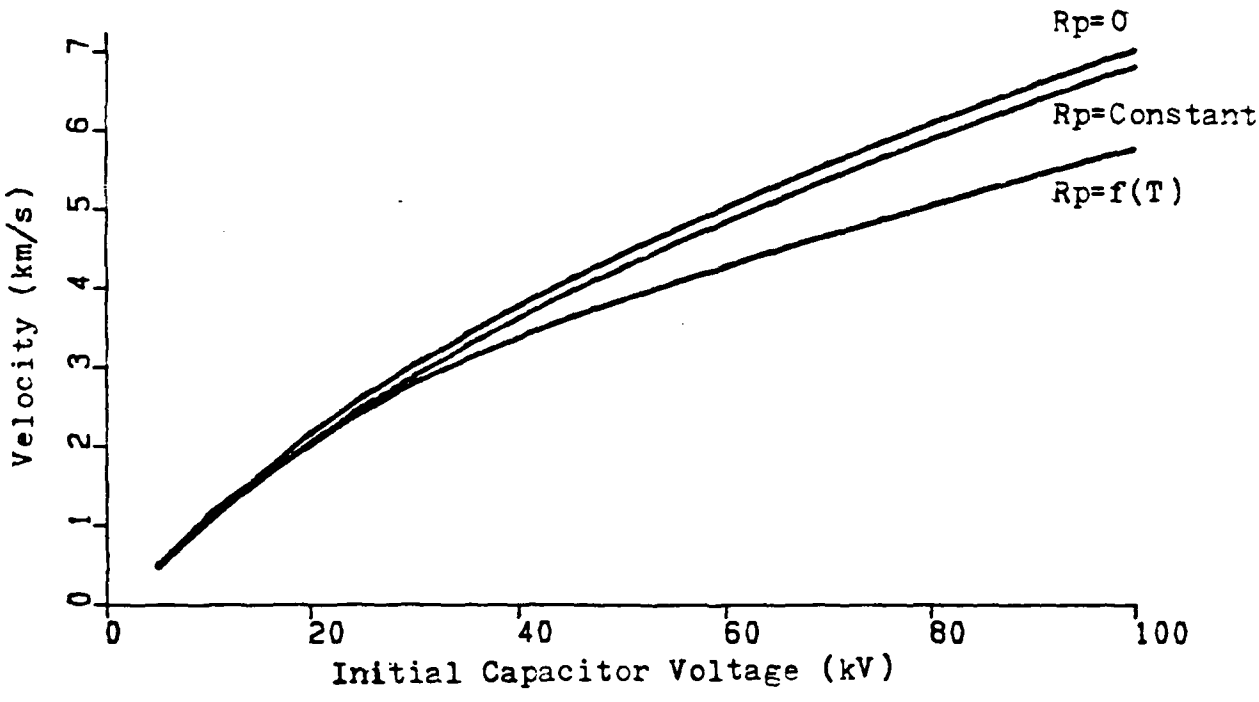

Figure 6.10: Resistance Effects on Aluminum Reaction Mass

6.3 Material Constraints

The performance of a metallic induction reaction engine system is not as limited by geometric constraints as it is by the material constraints of it's various components. There are three basic types of material constraints that should be considered, thermal, structural, and electrical.

6.3.1 Thermal

Stored energy that is not converted to kinetic energy during

the discharge cycle of the metallic induction reaction engine eventually turns up as heat in the drive coil, projectile coil and leads of the system. In the projectile coil, this ohmic heating effect is, to some extent, beneficial since it can cause the projectile coil to vaporize and thus, avoid the problem of a solid exhaust trail. However, ohmic heating of the drive coil and leads of the system can cause them to melt and fail structurally. Fortunately, the mass of these components is not as crucial as it is for the projectile coil and therefore, they can be designed to have a much lower temperature rise during the discharge cycle.

As an example, the thermal properties of some popular conducting materials are shown in table 6.1. Notice that the current integral given in equation 6.1.8 relates current to material temperature and is therefore, a good indication of a material's resistance to ohmic heating.

Table 6.1: Thermal Properties of Conductors

Material	Cv cal/g °k	Mp °k	Bp °k	Jmp A^2 s/cm	Jbp A^2 s/cm
Aluminum	0.23	933	2740	3.3x108	5.9x108
Copper	0.45	1356	2840	6.5	12.4
Magnesium	0.25	921	1363	0.7	1.6
Silver	0.056	1253	2485	4.9	10.0

Cv specific heat at 300°k, Mp melting point, Bp boiling point, Jmp current integral at melting point, Jbp current integral at boiling point [Knoepfel 70], [Ashby 80],

6.3.2 Structural

The magnetic forces generated in a drive coil during a discharge cycle can be astronaumical. Not only is there a force accelerating the projectile coil, there is also a large internal magnetic force which the drive coil must contend with. To understand the relationship between the material characteristics of a drive coil and the maximum magnetic field that can be generated, consider the thin cylindrical coil in figure 6.11.

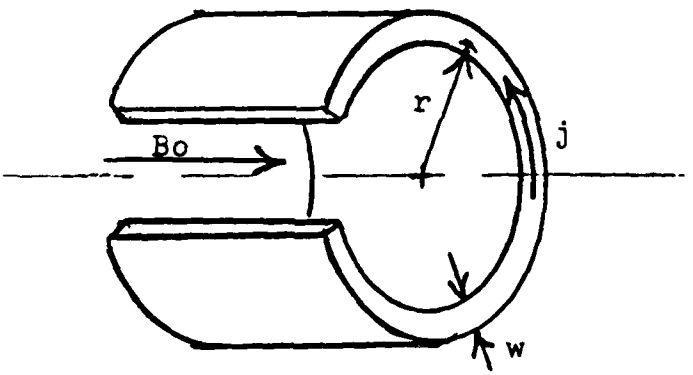

Figure 6.11: Cylindrical Drive Coil

The magnetic field generated by a current density, j, in the coil can be expressed from equation 6.1.6 as

$$Bo = -\mu w j \qquad (6.3.1)$$

Therefore, the magnetic pressure being exerted on this coil is

$$Pmag = \mu w^2 j^2/2 = Bo^2/2\mu \qquad (6.3.2)$$

This magnetic pressure is contained by a tensile stress, Qts. By equating the sum of the forces around the coil to zero, we obtain

$$Qts = Bo^2 r/2\mu w \qquad (6.3.3)$$

where r is the mean radius of the coil.

A similar relationship exists for the compressive stress in a thin face coil accelerating a projectile coil

$$Qc = Bo^2/2\mu \qquad (6.3.4)$$

As can be seen by these two equations, 6.3.3 and 6.3.4, the maximum magnetic field that can be generated by a drive coil is limited by the tensile and compressive strengths of the material it is made from. It should be noted that the largest repeatable magnetic field ever generated was about 100 tesla. This is equivalent to containing a pressure of 600,000 pounds per square inch. For reaction engine applications where size and weight are important, it is believed that a magnetic field of about 40 tesla is the maximum that can be safely contained. Table 6.2 contains some of the structural properties of various conducting materials.

Table 6.2: Structural Properties of Conductors

Material	R uΩ-mm	p Mg/m	E GN/m	Qy MN/m	Qts MN/m
Aluminum	27	2.7	69	40	200
Al alloys		2.8	73	300	500
Brass	62	8.0	110	450	600
Be-Copper		2.0	230	160	500
Copper	18	8.9	124	60	400
Cu alloys		8.0	130	700	800
Magnesium	45		40	80	200
Nickel	78	8.9	210	70	400
Ni alloys		9.0	220	1200	1500
Mild Steel	98	7.8	296	220	430
St. Steel		7.7	190	320	900

R resistivity, p density, E Young's modulus, Qy yield strength, Qts tensile strength [Ashby 80].

6.3.3 Electrical

All pulsed inductive systems such as the metallic induction reaction engine use insulating materials to restrict current to desired paths. When an insulating material fails, a high temperature arc forms. Gas pressure from the arc can be so severe that it will literally explode the materials surounding it. The maximum voltage that a material can standoff before this electrical breakdown occurs is known as the dielectric strength of the material. The properties of some insulating materials are shown in table 6.3. Notice that the structural strengths of some of these materials are greater then the conducting materials shown in table 6.2. Because of this, many of them can be used

for structural reinforcment as well as insulators. However, the large dynamic loads generated by pulse coils usually require that the difference in the modulus of elasticity between the conductor and the insulator be relatively small. Therefore, for most high performance systems, only a few combinations of conducting materials and insulating materials can be used effectively.

Table 6.3: Insulator Properties

Material	Dielectric Strength V/um	Qc MN/m	Qts MN/m	Tmax k
Nylon	11	103	76	390
Porcelain	16	138	800	1000
Teflon	17	117	34	600
Epoxy	18	117	62	500
Phenolic	20	172	76	390
G 10	22	414	276	390
Polyethylene	28	21	21	400
Cellophane	89	-	83	330
Acetate	158	-	76	400

Qc compressive strength, Qts tensile strength, Tmax maximum operating temperature [Mongeau 81].

CHAPTER 7

SUMMARY AND CONCLUSIONS

The metallic induction reaction engine is a type of space propulsion device which uses magnetic induction to convert stored electrical energy into kinetic energy. A solid metallic reaction mass such as aluminum or any other good conductor is used rather then a gas or plasma to achieve a high thrust density and efficiency. The reaction engine works by discharging stored electrical energy into a pulse coil. The current in the pulse coil magnetically induces a current in a coil formed from the reaction mass. This causes a magnetic force to develop between the two coils which accelerates them apart, thus producing thrust. By inducing a current in the reaction mass inductively rather then by direct mechnical contact, problems with erosion and wear of the engine are greatly reduced.

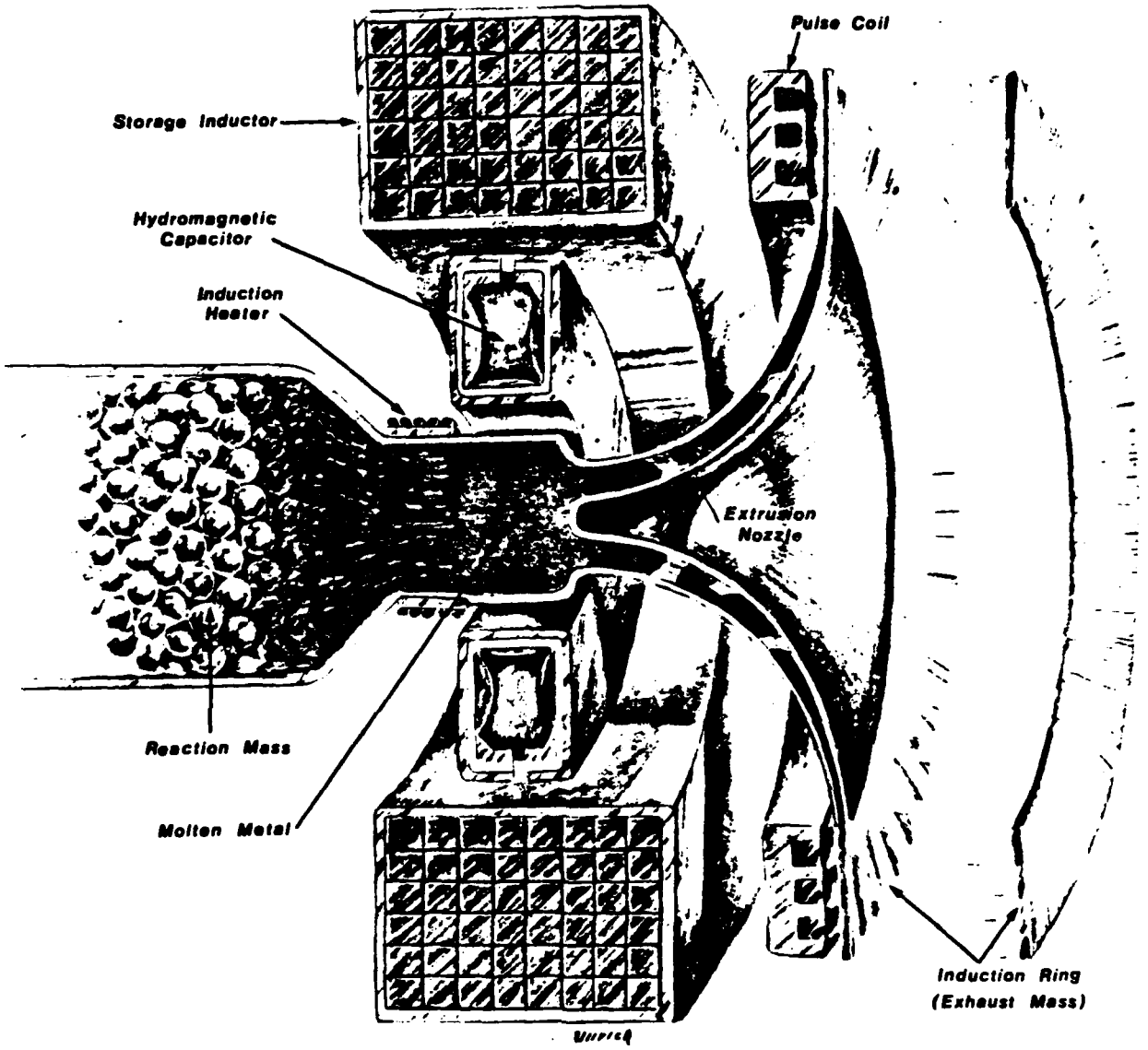

Figure 7.1: Artist's Conception

This thesis represents two years of an ongoing research program to determine the basic mechanisms and limits of the inductive conversion of electrical energy to kinetic energy by this engine. The fundamental principles of this energy conversion have been previously established [Mongeau 81]. However, the detailed effects of resistivity, coupling parameters, and material thermal properties had not. To analyse these effects, theoretical, experimental, and numerical methods were employed.

An experimental apparatus was constructed to observe the inductive acceleration process. This apparatus consists of an 18 inch diameter glass vacuum chamber mounted on a steel channel support structure. Removable end plates permit various pulse coil designs and diagnostic equipment to be readily installed. Aluminum and copper foil rings were placed on the face of the pulse coils and accelerated by a 90 microfarad, 20 kilovolt capacitor bank discharged through a dielectric switch. Measurments of velocity, current, and voltage were made as well as photographic observations of the rings in flight. Over one hundered tests were performed with this experimental apparatus including several tests with transfer efficiencies greater then 50%.

Many important parameters such as back EMF, resistive voltage drop, ring temperature, and induced current could not be measured directly. To understand the effects of these parameters, a

numerical model combining the magnetic coupling parameters with the phase and temperature dependent properties of the pulse coil/reaction mass system was developed. Using this model, various design tradeoffs could be observed quickly and in detail. The modeled results of velocity and current agree to within 15% of the experimental data over the entire observed range of operation. Extrapolation to higher performance operation has revealed that there are adverse coupling and circuit impedance effects which can limit the ultimate performance of the metallic induction reaction engine. Both the experimental tests and the numerical model indicate that the specific impulse of the engine is more dependent on the density of the reaction mass and the strength of the accelerating magnetic field than it is on material conductivity.

APPENDIX A

FUTURE WORK

The performance of the metallic induction reaction engine is largely dependent on the relationship between the discharge period of the drive circuit and the length of time the projectile coil remains magneticaly coupled to the drive coil. Ideally, stored electrical energy should be completely deposited in the drive coil and projectile coil before the projectile coil has time to move. However, this is generaly not what happens. For most drive coil designs, such as a face coil, the force that is exerted on a projectile coil is a function of the rate of energy input to the system. The greater the rate of energy input, the quicker the projectile coil decouples from the drive coil. In order to get around this limitation, a drive coil has been designed which, in effect, decouples the energy input to the system from the acceleration rate of the projectile coil. This drive coil design is known as a compound coil.

Compound Coil

All drive coils accelerate projectile coils at a rate proportional to the mutual inductance gradient between the two coils. In a face coil design, the mutual inductance between the

drive coil and the projectile coil is large when the two coils are closely coupled and decreases as they move apart. Therefore, the projectile coil's rate of acceleration is high at a time when energy input is the most crucial. The compound coil avoids this problem by coupling to the projectile coil in such a way that the mutual inductance gradient starts out low during the initial part of the acceleration process, grows as the two coils begin to decouple, and then decays to zero as they move further away from each other (see figure A.1). A compound coil is actually two coils, one placed inside the other. These coils are designed so that a projectile coil can be placed between them (see figure A.2).

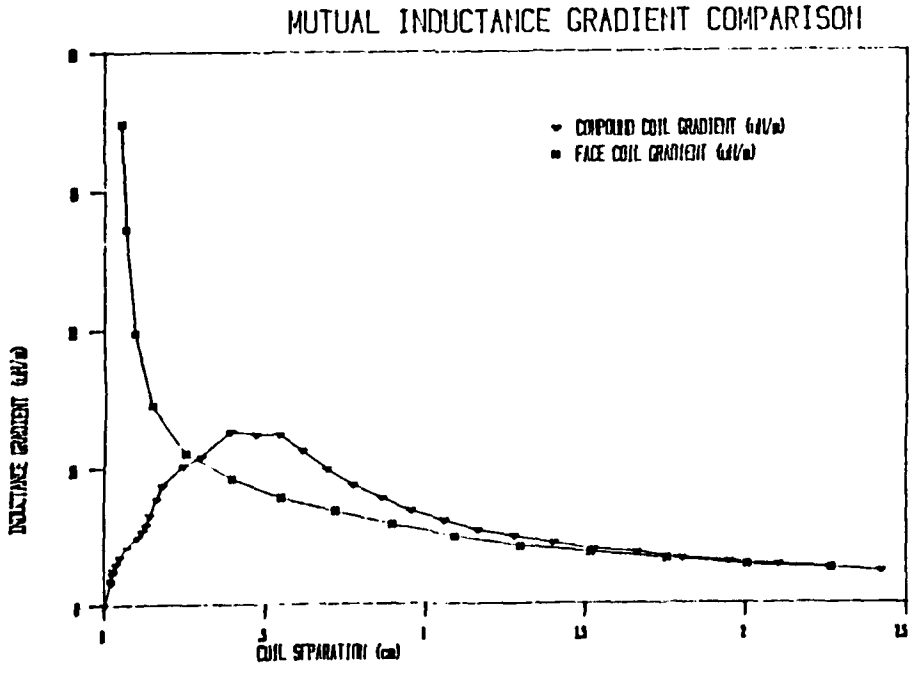

Figure A.1: Mutual Inductance Gradient Comparison

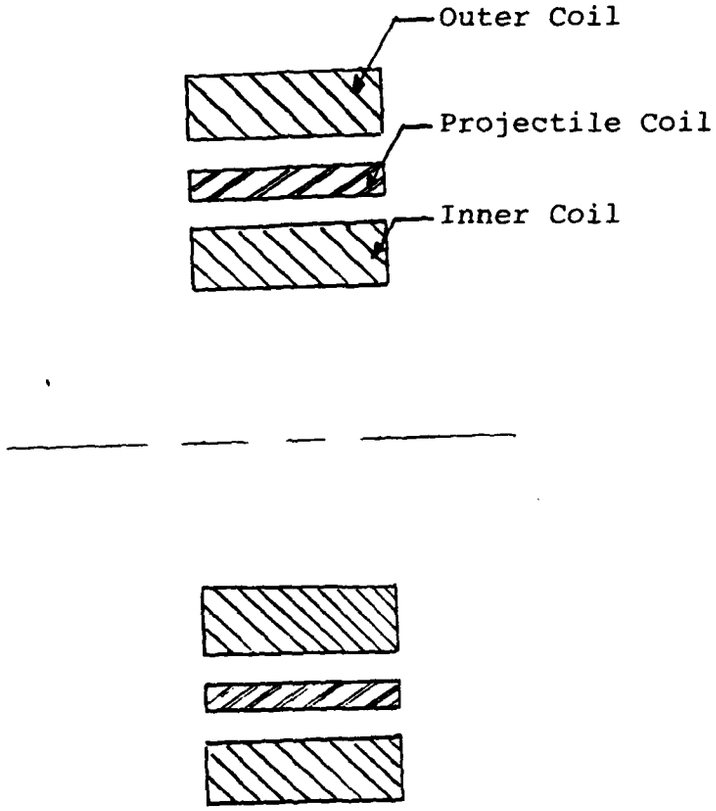

Figure A.2: Compound Drive Coil

If the projectile coil is placed at the exact center of the compound coil, the mutual inductance between it and the compound coil is very large but, the mutual inductance gradient is zero. In this way, the compound coil and the projectile coil act like a transformer with the projectile coil as the secondary and the compound coil as the primary. There is no force acting on the projectile coil, so it will remain where it is while energy is fed into the two coils. If the projectile coil is then perturbed in some way, a force is immediately established between it and the compound coil and the two will accelerate apart. Note that this is essentialy a magnetic adiabatic acceleration type of process. In practice, it is impossible to locate the projectile coil at the exact center of the drive coil and therefore, the projectile coil will begin to accelerate as soon as energy enters the system. However, placing the projectile coil near the center greatly reduces the initial accelerating force and increases the coupling time between the coils.

At the time this thesis was written, a compound coil had been built and some preliminary testing performed. Unfortunately, instrumentation difficulties prevented an analysis of this coil's performance (see figure A.3).

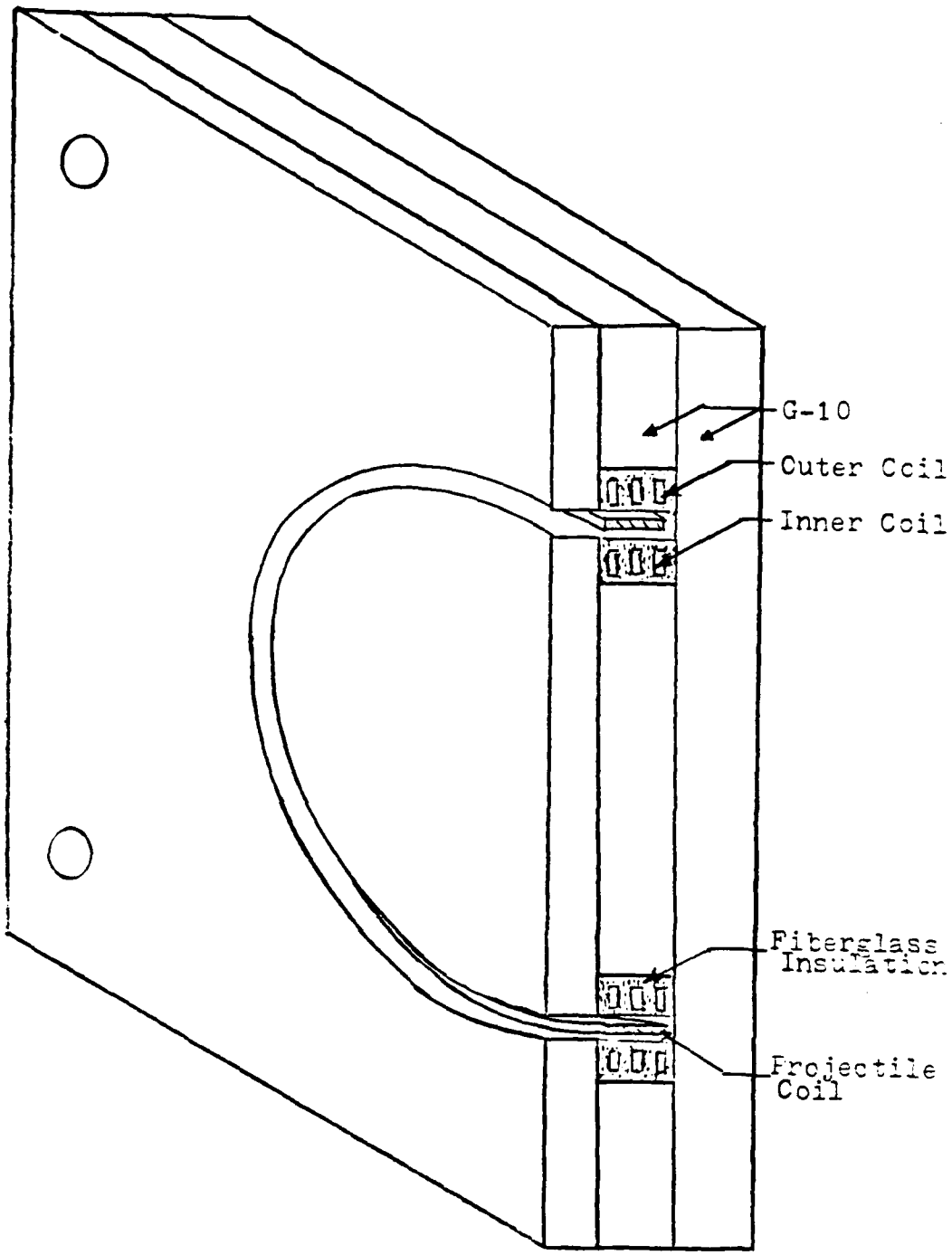

Figure A.3: Experimental Compound Coil

Projectile Ionization

Aside from poor geometric coupling between the drive coil and the projectile coil, there also exist large resistive losses in the projectile coil which can adversly effect the performance of the metallic induction reaction engine. Near the vaporization point of the projectile coil material, the resistance of the coil can be so large that it appears more like an insulator then it does a conductor. This can limit the acceleration process to the conduction period available in the current integral. It is assumed, however, that a high induced voltage around the projectile coil can cause it to ionize and conduct electricity past the vaporization point. Tests conducted on metal wires indicate that this is fact what happens, but these tests were performed by direct mechanical contact with the wire and not by a magnetically induced current [Reithel 59]. To demonstrate that a projectile coil can be ionized inductively and to observe the effect of this ionization, an experimental apparatus has been designed. This apparatus consists of a thin glass vacuum chamber formed from 1/4 inch tempered glass and mounted to a magnetic pulse coil (see figure A.4). This glass chamber will hold the projectile coil stationary during a test thus, permiting material ionization to be observed in a controlled geometry. Instrumentation will include a Rogowski coil to measure current in the drive circuit and a small coil placed on top of the vacuum

chamber to measure the magnetic field around the drive coil and projectile coil. Observations of the ionization process will be made with an open shuttered camera.

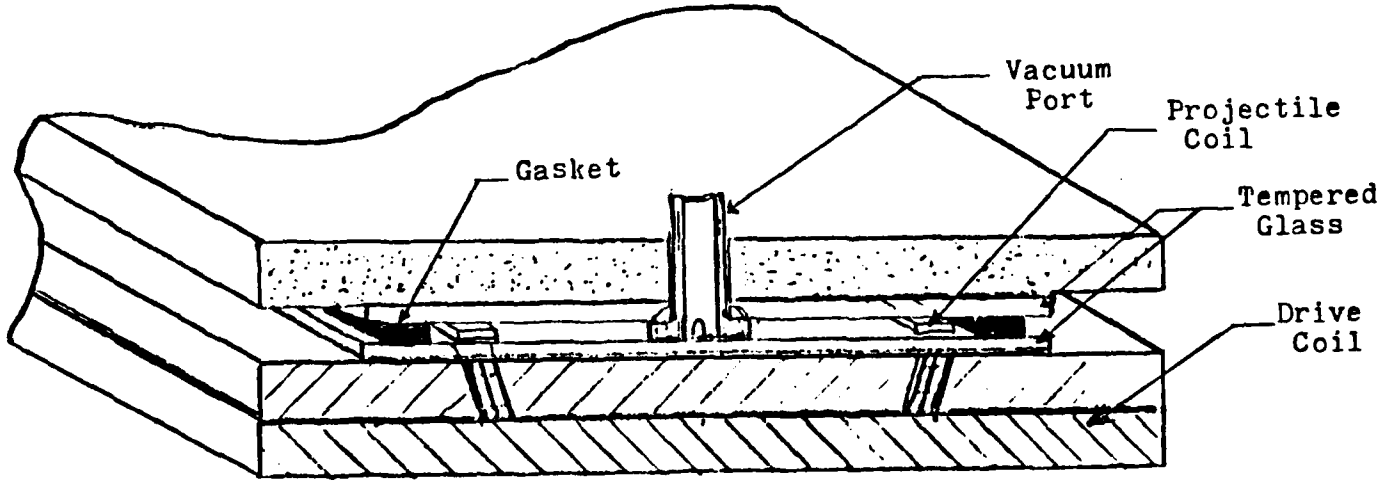

Figure A.4: Ionization Experiment

Because of the difficulties encountered during previous experiments, a pulse coil has been designed for this apparatus

that can be quickly rebuilt should it fail.

Rebuildable Coil

The rebuildable coil is a type of face coil constructed from 1/2 x 0.02 inch beryllium copper ribbon. G-10 strips are used to insulate the turns of the coil and two 3/4 inch G-10 plates encase the coil providing it with structural support. There are two unique features to this coil. One is that the coil can be pretensioned. This is acomplished by tightening the bolts on a tapered G-10 plug that fits around the inside of the coil. In order to get an even distribution of pressure, a 1/8 inch strip of rubber is placed around the outermost turn of the coil (see figure A.5). The other unique feature to this coil is that instead of potting it in an epoxy dielectric, mineral oil is used to prevent surface flashover (Simple experimental tests are expected to be conducted to determine the effectiveness of the mineral oil). The entire coil is bolted together with a G-10 or glass cover plate and two O-rings to prevent the mineral oil from leaking. The only parts of the coil that can not be quickly disassembled and reassembled are the leads. They exit from the rear of the coil and must be caulked to prevent leaks.

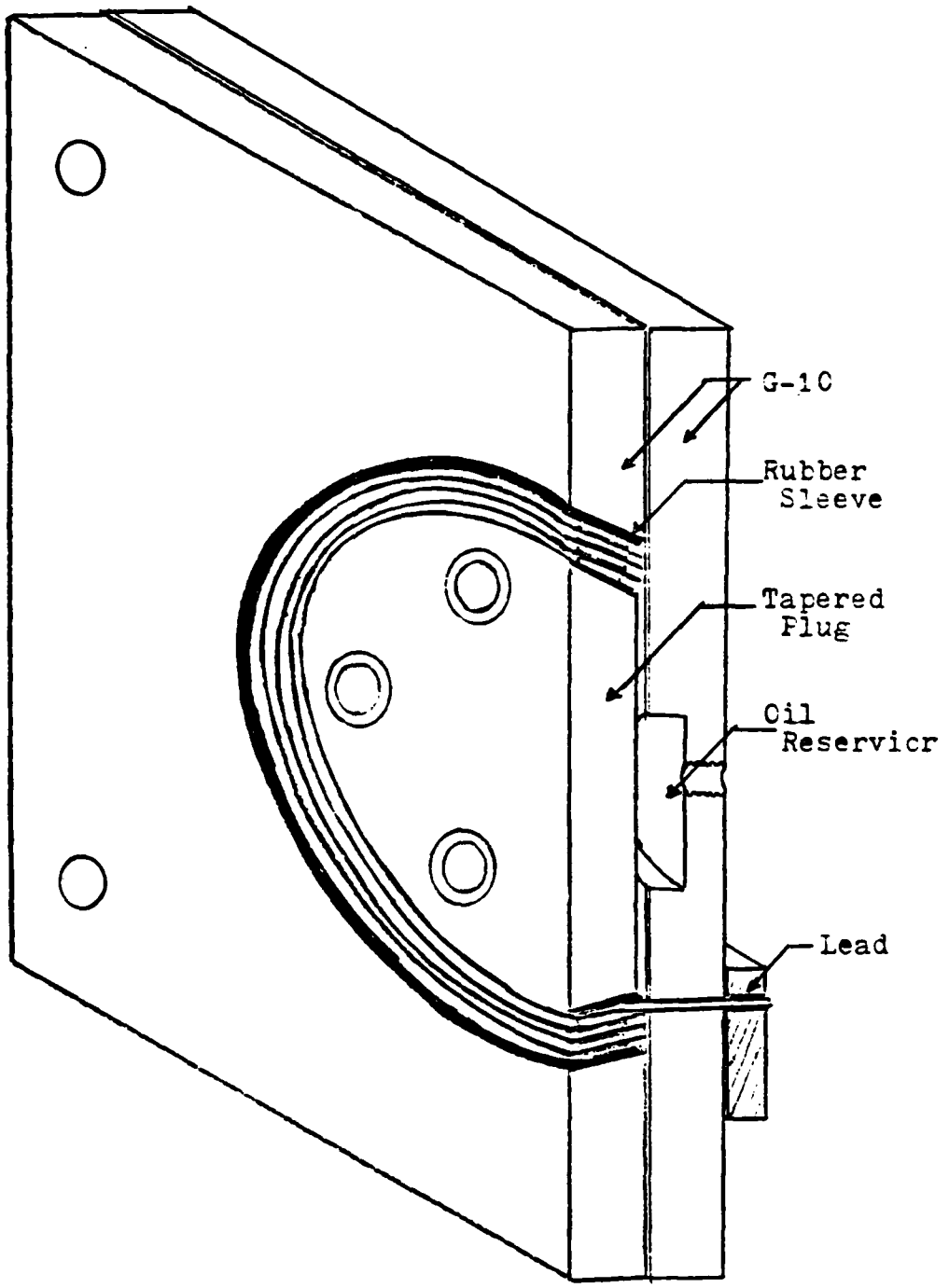

Figure A.5: Rebuildable Coil

APPENDIX B

POLYNOMIAL APPROXIMATION OF ELLIPTIC INTEGRALS

Elliptic Integral of the Fist Kind;

$$K(m) = \int_0^{\pi/2} [1-m\sin^2\theta] \quad d\theta$$

$$K(m) = [A0+A1*m1+\ldots A4*m1^4] + [B0+B1*m1+\ldots B4*m1^4]*\ln(1/m1) + e(m)$$

where e(m) is the error,

$$e(m) < 2E\text{-}08$$

$$m1 = 1-m$$

and

A0 = 1.38629436112	B0 = 0.5
A1 = 0.09666344259	B1 = 0.12498593597
A2 = 0.03590092383	B2 = 0.06880248576
A3 = 0.03742563713	B3 = 0.03328355346
A4 = 0.01451196212	B4 = 0.00441787012

Elliptic Integral of the Second Kind;

$$E(m) = \int_0^{\pi/2} [1-m\sin^2\theta] \quad d\theta$$

$$E(m) = [1+a1*m1+\ldots a4*m1^4] + [b1*m1+\ldots b4*m1^4]*\ln(1/m1) + e(m)$$

where

$$e(m) < 2E\text{-}8$$

$$m1 = 1-m$$

and

a1 = 0.44325141463	b1 = 0.24998368310
a2 = 0.06260601220	b2 = 0.09200180037
a3 = 0.04757383546	b3 = 0.04069697526
a4 = 0.01736506451	b4 = 0.00526449636

BIBLIOGRAPHY

[Anderson 84] D.A. Anderson, J.C. Tennehill and R.H. Pletcher, Computational Fluid Mechanics and Heat Transfer, McGraw-Hill, New York, 1984.

[Ashby 80] M.F. Ashby and D.R.H. Johns, Engineering Materials An Introduction to their Properties and Applications, Pergamon Press, New York, 1980.

[Bondaletov 67] V.N. Bondaletov, Induction Acceleration of Conductors, Soviet Physics-Technical Physics 12(2), August, 1967.

[Bondaletov 77] V.N. Bondaletov and E.N. Ivanov, Ultrahigh axial acceleration of Conducting Rings. Soviet Physics-Technical Physics 22(2), Febuary, 1977.

[Byers 79] D.C. Byers, Characteristics of Primary Electric Propulsion Systems, Princeton/AIAA/DGLR 14th International Electric Propulsion Conference, AIAA Paper, October 1979.

[Daily 81] C.L. Daily, H.F. Meissinger, R.H. Loveberg, and S. Zafren, *Integrated Propulsion for Near-Earth Space Missions*, NASA Paper No. CR 167889, October 1981.

[Daily 79] C.L. Daily and R.H. Loveberg, Large Diameter Inductive Plasma Thrusters, AIAA Paper No. 79-2093, October 1979.

[Grover 62] Fredrick W. Grover, Ph.D. Inductance Calculations, Working Formulas and Tables, Dover Publications, Inc., New York, 1962.

[Hildebrand 74] F.B. Hildebrand, Introduction To Numerical Analysis, McGraw-Hill Inc., New York, 1974.

[Knoepfel 70] H. Knoepfel, Pulsed High Magnetic Fields. American Elsevier Publishing Company Inc., New York, 1970.

[Kraus 73] J.D. Kraus and K.R. Carver, Electromagnetics, McGraw-Hill, New York, 1973.

[Medearis 74] Kenneth Medearis, Numerical-Computer Methods for Engineers and Physical Scientists, KMA Research, Denver-Fort Collins, 1974.

[McKinney 81] Kenelm Lee McKinney, Computer Assisted Inductance Calculations, Massachusetts Institute of Technology, January, 1984.

[McKinney 84] K.L. McKinney, Pulsed Induction Acceleration, Master's Thesis, Massachusetts Institute of Technology, January, 1984.

[Milne 70] W.E. Milne, Numerical Solutions of Differential Equations, second edition, Dover Publishing Inc., New York, 1970.

[Mongeau 81] Peter Mongeau, Coaxial Air Core Electromagnetic Accelerators, Ph.D. Thesis, Massachusette Institute of Technology, October, 1981.

[Mongeau 82] Peter Mongeau and Henery Kolm, Metallic Induction Reaction Engine, 1982.

[Patera 84] A.T. Patera, unpublished notes on numerical methods for solving fluid dynamic and thermodynamic problems, 1984.

[Reithel 59] R.J. Reithel, J.H. Blackburn, G.E. Seay, and S. Skoinick, The Current Pause in Exploding Wire, Exploding Wires, edited by W. Chace and H, Moore, Plenum Press, New York, 1959

[Rohsenow 61] W.M. Rohsenow and H.Y. Choi, Heat, Mass and Momentum Transfer, Prentice-Hall Inc., Englewood Cliffs, New Jersey, 1961.

[Trick 77] Timothy N. Trick, Introduction to Circuit Analysis, John Wiley & Sons, New York, 1977.

END

FILMED

11-85

DTIC